High Vocational Libyan Center of Casting

Scientific Research Journal for Metal Engineering and Technologies

Vol. 2 No. 1 Year 2021

SRJMET

International Standard Serial Number

ISSN: 399 - 2107

ISO: 3297

High Vocational Libyan Center of Casting 2021

مجمـوعة السهـل
Al-Sahl Group

الشركة الليبية للحديد والصلب
LIBYAN IRON AND STELL COMPANY

المؤتمـــر الليبـــي الثاني لسبـــاكة المعـــادن

والصنـــاعات المعدنيـــة

Second Libyan Conference on Metal Casting and Processing Technologies

تحت شعار

"نبحث ونواكب لنصل"

تـــنـــويـــه

الأوراق المنشورة في العدد الثاني من المجلة هي الاوراق التي تمت المشاركة بها في مؤتمر المركز العلمي الثاني والذي عقد بتاريخ 2021/09/28 م

المجلة

المجلة العلمية لدراسات وأبحاث العلوم الهندسية وتقنيات المعادن هي مجلة علمية محكمة نصف سنوية تصدر عن المركز العالي المهني للسباكة التابع لهيئة أبحاث العلوم الطبيعية والتكنولوجيا.

تعنى المجلة بنشر البحوث العلمية في مجالات سباكة المعادن ومختلف التطبيقات الهندسية ذات العلاقة .

دعوة للمشاركة :

تدعوا هيئة تحرير المجلة السادة الباحثين بالمراكز البحثية واكاديمية الدراسات العليا واعضاء هيئة التدريس والطلبة بالجامعات والمعاهد العليا والمهتمين داخل وخارج ليبيا للمشاركة .

قواعد النشر :

1- يجب أن لا تكون الورقات والتقارير العلمية المقدمة للنشر قد سبق نشرها في مجلات علمية اخرى.
2- تخضع جميع الورقات العلمية والتقارير للتقييم العلمي من ثلاثة مقيمين من ذوي الكفاءة ولن يتم نشر أي ورقة الا بعد اتمام التعديلات المطلوبة في حالة وجودها والالتزام بقواعد النشر.
3- يجب ترقيم كل الصفحات بما فيها التي تحتوي علي مخططات وجدول واشكال وجميعها يجب ان تدرج بعد الفقرة الخاصة بها مباشرة ويجب ان لا يزيد عدد الصفحات عن15 صفحة.
4- تقبل الورقات باللغتين العربية والانجليزية فقط وفي حالة استخدام اللغة العربية يجب كتابة المصطلحات العلمية باللغة الانجليزية بين قوسين اما عند استخدام اللغة الانجليزية يجب ارسال نسخة من ملخص الورقة باللغة العربية .
5- حقوق النشر: يتعهد الباحث على نماذج خاصة , بحق المركز الحصري بنشر الورقة أو البحث أو التقارير , عند قبوله النشر.

للاطلاع على كامل شروط المشاركة يرجي زيارة الموقع الإلكتروني: WWW.HVCC.LY

لأي استفسار على نشاطات المجلة، نأمل مراسلة هيئة التحرير علي البريد الإلكتروني الخاص بالمجلة:

SRJMET@HVCC.LY

لمركـــز الليبي العالـــي المهنـــي للسباكـــة

المجلة العلمية لدراسات وأبحاث العلوم الهندسية وتقنيات المعادن

المجلد الثاني – العدد الأول - سبتمبر 2021

Eng. MOHAMED ABDULJALIL ELMKHARRAM	High Vocational Libyan Center of Casting
Prof. RAMADAN ALHADE ALMADANE	Libyan Academy
Prof. MUSTAFA JARNAZ	Libyan Academy

Scientific Committee

المجلة العلمية لدراسات وأبحاث العلوم الهندسية وتقنيات المعادن

المركز الليبي العالي المهني للسباكة 2021م

The Journal

The Scientific Research Journal for Metal Engineering and Technologies, is a semi-annual engineering scientific journals published by the High Vocational Center of Casting which belongs to The authority of Natural Science, Research and Technology - Ministry of education.

The Journal publishes engineering and scientific research in various fields of metal shaping, treating and fabrication technologies. Research related to the metal casting technology is of special interest.

Invitation to Participate

The editorial board of the journal would like to invite researchers in the Libyan Research Centers, Post graduate Academies, Universities and High Institutes to submit their research papers and scientific articles for publishing in the Scientific Research Journal for Metal Engineering and Technologies.

General Roles of Preparing Manuscript foe Publication

1. Manuscripts submitted for publication, must be original (three copies) and must not have been submitted to any other publication.
2. Submitted manuscripts should be evaluated by a board of three reviewers of high eminence.
3. All manuscript pages should be numbered consecutively, including those containing diagrams, figures and tables. Figures and tables should be placed after the text.
4. Manuscripts are accepted in Arabic and English only. A manuscript should not exceed 15 pages, this includes: diagrams, tables, figures and abstracts.

In order to see the full list of rules for publication in the Scientific Research Journal for Metal Engineering and Technologies (SRJMET), kindly visit the web site of the High Vocational Center of Casting : **www.hvcc.ly** or send email to **srjmet@hvcc.ly**

High Vocational Libyan Center of Casting (HVLCC)

Scientific Research Journal for Metal Engineering and Technologies (SRJMET)

Volume.2- Number.1- Year 2021

High Vocational Libyan Center of Casting Scientific Research Journal for Metal Engineering and Technologies

Vol. 2 No. 1 Year 2021

SRJMET
Scientific Research Journal for Metal Engineering and Technologies
Volume No.02 Issue No. 01,pp:1-15
ISSN:399-2017
01. Aug .2021

Synthesis and Characterization of Plasma Polymerized Thin Films on Stainless Steel Using Microwave (PECVD) Method for Medical Applications

Sana Sbeta[a], Abdulmagid Bouzed[b], Omran Musbah[c], Chin Oi Hoong[d], Wong Chiow San[e]

[a,b]Libyan Center for Plasma Research, Libyan Authority of Scientific Research, Libya
[c]Materials & Metallurgy Engineering Department, Faculty of Engineering University of Tripoli, Libya
[d,e]Plasma Technology Research Center, Department of Physics, Faculty of Science, University of Malaya, Malaysia

[a]sbeta_62@yahoo.com, [b]a_bouzed@yahoo.com, [c]oamusbah@gmail.com,

[d]ohchin@um.edu.my, [e]cswong@um.edu.my

Abstract

A home-made microwave Plasma Enhanced Chemical Vapor Deposition (PECVD) system was constructed for the deposition of polymer-like thin films on 304L stainless steel substrates that are used in medical applications and on glass substrates by using benzene (C_6H_6) and argon (Ar) as precursor and carrier gas respectively. The surface properties of the deposited thin films such as chemical structure and wettability were characterized by Fourier Transform Infrared spectroscopy (FTIR) and Water Contact Angle (WCA) measured by Optical Tensiometer respectively. The corrosion behavior of the deposited thin film on stainless steel was evaluated by Electrochemical Impedance Spectroscopy (EIS). The effects of the deposition parameters, such as working pressure and time of deposition on the surface properties of the deposited thin films were investigated. FTIR analysis indicated the decomposition of the benzene ring and formation of a-C:H films in aliphatic group. The chemical structure of the thin films was changed by decreasing the working pressure in which the C≡C absorption bands became more prominent. All the samples had WCA (θ) lower than 90° so they are classified as hydrophilic (wettable) surfaces. The deposition time had the greatest influence on the WCA measured. It was observed that wettability can be adjusted by the plasma parameters, which would enable the production of coatings with properties suitable for specific practical applications, such as in biomedical devices. The collected (EIS) data showed higher Z modulus of film coating at lower test frequency which indicated a better corrosion resistant of the metal substrate.

Keywords— Thin Film Deposition, PECVD, FTIR, WCA, EIS.

1. Introduction

Surface modification includes all types of surface treatments and coatings that result in a change in the composition and the microstructure of the surface layer [1]. It is often performed to improve the biological, chemical and mechanical properties of the surface layer of materials [2]. Over the past 40 years, plasma has become a very useful method for surface modification and deposition of various materials [3]. Plasma Surface Modification (PSM) is an economical and an effective material processing technique used in the biomedical field because it offers the unique advantage of allowing surface properties and biocompatibility to be engineered selectively, while the bulk of the properties of the material remain unchanged. Changes in the chemical composition and properties of the surface layer of materials (e.g. wettability, metal adhesion, refractive index, hardness and biocompatibility) can be induced using PSM [4]. PSM can be classified into three categories: 1) removing materials from the surface such as plasma etching; 2) changing materials in the surface such as plasma treatment and 3) adding new materials on the surface such as thin film deposition [4-6]. The most commonly used method for thin film deposition is Plasma Enhanced Chemical Vapor Deposition (PECVD). The use of PECVD, or simply plasma polymerization, is increasing [7-9] because it is very efficient method to produce homogeneous organic thin films on large area substrates, such as metals, ceramics and plastics, and offers good control over the film properties [10]. Also, polymeric thin films obtained by PECVD have several advantages over films produced by conventional polymerization [11]. Moreover, it is a green technology (i.e. environmentally benign) compared to other material processing methods. In addition, it can occur at moderate temperature compared to conventional chemical reaction. It refers to the deposition of polymer thin film through plasma dissociation due to the excitation of an organic monomer gas and subsequent deposition and polymerization of the excited species on the surface of a substrate [3]. Plasma polymerization can be used to fabricate polymer thin films (100Å-1μm) from a variety of organic and organometallic starting materials. In PECVD processes, plasma can be generated by direct current (DC), radio frequency (RF) and microwave (MW) discharges [12]. Microwave discharges are widely used for generating cold plasma at pressures from 10^{-5} Torr up to an atmospheric pressure of 760 Torr in the pulse and continuum wave regimes at incident powers ranging from several Watts to hundreds of kW for different applications [13]. Magnetrons are the most common microwave generators because of their low cost and availability in the market for domestic use, such as in microwave ovens [14]. There are several classes of the microwave plasma generators include the waveguide microwave plasma generators [13] which was used in this study. Microwave-plasma polymerization is an attractive method for obtaining thin films [12]. A variety of medical devices such as artificial hips and knee joints, coronary stents and heart valves are routinely implanted into the human body. These devices may come in contact with body fluids which contain about 1% NaCl; increasing the likelihood of corrosion that may have harmful effects on both the body and implants [7]. The ideal biomedical implants should have good mechanical properties while the surface should have good biocompatibility [4]. Many types of

materials are being used in biomedical applications including metals, alloys, polymers, ceramics, composites, and glasses [4,15]. For structural applications in the body (i.e. implants), the principal metals used are titanium-based alloys, cobalt-based alloys and stainless steels [15]. The common grades of stainless steels used in this field are the Austenitic stainless steel 316 and 304. The Austenitic stainless steel 304 is widely used in many engineering applications such as in the manufacturing, nuclear, chemical, oil and petrochemical, and food industries, as well as in the medical industry for biomedical implants [16]. There are different versions of stainless steel 304 with improved material properties for specific applications such as 304L (the low carbon version) [17]. Stainless steel is naturally a biocompatible material. Its biocompatibility can be further improved by modification of its surface energetics. Plasma polymerization is one of the most important processes used to modify the surfaces of many materials by deposition of polymeric thin films. The biocompatibility of a material is determined by the interactions between the implant and biological system on the micrometer and nanometer scale, and the physicochemical surface properties (such as chemical composition, wettability and surface energy) play an important role. PSM has recently drawn much interest from the field of medicine and it is now used to improve the function and the longevity of biomedical materials [4]. The development of chemical and biological stability of biomedical materials against corrosive body-fluid environments is a widespread research interest. In this research, a microwave PECVD system was constructed to deposit polymer-like thin films on 304L stainless steel substrates and on glass substrates (for FTIR analysis). Benzene and argon were used as precursor and carrier gas respectively. The main objectives of this research are: 1) to deposit thin films on stainless steel via microwave PECVD and 2) to investigate the effect of deposition parameters (i.e. working pressure and time of deposition) on the surface properties such as chemical structure, surface wettability and corrosion behavior of the deposited thin films. These films are characterized by Fourier Transform Infrared Spectroscopy (FTIR) for chemical structure and functional group identification, Optical Tensiometer for contact angle measurements to analyze the surface wettability (hydrophilicity/hydrophobicity) and Electrochemical Impedance Spectroscopy (EIS) to evaluate the corrosion behavior of the polymer coated metal.

1.1 Display Problem

Austenitic stainless steel 304L is known for its good corrosion resistance in many corrosive environments, but in the presence of chloride ions is susceptible to localized corrosion. For extremely corrosive environments, stainless steel 304L also offers a greater resistance to inter-granular corrosion, than similar grades of stainless steel [17], but it is prone to inter-granular corrosion when used in chloride environments due to precipitation of chromium as chromium carbide ($Cr_{23}C_6$) at grain boundaries. Though corrosion is inevitable and the rate of corrosion can be reduced by a proper choice of material combination by: (a) using corrosion inhibitors, (b) protective films and coatings deposited onto the metal surface and (c) surface modification [21,22].

1.2 Research Method

1. Thin Film Deposition Technology

Thin film technology is simultaneously one of the oldest arts and one of the newest sciences. Today, thin films of any material are widely used in electrical, optical, thermal, and protective applications. Surface properties such as corrodibility, wear resistance, hardness, and wettability can be changed fundamentally due to coatings with specific thin films [7]. Thin-film deposition technologies for forming layers in the thickness range of a few nanometers to about ten micrometers can be classified into: 1) evaporative methods, 2) glow discharge processes, 3) gas phase chemical processes and 4) liquid phase chemical techniques [23]. The thin film deposition by glow discharge processes can be subdivided into two groups: sputtering deposition and plasma enhanced chemical vapor deposition [24].

2. Plasma Enhanced Chemical Vapor Deposition

Among many chemical vapor deposition (CVD) methods, plasma-enhanced chemical vapor deposition (PECVD) process is very efficient method to produce thin films [25]. A recent development has been the use of PECVD to produce polymeric and inorganic coatings with properties completely different from those of conventional materials [26]. Polymer films fabricated by PECVD have unique properties due to their dense crosslinked bulk structure. These spatially uniform films exhibit good adhesion to a variety of substrates, excellent chemical inertness, high thermal resistance, and are formed from an inexpensive, solvent-free and room temperature process [27]. PECVD is curried out using low pressure (glow discharge) plasmas in which the energy to sustain the ionized state is supplied by an externally applied electric field. The energetic species in these plasmas are the free electrons. They gain energy from the electric field faster than the ions do and are thermally isolated from the atoms and molecules, as far as elastic collisions are concerned, by the mass difference. Consequently, the electrons accumulate sufficient kinetic energy to undergo inelastic collisions and to sustain the ionization, while the heavy particle (molecule) temperature remains low [25]. In PECVD process shown in figure 1, the radicals were produced in the plasma and the supplied feed gas drift to the surface. The radicals do not chemically react with the substrate surface. Instead the radicals combine to form stable chemicals. Ions accelerated across the sheath deliver energy that tends to “cross-link” these chemical bonds. Plasma bombardment can have an important influence on the properties of the growing coatings.

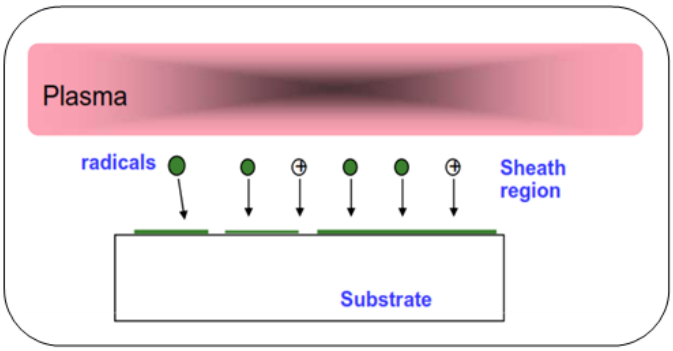

Figure 1: Plasma Enhanced Chemical Vapor Deposition (PECVD) Process

2. Experimental Equipment's and Procedure

2.1 Deposition System

The deposition system used in this work is a home-made microwave PECVD designed system which is illustrated in figure 2 (a&b). It is a multi-purpose system for the treatment by plasma processes such as thin film deposition, surface cleaning, nitriding and etc. The system consists of deposition chamber, vacuum system and microwave generator (plasma source). The deposition chamber composed of a stainless steel cylindrical chamber 25 cm long and 14.5 cm in diameter provided with four ports for: 1) vacuum system- turbo-molecular pump backed by mechanical pump and pressure gauges, 2) gas inlet, 3) wave-guide and 4) the last port with a glass window for observing the deposition process. The microwave is generated by the microwave furnace (commercial magnetron) at frequency of 2.45 GHz with maximum power of 900 W which was transmitted to the chamber via a wave-guide.

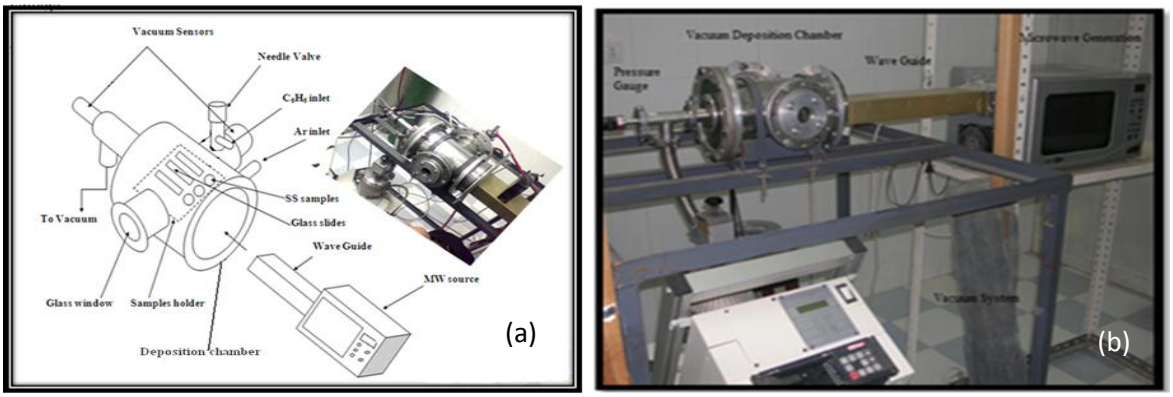

Figure 2: (a) Schematic diagram and (b) Photograph of the home-made microwave plasma system

2.2 Sample Preparation

Two types of materials were used in this experiment. The first type was disc shaped 304L Stainless Steel (SS) samples of 16 mm diameter and 8 mm thick. The second type was glass slide of dimension 85x25x1 mm suitable for FTIR analysis. The surfaces of SS samples were mechanically wet ground on SiC papers down to 2000 grit and then polished with alumina paste and rinsed with distilled water. Both types of samples (SS and glass) and the deposition chamber were cleaned by acetone just before the deposition process. The 304L SS sample is a biomedical grade austenitic type of stainless steel which is a common grade used in biomedical applications. This alloy contains mostly iron, about 17wt% chromium, 10wt% nickel and small amounts of other alloying species as given in table [1].

Table 1: Chemical analysis of 304L stainless steel

Element	Fe	C	Mn	Si	Mo	Co	Cr	Cu	Ni	Others
Wt %	69.4	0.0269	1.52	0.671	0.375	0.0699	17.0	0.361	10.1	0.5762

2.3Deposition Procedure

After chamber evacuation to a certain base pressure (~0.1 mTorr), benzene precursor gas was introduced to the chamber with certain working pressure and the plasma was generated by microwaves. Before deposition, the microwave plasma of argon (Ar) gas was applied to some samples at power of 180 watt for 15min and working pressure of 3.7 mTorr (~0.5 Pa). This process was carried out at base pressure of 0.73 mTorr to remove any contaminations or organic oxides from the surface of samples and the chamber (i.e. pre-cleaning process for both chamber and samples).
Thin film deposition processes were conducted at various parameters as indicated in table 2. Argon gas (Ar) used as a carrier gas with (Ar/C_6H_6) ratio of (30:70) respectively. The working power P was adjusted at 540 W.

Table 2: Parameters of the deposition process

Parameter	Value
Power	**540 W**
Base pressure	**0.1 mTorr**
Working pressure	**10, 30, and 50 mTorr**
Deposition time	**5, 15, and 30 min**
Ar/C_6H_6 ratio	**30:70**

By adjusting the deposition parameters; working pressure and deposition time, the nature and properties of the deposited thin films were varied. In this research the effect of working pressure and deposition time on the deposited thin film properties have been investigated.

2.4 Characterization of the Deposited Thin Films

The deposited thin films were analyzed by the following characterization techniques using glass slide samples for FTIR analysis and stainless steel samples for the other characterization:

1. Fourier Transform Infrared Spectroscopy (FTIR) for chemical structure and functional group identification.
2. Optical Tensiometer for contact angle measurements to analyze the surface wettability (hydrophilicity/ hydrophobicity).
3. Field Emission Scanning Electron Microscope (FESEM) for surface morphology.
4. Electrochemical Impedance Spectroscopy (EIS) to evaluate the corrosion behavior of the polymer coated metals.

3. Results & Discussion

During plasma deposition, the benzene decomposed into fragments and radicals [28] and thin film of amorphous hydrogenated carbon (a-C:H) was formed with different chemical structures.

3.1 FTIR Analysis

The compositional changes in the molecular structure of the thin films deposited on the glass slides from benzene vapor under present experimental test conditions were observed clearly by comparison of benzene infrared spectrum shown in figure 3 with the other spectra of the deposited thin films given in figures 4 to 6. The bands in the aromatic ring did not appear in the spectra of the deposited thin film which is an indication of complete decomposition of benzene vapor. The bond frequency, absorption and functional groups of the thin films deposited on glass slides are illustrated in table 3. This identification was made with assistance of Spectroscopic Handbook on Chemistry Data [29]. The bands related to the (O-H) group with different intensities were detected in the deposited thin films spectra. Since there was no oxygenated compound in the reacting species, the presence of these bands could be attributed to presence of some humidity in the deposition chamber. This was confirmed by analyzing the spectra of deposited thin films shown in figure 4 after doing a pre-cleaning step and using argon as a carrier gas with (Ar/C_6H_6) ratio of 30:70. The effect of working pressure on the structure of deposited thin films at 30 min deposition time is shown in figures 5 and 7. The chemical structure was changed when the working pressure was increased. For instance, the weak peaks of the carbon triple bond (C≡C) were recorded at 2177 & 2185 cm^{-1} at 10 and 30mTorr respectively, these peaks disappeared when the working pressure was raised to 50mTorr. Instead the hydrogenated carbon bond (C-H) was detected at 2945 cm^{-1}. This change in nature of the chemical structure of the deposited thin films could be attributed to increasing amount of benzene gas entering the deposition chamber. The absorption intensity increased by increasing the deposition time as shown in figures 6 and 8, and the films formed become thicker though the film formed exhibited the same chemical structures (i.e. same functional groups). The FTIR analysis indicated that the deposition process in this work was more effective at 30 min deposition time.

Table 3: Identification of Bond frequency, absorption & functional groups of the thin films deposited on glass slides

Bond	Wave number (cm^{-1})	Intensity	Functional group
O – H str	**3428 - 3296**	**s, br**	**Polymeric-alcohol**
C – H str	**2945 - 2939**	**m**	**Alkanes**
C ≡ C str	**2186 - 2177**	**w**	**Alkynes**
C = C str	**1683 - 1669**	**v**	**Alkenes**
C – H str	**1457 - 1385**	**m-w**	**Alkanes**

s: strong, w: weak, br: broad, m: medium, v: variable intensity

SRJMET
Scientific Research Journal for Metal Engineering and Technologies
Volume No.02 Issue No. 01,pp:1-15
ISSN:399-2017
01. Aug .2021

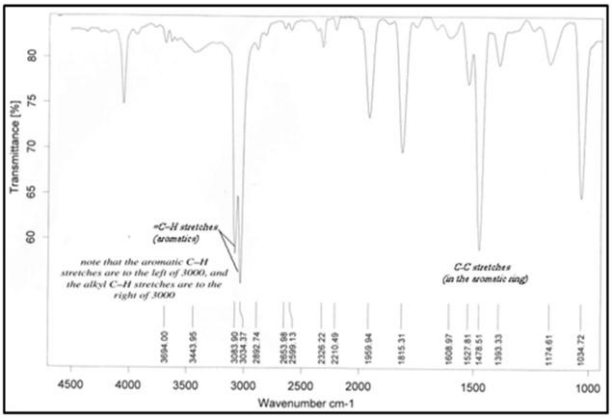

Figure 3: IR spectrum of benzene C_6H_6

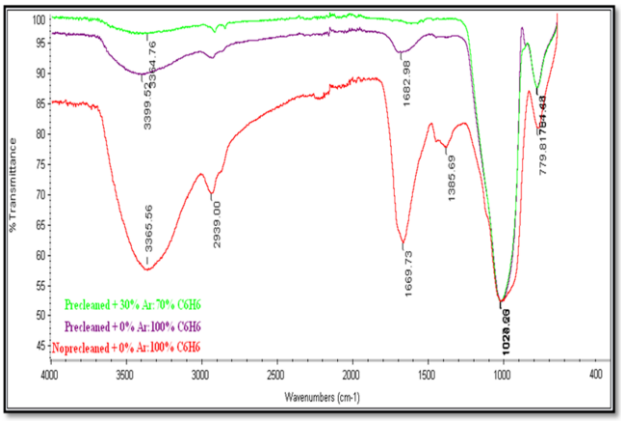

Figure 4: IR spectra of thin films deposited with/without pre-cleaning and Ar: C_6H_6 (30:70)

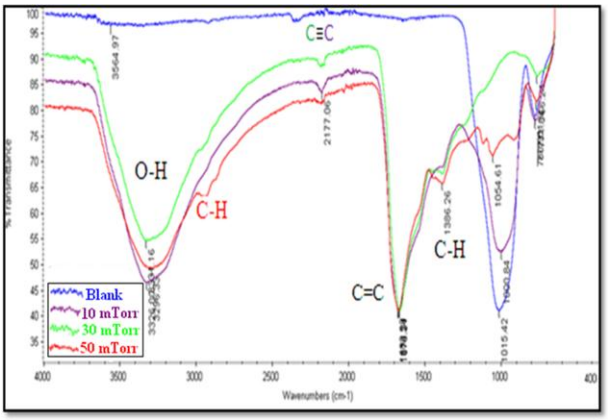

Figure 5: IR spectra of thin films deposited for 30 min deposition time.

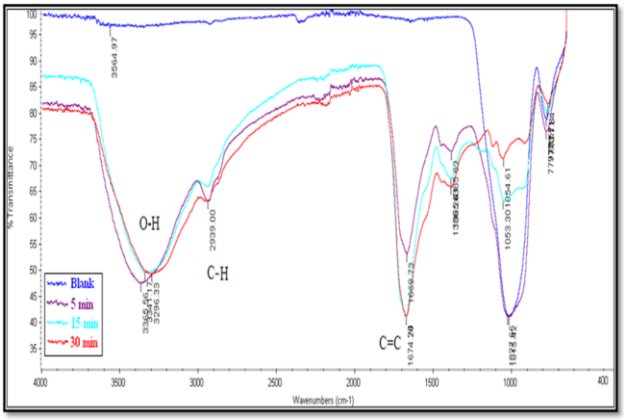

Figure 6: IR spectra of thin films deposited at 50mTorr working pressure

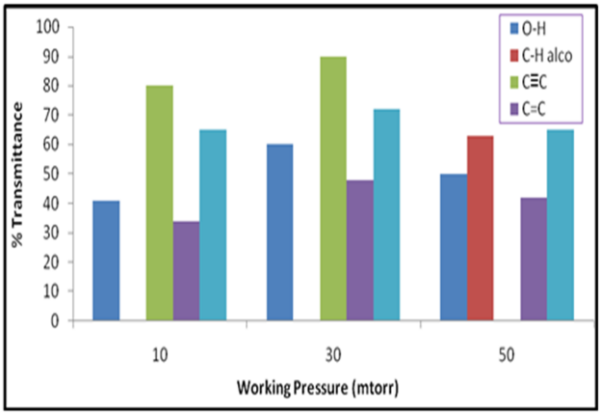

Figure 7: Effect of working pressure on the absorption intensity (%Transmittance) of the deposited thin films bonds.

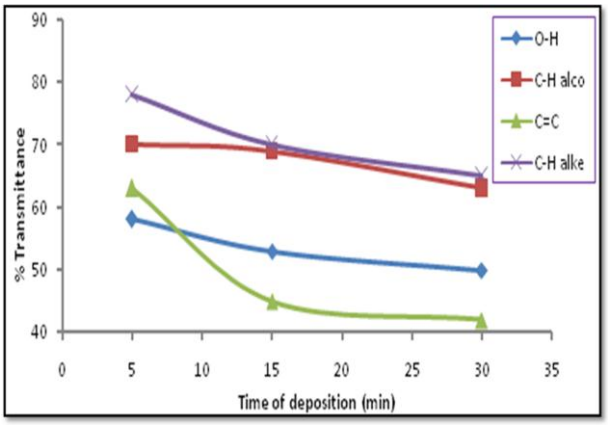

Figure 8: Effect of deposition time on the absorption intensity (%Transmittance) of the deposited thin films bonds

3.2 Surface Wettability

The surface wettability of the films deposited on stainless steel substrate was analyzed by measuring the water contact angle (WCA) at the chosen test parameters; working pressure and deposition time. Table 4 illustrates the contact angle and surface free energy measurements.

SRJMET
Scientific Research Journal for Metal Engineering and Technologies
Volume No.02 Issue No. 01,pp:1-15
ISSN:399-2017
01. Aug .2021

Table 4: Results of contact angle & surface free energy measurements

Samples No	Working pressure (mTorr)	Time of deposition (minutes)	Contact angle degrees [θ°]	S F E [mN/m]
Bare metal			81	35
T1	50	5	71	46
T2	50	15	67	49
T3	50	30	44	57
T4	30	30	30	65
T5	10	30	33	63

S F E=surface free energy

According to data given in the table above the deposition time seems to have the greater influence on the measured contact angle (film surface wettability) when compared with the effect of working pressure. On coated stainless steel at constant working pressure of 50 mTorr, the measured contact angle drops from 71°(at 5 minutes) to 44°(at 30 minutes) deposition time. At constant deposition time of 30 minutes, the measured contact angle decreases from 44° (at 50 mTorr) to 30° (at 30 mTorr) working pressure. But at lower working pressure (10 mTorr) the measured contact angle slightly increases (33°). This is due to the change of the chemical structure of the thin film deposited. This is confirmed by the FTIR spectra figure 5. In parallel to that, the surface free energy recorded an increase from 35mN/m on bare stainless steel to about 65mN/m on coated steel at the maximum deposition time of 30 minutes and a working pressure of 30mTorr. The effects of deposition time and working pressure on measured WCA and SFE of bare and coated stainless steel were shown in figures 9 and 10 respectively. From these results, the lowest stable contact angle that could be achieved at 50 mTorr working pressure and 30 minutes deposition time is ~44° as shown in figure 11. It can be inferred that film wettability on coated stainless steel can further be improved by longer deposition time which will create better possibility for the formation of more hydrogen bonds between water molecules and the film. However, it is not advisable to grow films for extended periods of time since this will lead to poor film adhesion to substrate due to the intrinsic stress caused by increasing film thickness due to increasing in deposition time as mentioned by Schauer in reference [7] and probably affect (in a negative way) other physical and mechanical properties.

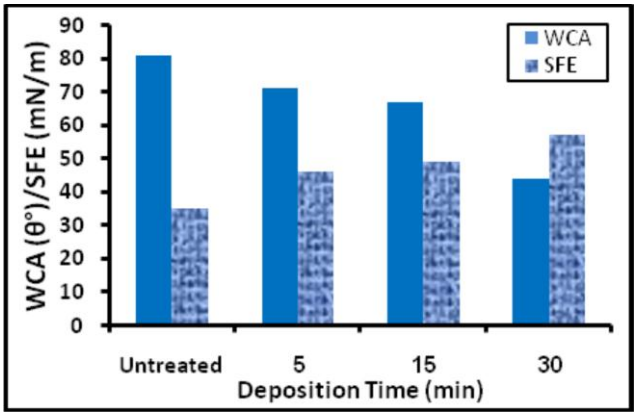

Figure 9: The effect of deposition time on WCA and SFE of the thin films deposited for 50 mTorr.

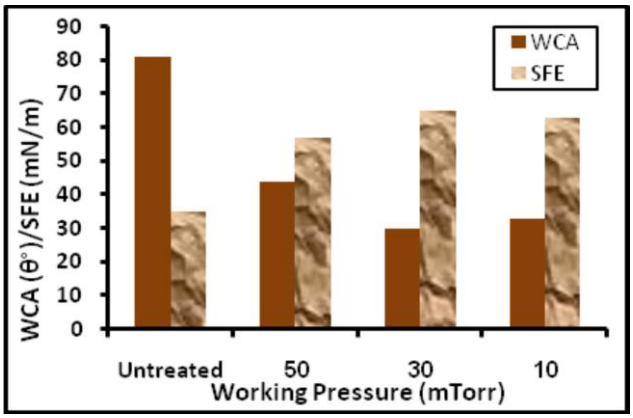

Figure 10: The Effect of Working Pressure on WCA and SFE of the Thin Films Deposited for 30 min.

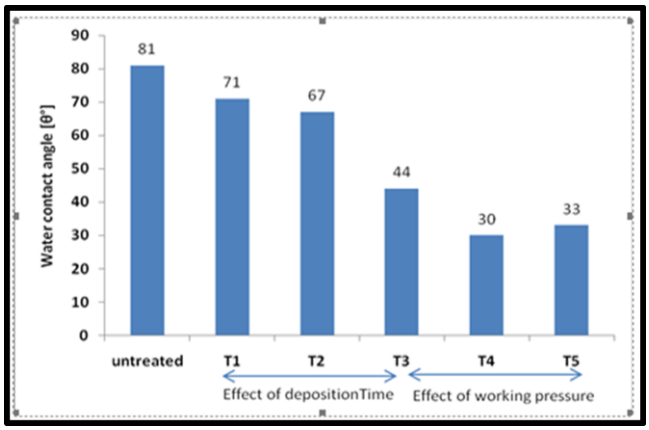

Figure 11: Water Contact Angle measured for bare and coated stainless steel

3.4 Surface Morphology by FESEM Analysis

Figures 12 (a, b, c) show the FESEM images of the untreated sample surface, flaking of the thin films deposited at 30 mTorr for 30 min (i.e. poor quality deposition) and the uniform thin films deposited at 50 mTorr for 5 min (i.e. better quality deposition). The low adhesion of the (C–H) films on stainless steel was attributed to poor chemical binding between a-C:H and metal and/or high internal stresses inside the deposited films leading to film flaking, then peeling off from the sample edge as shown in figure 12 (b). The intrinsic stress of the film is increased by (i) increasing the deposition time as evident in figures 13 (a, b, c), (ii) the nature of the film chemical structure as presented in IR spectra shown in figure 5, and (iii) the type of substrate. The problem of low adhesion can be solved by the deposition of a very thin intermediate layer between the metal surface and the (C–H) films. An amorphous hydrogenated silicon (a-Si:H) film is commonly used as an intermediate layer between metal and deposited film especially for coating of toxic substrates [7]. The effect of pre-cleaning on the surface of the sample before deposition was clearly observed. The contaminations under the thin films as shown in figure 14 (a) were removed and so a smooth deposited thin films from only benzene were obtained as shown in figure 14 (b). The roughness of the deposited thin films was increased by using a mixture of argon and benzene with ($Ar:C_6H_6$) ratio of (30:70) after the pre-cleaning step, as shown in figure 14 (c).

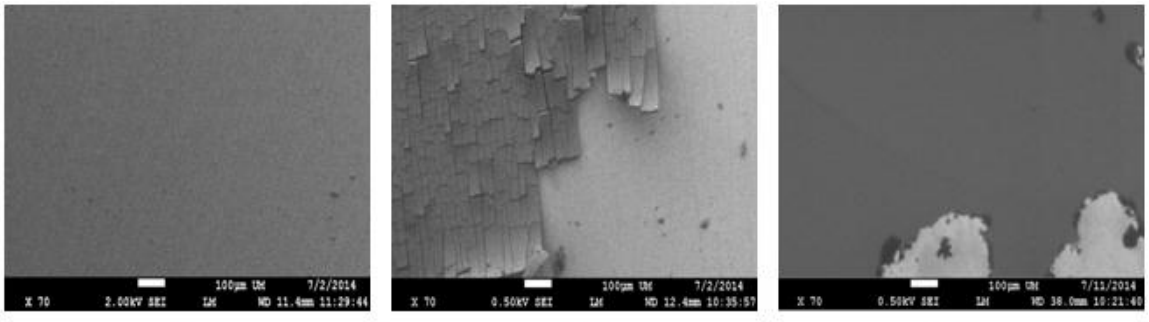

(a) (b) (c)

Figure 12 (a,b,c). FESEM images of (a) untreated sample, (b) the shape of flakes formed in thin film deposition at 30 mTorr for 30 min and (c) uniform thin film deposited at 50 mTorr for 5 min (X 70).

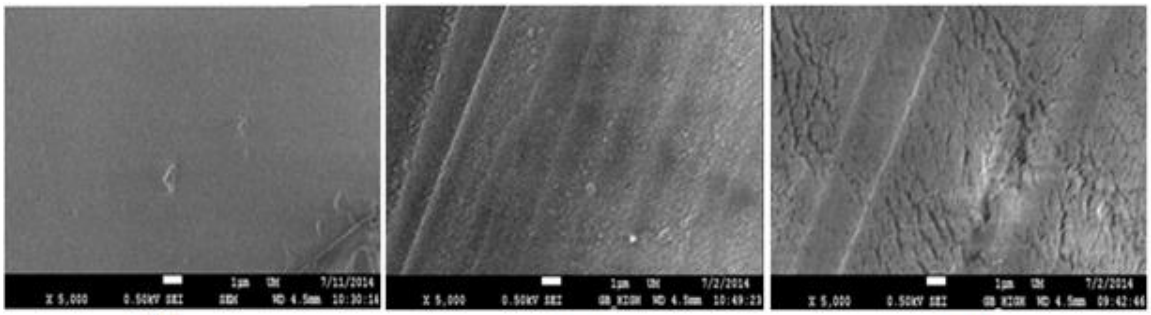

(a) (b) (c)

Figure 13 (a,b,c). FESEM images of thin film deposited for different deposition time (a) 5 min, (b) 15 min and (c) 30 min (X 5000).

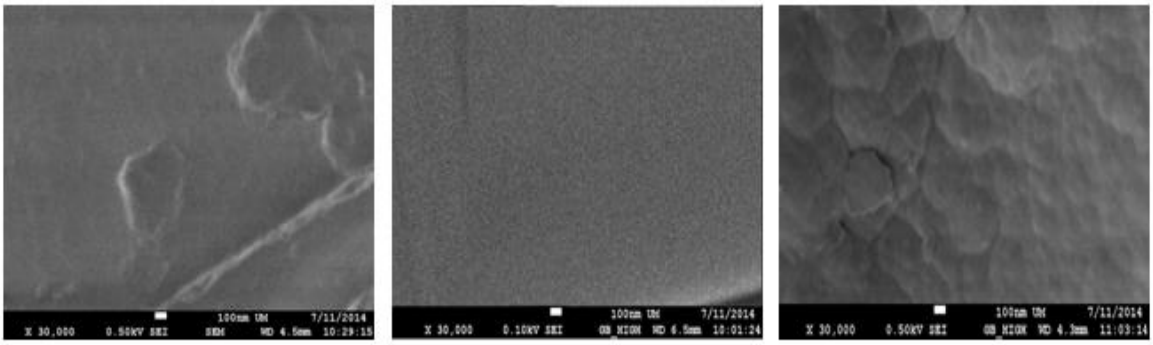

(a) (b) (c)

Figure 14 (a,b,c): FESEM images of thin film deposited (a) without pre-cleaning 100% C_6H_6, (b) with pre-cleaning 100% C_6H_6 and (c) with pre-cleaning 30%Ar:70%C_6H_6 (X 30,000).

3.5 Electrochemical Characterization

Two types of corrosion measurements were conducted; open-circuit corrosion test survey in neutral chloride solution and an electrochemical impedance spectroscopy characterization. The operating parameters of these measurements are illustrated in table 5. Seven stainless steel samples were used in this characterization as clarified in table 6.

Table 5: Operating parameters of the corrosion test

Parameter	Value
AC Voltage (mV_{rms})	10
Initial Frequency (Hz)	100,000
Final Frequency (Hz)	0.01
Time of Immersion (sec)	60

Table 6: The stainless steel samples used in electrochemical characterization

Samples No. / Deposition parameters	T_1	T_2	T_3	T_4	T_5	T_6	T_7
Deposition time (min)	5	15	30	30	30	5	5
Working pressure (mTorr)	50	50	50	30	10	30	30
Ar/C_6H_6 ratio after pre-cleaning	-	-	-	-	-	0/100	30/70

Figures 15 and 16 show the test results of the open-circuit potential measurements for the coated samples. In figure 15, the initial potential was about -138mv (SCE) and drift in the noble direction until reach almost steady state condition at around -122mv (SCE) after 60 seconds of immersion in 3% NaCl solution. By the end of this time period there was no significant change in E_{corr} which is an indication that this specimen approaches a passive state with minimum degradation rate. In this test result, the potential drift in the noble direction means that the film exposed to test solution is resisting active dissolution. On the other hand, the drift in the open-circuit potential was in the active direction for badly coated sample as shown in figure 16 which is indication of active direction or bad resistance of film for the effects of environmental electrolyte.

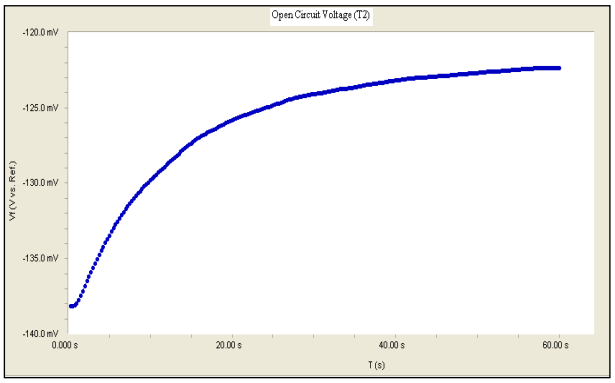

Figure 15: Open-circuit potential measurement for coated stainless steel (T_2) at 50 mTorr for 15 min

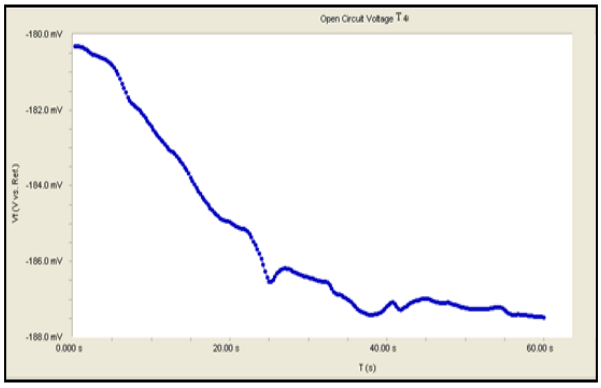

Figure 16: Potential-time survey for badly coated stainless steel (T_4) at 30mTorr for 30 min

The electrochemical test results for impedance measurements for sample T3 are shown in figures 17 and 18 as Bode and Nequist representation of impedance spectra respectively. Generally, higher Z modulus of the coating at lower frequency as shown in the figure17 indicates a better corrosion resistance. Also the shape of plot given in figure 18 gives indication of the coating impedance behavior.

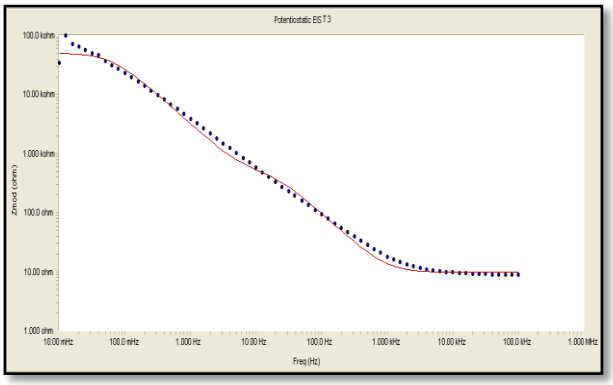

Figure 17: Bode Plot representation of Impedance data for coated steel sample (T_3)

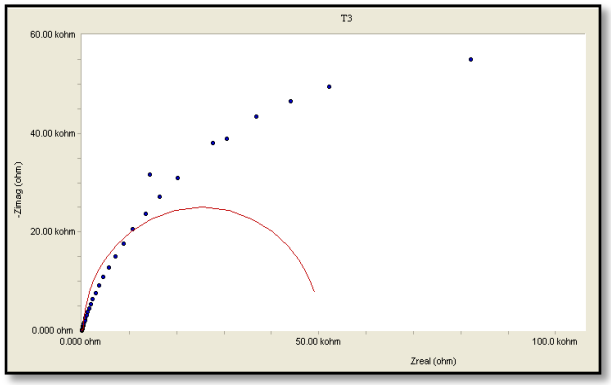

Figure 18: Impedance data of coated steel (T_3), Nyquist representation

The results of the fitting for obtained spectra of the polymer-like coated stainless steel samples are plotted in Bode diagram to make a comparison of these spectra (as shown in figure 19). As can be seen in the figure, it is possible to conclude that sample T_3 has a highest value R_f (~50 kΩ) while sample T_4 has the lowest value (~3 kΩ). So the deposition process is more effective at 30 minutes and 50 mTorr (T3) in our home-made deposition system.

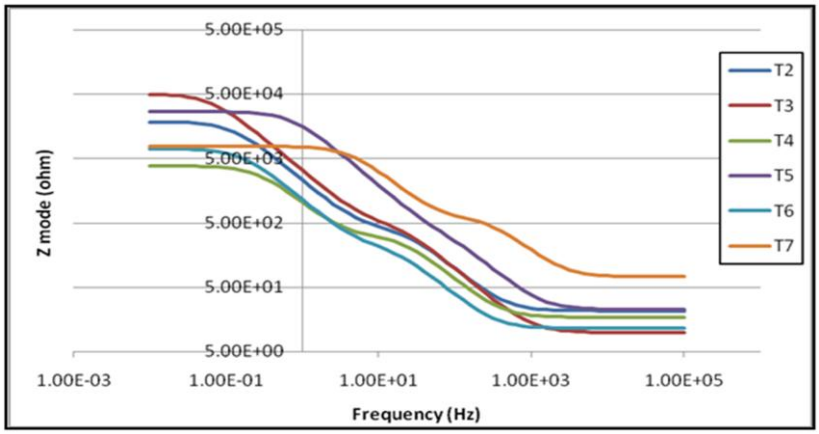

Figure 19: EIS spectra of coated steels at different deposition parameters (Bode mode)

4. Conclusion

Plasma polymerized thin films have been deposited on stainless steel and glass substrates at room temperature using benzene as precursor gas by PECVD method. Pulsed microwave with frequency of 2.45GHz and 540W was applied for the ignition of the plasma. From this study, the following conclusions can be drawn:

1. FTIR analysis indicated the decomposition of the benzene ring and formation of a-C:H films in aliphatic group.
2. According to the effect of deposition parameters, the chemical structure of the thin films was changed by decreasing the working pressure in which the C≡C absorption bands became more prominent.
3. The absorption of the (O-H) group band was minimized after doing pre-cleaning step and using Ar as a carrier gas with (Ar/C_6H_6) ratio of 30:70. This indicates the importance of this process in thin film deposition technique.
4. All the samples had contact angle (θ) lower than 90º so they are classified as hydrophilic (i.e. wettable) surface. More hydrophilicity (wettability) of 304L SS surface and higher SFE indicate better biocompatibility.
5. Wettability can be adjusted by the plasma parameters, which would enable the production of coatings with properties suitable for specific practical applications.
6. Among our test parameters, time of film deposition was the most influential factor on the film surface wettability.
7. Flaking of the thin films deposited at 30 mTorr for 30 min (i.e. poor quality deposition) due to poor chemical binding between film and metal and/or high internal stresses inside the deposited films.
8. Recorded higher (Z) modulus of film coating at lower tests frequency indicates better corrosion resistance to the metal substrate.
9. According to the effect of deposition parameters, the deposition process is more effective at working pressure of 50 mTorr for 30 minutes deposition time.

5. References

[1] D.M. Mattox, "Introduction", in *Handbook of Physical Vapor Deposition (PVD) Processing*, edited by D.M. Mattox, Albuquerque: William Andrew Publishing, 1998, pp. 29-55. doi: 10.1016/B978-081551422-0.50002-4

[2] X.Y. Liu, P.K. Chu and C.X. Ding, Surface modification of titanium, titanium alloys and related materials for biomedical applications, *Mater. Sci. Eng. R Rep.*, 47, 49–121 (2004). doi: 10.1016/j.mser.2004.11.001

[3] Z.H. Zhang, "Surface Modification by Plasma Polymerization and Application of Plasma Polymers as Biomaterials", Ph.D. Thesis, Johannes Gutenberg University Mainz, 2003, pp. 1-17.

[4] P.K. Chu. J.Y. Chen, L.P. Wang and N. Huang, Plasma-surface modification of biomaterials, *Mater. Sci. Eng. R Rep.*, 36**,** 143–206 (2002). doi: 10.1016/j.mser.2004.11.001

[5] P. Favia and R. d'Agostino, Plasma treatments and plasma deposition of polymers for biomedical applications, *Surf. Coat. Tech.* 98, 1102-1106 (1998). doi: 10.1016/S0257-8972(97)00285-5

[6] G. Szabó, L. Kovács, K. Vargha, J. Barabás and Z. Németh, A new advanced surface modification technique – titanium oxide ceramic surface implants: the background and long-term results, *J. Long Term Eff. Med. Implants*, 9 (3), 247-259 (1999). PMID: 10847966

[7] J.-C. Schauer, "PECVD-Deposition and Characterization of C-Si Thin Film Systems on Metals", Ph.D. Thesis, Ruhr University, 2007, pp.19-23.

[8] T. Lu, Y.Q. Qiao and X.Y. Liu, Surface modification of biomaterials using plasma immersion ion implantation and deposition, *Interface Focus*, 2, 325–336 (2012). doi: 10.1098/rsfs.2012.0003

[9] S.J. Bull, "Notes on Surface Engineering" (6 July 2000), Retrieved 20 July 2018, from University of Newcastle: https://www.staff.ncl.ac.uk/s.j.bull/SENotes.html.

[10] H.M. Abourayana, N.A. Zreiba and A.M. Elamin, Synthesis and Characterization of Plasma Polymerized Thin Films Deposited from Benzene and Hexamethyldisiloxane using (PECVD) Method, *International Journal of Chemical, Molecular, Nuclear, Materials and Metallurgical Engineering*, 5 (2), 117-123 (2011)

[11] H.M. Abourayana and D.P. Dowling, "Plasma Processing for Tailoring the Surface Properties of Polymers", in *Surface Energy*, edited by M. Aliofkhazraei, IntechOpen, 2015, pp. 123 -152. doi: 10.5772/60927

[12] C.S. Wong, R. Mongkolnavin, "Methods of Plasma Generation", in *Elements of Plasma Technology*, Singapore: SpringerNature, 2016, pp. 15-48.

[13] Y.A. Lebedev, "Microwave Discharges: Generation and Diagnostics", in *25th Summer School and International Symposium on the Physics of Ionized Gases – SPIG2010*, edited by L.Č. Popović and M. Kuraica, J. Phys.: Conf. Ser., 257, 012016 (2010). Doi: 10.1088/1742-6596/257/1/012016

[14] C.A. Destefani, E. Siores and A.B. Murphy, Generation of Microwave-Induced Plasmas in Automotive Exhaust Gas Mixtures Using Pulsed Microwave Energy, *J. Microw. Power Electromagn. Energy*, 38 (2), 95-101 (2003). doi: 10.1080/08327823.2003.11688491.

[15] J.R. Davis, "Overview of biomaterials and their use in medical devices" and "Metallic Materials", in *Handbook of Materials for Medical Devices*, edited by J.R. Davis, Materials Park Ohio: ASM International, 2003, pp. 1-11 & 21-50.

[16] F.J. Baldenebro-Lopez, C.D. Gomez-Esparza, R. Corral-Higuera, S.P. Arredondo-Rea, M.J. Pellegrini-Cervantes, J.E. Ledezma-Sillas, R. Martinez-Sanchez and J.M. Herrera-Ramirez, Influence of Size on the Microstructure and Mechanical Properties of an AISI 304L Stainless Steel—A Comparison between Bulk and Fibers, Materials, 8 (2), 451-461 (2015). doi: *10.3390/ma8020451*

[17] Medical Applications of Stainless Steel 304 (UNS S30400), *http://www.azom.com/article.aspx?ArticleID=6641*, 2013

[18] H.G. Kim, S.H. Ahn, J.G. Kim, S.J. Park and K.R. Lee, Electrochemical behavior of diamond-like carbon films for biomedical applications, *Thin Solid Films*, 475, 291-297 (2005). doi: *10.1016/j.tsf.2004.07.052*

[19] H.G. Kim, S.H. Ahn, J.G. Kim, S.J. Park and K.R. Lee, Corrosion performance of diamond-like carbon (DLC)-coated Ti alloy in the simulated body fluid environment, *Diamond Relat. Mater.*, 14 (1), 35-41 (2005). doi: *10.1016/j.diamond.2004.06.034*

[20] P. Qi, Y. Yang, S. Zhao, J. Wang, X. Li, Q. Tu, Z. Yang and N. Huang, Improvement of corrosion resistance and biocompatibility of biodegradable metallic vascular stent via plasma allylamine polymerized coating, Mater. Des., 96, 341-349 (2016). doi: *10.1016/j.matdes.2016.02.039*

[21] A Uma Maheswari, "Corrosion Resistance of 304L SS Spray Coated with Zirconia Nanoparticles", Materials Science and Engineering 149 (2016), doi: *10.1088/1757-899X/149/1/012068*

[22] L. Curkovic, H. O. Curkovic, S. Salopek, M. M. Renjo, S. Šegota; "Enhancement of corrosion protection of AISI 304 stainless steel by nanostructured sol–gel TiO films"; Corrosion Science 77, 176-184, (2013). *http://dx.doi.org/10.1016/j.corsci.2013.07.045*

[23] Werner Kern, Klaus K. Schuegraf, "Handbook of thin-film Deposition Processes and Techniques", Deposition Technologies and Applications Introduction and Overview, 2nd edition, California, (2002).

[24] A. Bogaerts, E. Neyts, R. Gijbels, Joost van der Mullen, "Gas discharge plasmas and their applications", Spectrochimica Acta Part B 57, 609–658, (2002).

[25] H. M. Abourayana, N. A. Zreiba, A. M. Elamin, "Polymerized Thin Films Deposited from Benzene and Hexamethyldisiloxane using (PECVD) Method", International Journal of Chemical, Molecular, Nuclear, Materials and Metallurgical Engineering Vol:5, No:2, (2011).

[26] G. R. Prasad, S. Daniels, D.C. Cameron, E. Tully, R. O'Kennedy; "Biocompatible Coatings with Silicon and Titanium Oxides Deposited by PECVD", 3rd Mikkeli International Industrial Coating Seminar, Mikkeli, Finland, (2006)

[27] L. E. Elzawi, N. A. Zreiba, A. M. Elamin " Investigation of Characteristics of a Polymer Film Deposited on Al-alloy Via Microwave Plasma", MSc. Thesis, 5-11, Libya (2013).

[28] J. Friedrich; "Plasma Polymerization Mechanism", Federal Institute for Materials Research and Testing, 12200 Berlin, Germany, (2011).

[29] B.D. Mistry, "A Handbook of Spectroscopic Data, Chemistry", (UV, IR, PMR, ^{13}CNMR and Mass Spectroscopy), India, (2009), 34-45.

SRJMET
Scientific Research Journal for Metal Engineering and Technologies
Volume No.02 Issue No. 01,pp:pp: 16-32
ISSN:399-2017
01. Aug .2021

The Effect Of Cold Rolling On Corrosion Performance For Plane Carbon Steel In 3.5wt% Sodium Chloride

M. Aboulsayan[1], A. Elbasir[2], Hesham.Mraied [3]

Materials engineering department, University of Tripoli, P. O. Box 13292, Tripoli-Libya
monderaboulsayan@gmail.com[1], aelbasir.55@gmail.com[2] , h.maried@uot.edu.ly[3]

ABSTRACT

Corrosion performance of cold rolled mild steel in 3.5% sodium chloride solutions was examined. The cold rolling was achieved by reducing the original thickness of as received steel plates to the levels of 10%, 20%, 30% and 40%. The impedance spectroscopy and the polarization electrochemical techniques were applied to determine the corrosion characteristics. Themeasured corrosion rates from these two different techniques are slightly different. The corrosion rates measured by the impedance technique are lower than those determined by the polarization technique. The difference in the corrosion rates is mainly attributed to the different polarization intervals in terms of cathodic and anodic potentials. Cold rolling of steel to 10٪, 20 ٪ and 40 ٪showed better corrosion performance than the as received steel sample. This was explained that each cold deformation created compact surface texture which has less preferable sites for corrosion. Whereas the cold rolling of steel to 30% reduced the corrosion resistance of the evaluated samples. This reduction in corrosion resistance was attributed to the subsurface defects such as inclusions converted to surface defects after the 30% cold rolling and became in contact with the corrosive media. Corrosion morphology shows localized corrosion of as received and each cold rolled samples. On the other hand, the 30 ٪cold rolled sample showed scattering of less size corrosion pits.

Keywords: Cold rolling, Mild steel, Impedance, Polarization, Corrosion.

1. Introduction.

Mild steel is used as the preferred construction material across industries and are considered the more economical option than the costly corrosion-resistant alloys in a wide range of applications, such as structural components, pipes, storage tanks and other functions (Kooliyat et al.,2019) (Renton et al., 2011). Cold deformation is always present in metal components due to fabrication techniques used in machining, bending and rolling. During cold deformation of a steel structure, changes of the original microstructure are generated based on the deformation level and hence the grains are divided and changes in their shapes and elongating in the direction of the applied stresses cause considerable changes in the important mechanical and corrosion properties of the material (Renton et al., 2011), (Zidani, et al., 2014), (Kain et al., 2004) (Mudali et al., 2002). It is well known that cold working of metals

generally introduces imperfections such as the substructures dislocation networks, twins, deformation bands, cell structures and emerging slip steps at the surface. Crystal defects, metallurgical structure, and composition affect the properties of the protective passive films, such as thickness, strength solubility, and porosity, and hence the susceptibility to localized breakdown and pitting of the alloy (Barbucci et al., 2002), (Mudali et al., 2002). Surface defects on the rolled steel are closely associated with the melting and casting process. Large-sized nonmetallic inclusions distributed on the subsurface of continuous casting are crushed, prolonged and exposed to the surface during the subsequent rolling process and they are apparently very detrimental to the surface quality (Deng et al., 2015). The defects generated on the surface during cold deformation of steel are more important affecting the surface quality than the deformation texture (Dwivedi et al., 2017). The objective of this study is to determine the corrosion characteristics of cold rolled mild steel samples after different levels of thickness reduction to 10٪, 20٪, 30٪, 40 ٪using the electrochemical corrosion techniques.

2.Experimental.

2.1 Materials.

The as received material is a cold rolled plate of mild steel (1020) having chemical composition (wt%) 0.2C, 0.3Mn, 0.04P, 0.05S, and the remainder is Fe. In addition to the as received condition, test samples were prepared from plates after receiving reduction in thickness by cold rolling to 10%, 20%, 30% and 40%. Figure 1(A) shows an example of test samples with surface area of 1cm^2 cut from the as received plate and utilized as working electrodes in the corrosion experiments. A copper wire was connected with each sample and then cold mounted to ensure the electric connection of the exposed surface with the rest of the corrosion cell during the immersion into the test media. The mounting is aimed to isolate the edges and to simplify the surface preparation using grit papers of several roughness i.e. 200, 400, 600, 800, 1000. The samples were cleaned with distilled water, acetone and dried before immersion into the test environment of 3.5 ٪NaCl solution.

2.2 Electrochemical Tests.

The electrochemical nature of as received and cold rolled steel samples were investigated by impedance spectroscopy and polarization techniques utilizing GAMRY electrochemical system. Figure 1 (B-D) shows the set-up of the electrochemical corrosion experiments involving the electrochemical corrosion cell consisting of a three electrode system has a reference electrode SCE, platinum auxiliary electrode (AE), steel working electrode (WE), Faraday cage and the impedance/potentiostate equipment. The three electrodes were submerged in the test environment of 3.5% sodium chloride as illustrated in the schematic of Figure 1(D) and kept until the Open Cycle Potential (OCP) was settled. Impedance signals (AC) were performed in the frequency range from 100 kHz to 0.1 Hz with amplitude of 10 mV at open circuit potential. The impedance outcomes and impedance modulus were collected from the Nyquist spectra circle and Bode graphs. The polarization

experiments were implemented immediately after the completion of each impedance test. The cathodic toward anodic polarizations were achieved using a scanning rate of 0.1mV/s. The corrosion rates the impedance and polarization graphs and data. From impedance data the corrosion current I_{corr} (µA/cm^2) with respect to the polarization resistance R_p (k ohm) was measured using Stern &Geary equation *(Stern & Geary 1957)* to determine the corrosion rates:

$$I_{corr} = B/R_pA \ldots\ldots\ldots\ldots \quad (1)$$

where B (Tafel slopes B = 26 mV) is usually assumed *(Alonso et al., 1988), (Rodriguez et al., 1995)* and A is the polarized area (cm^2).

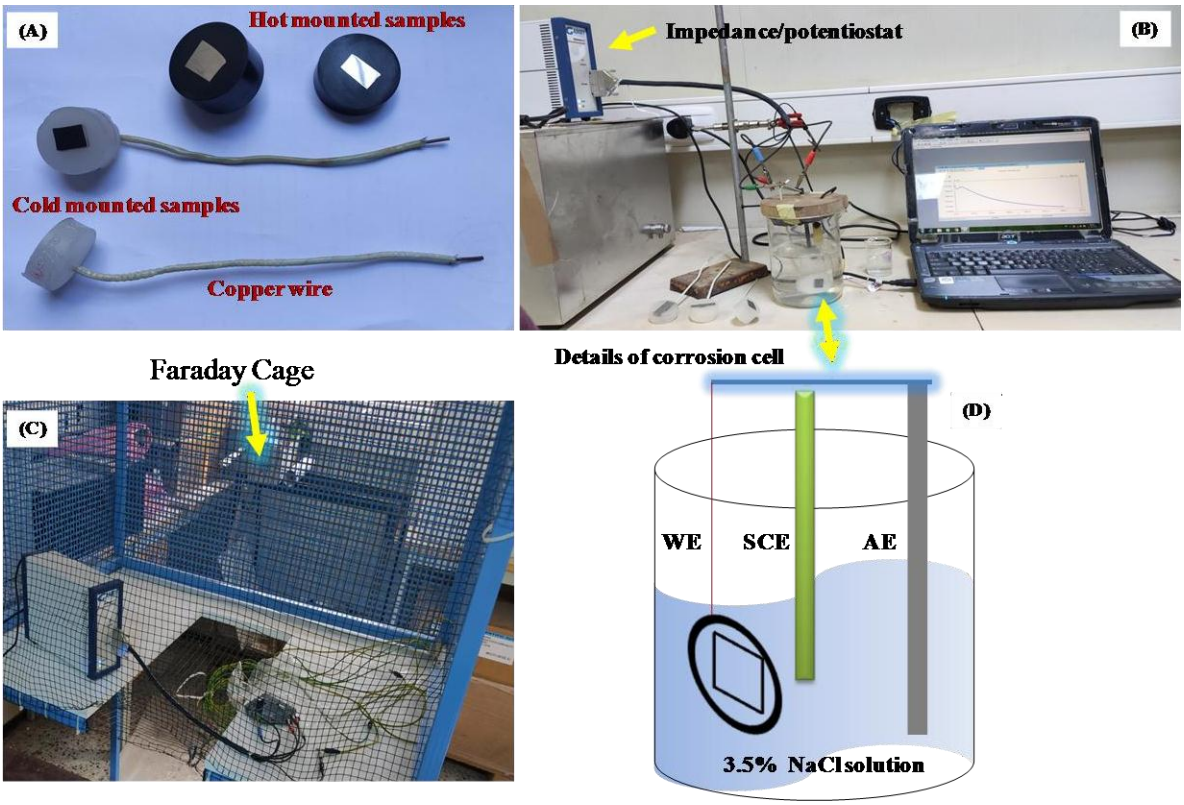

Figure 1. Experimental set-up for electrochemical experiment involving samples, impedancepotentiostat, faraday cage and corrosion cell electrodes.

3.Results and Discussion.

3.1 Microstructure.

The microstructure of the as received and 10%, 20%, 30% and 40% cold rolled mild steel samples are displayed in Figure 2. Figure 2(A) illustrates the microstructure of the as received steel. It shows that the dual microstructure is dominated by white ferrite grains matrix with less volume fraction of dark pearlite (ferrite pearlite) grains. Figure 2(B-D) shows the microstructure of 10, 20 and 30 ٪ cold rolled steels. The microstructure features indicate the decrease of the grain size

and elongation of the grain shape in the rolling direction as the reduction of thickness by cold rolling increased. The microstructure of the sample cold rolling to 40 % reduction in thickness is displayed in Figure 2(E). It reveals the most deformed microstructure in terms of disordered grains than the as received and 10%, 20%, 30% cold rolled samples. The microstructure of cold rolled steel has been examined by number of researchers. Tewary N. K et al. carried out Optical and TEM investigations and they observed that the cold rolled steels at 10-30 %exhibited dislocations, micro shear bands, deformation twins and the interaction of dislocations and twins. Deming Xu et al., showed that 10 %cold rolling to 316LN austenitic stainless steel caused dislocations gathered at the shear bands and twin boundaries. The authors found that cold rolling to 30 %resulted in more dislocations gathered with martensite phase.

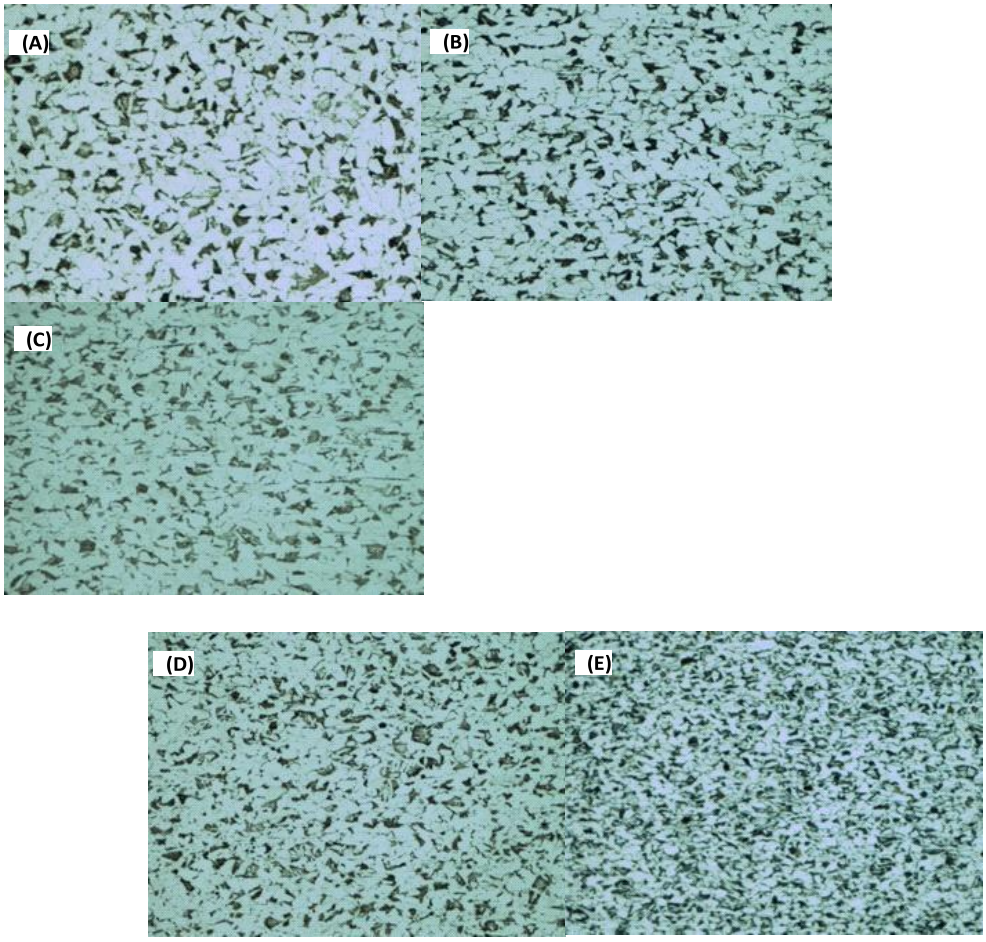

Figure 2. Microstructure 100 (µm) ; A) as received, B)- 10%, C)- 20%, D)-30 %and E)- 40 % coldrolled carbon steel samples.

3.2 Impedance Results.

Impedance measurements of as received and cold rolled steel samples immersed in 3.5 NaCl solutions were determined. The impedance spectrums of as received and 10 ٪cold rolled samples are shown in Figure 3. Figure 3(A) presents the Nyquist plots of as received and 10% cold rolled samples. It can be seen that the diameter of the capacitive semicircle of 10 ٪cold rolled sample is slightly bigger than the capacitive semicircle diameter of as received steel sample. Both samples revealed only one depressed capacitive semicircle shape features in the complex plane. This type of complex plane features is frequently explained as a mechanism of charge transfer on an inhomogeneous surface *(Haung et al., 2019)*. The Nyquist behaviour of 20% cold rolling sample is displayed in Figure 4(A). It shows that the diameter of the capacitive semicircle is increased by increasing the cold deformation to 20٪. Figure 5(A) shows the Nyquist performance of 30% cold rolled sample. At this level of deformation, a remarkable reduction of the capacitive semicircle diameter compared with the capacitive semicircle of as received, 10 and 20 ٪cold rolled samples. Deformation at 40% cold rolling improved the performance of the steel as indicated by Nyquist shape in Figure 6(A). It is apparently that the capacitive semicircle of 40 ٪ cold rolled sample is slightly reduced compared to 20 ٪cold rolled sample but still larger than the capacitive semicircle of as received, 10 and 30 ٪cold rolled samples. For further clarification, the capacitive semicircles of as received and cold rolled samples are combined in Figure 7. It can be seen that the graphs of the Nyquist impedance are not ideal semicircles, this type of performance is attributed to the frequency dispersion as reported by Hossain et al., 2006

The bode diagrams of as received and cold rolled samples are displayed in Figures (3B, 4B, 5B, 6B). Figure 3(B) shows the bode curves of the as received and 10 ٪cold rolled samples. Both samples have a zero-phase angle at the high frequency. The impedance of 10 ٪cold rolled sample is slightly higher than the impedance of the as received sample as can be seen from the impedance modulusat Y axes of the bode diagram. The modulus impedance of the as received steel sample is around 250Ω. Cold deformation of 10 ٪developed the impedance to 345Ω. Figure 4B indicated that the cold rolling to 20 ٪caused the highest shift of the impedance to 3.265KΩ. In contrary the increaseof cold rolling level to 30 ٪reduced the impedance of the steel to 180Ω. Thereafter, further cold deformation to 40 ٪enhanced the resistance to corrosion and increased the impedance to 1.214KΩ,as can be seen in Figure 6B. The 40% cold rolled sample has better impedance than 10 and 30 ٪cold rolled samples but it has less impedance than the 20 ٪cold rolled sample.
The increase in the Nyquist capacitive semicircles and the impedance modulus of the cold rolled samples to the levels of 10٪, 20 ٪and 40 ٪indicated the increase of the corrosion resistance. These observations can be attributed to the changes in the surface textures caused by the cold deformation (rolling) developed the charge transfer resistance and delayed the penetration of the corrosive elements toward the anodic sites and delayed the autocatalytic corrosion reactions to proceed. The

corrosion behaviour tendency of these cold deformed steels is in a good agreement with the findings of a number of researches cited in reference *(Renton e al., 2011)*.

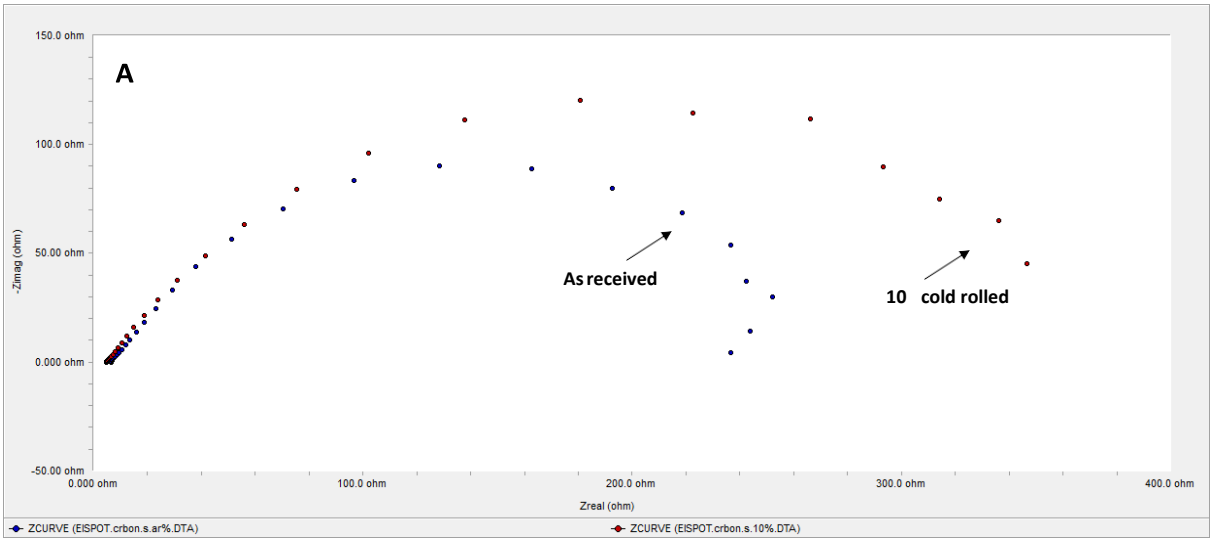

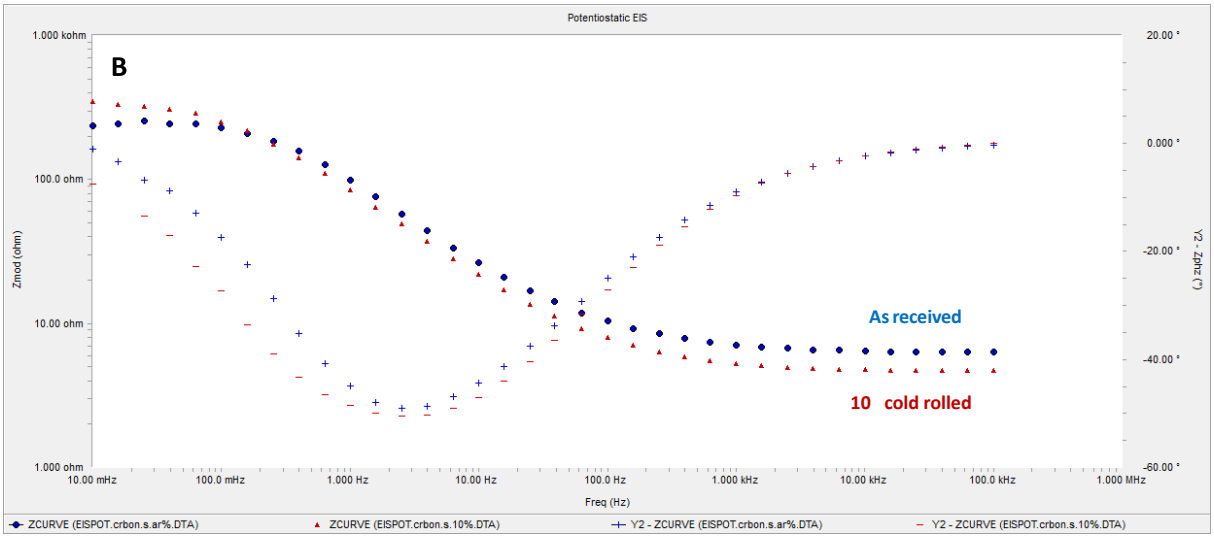

Figure 3. A)- Nyquist plot, B)- Bode plot of the as received and 10% cold rolled carbon steel samples.

SRJMET
Scientific Research Journal for Metal Engineering and Technologies
Volume No.02 Issue No. 01,pp:pp: 16-32
ISSN:399-2017
01. Aug .2021

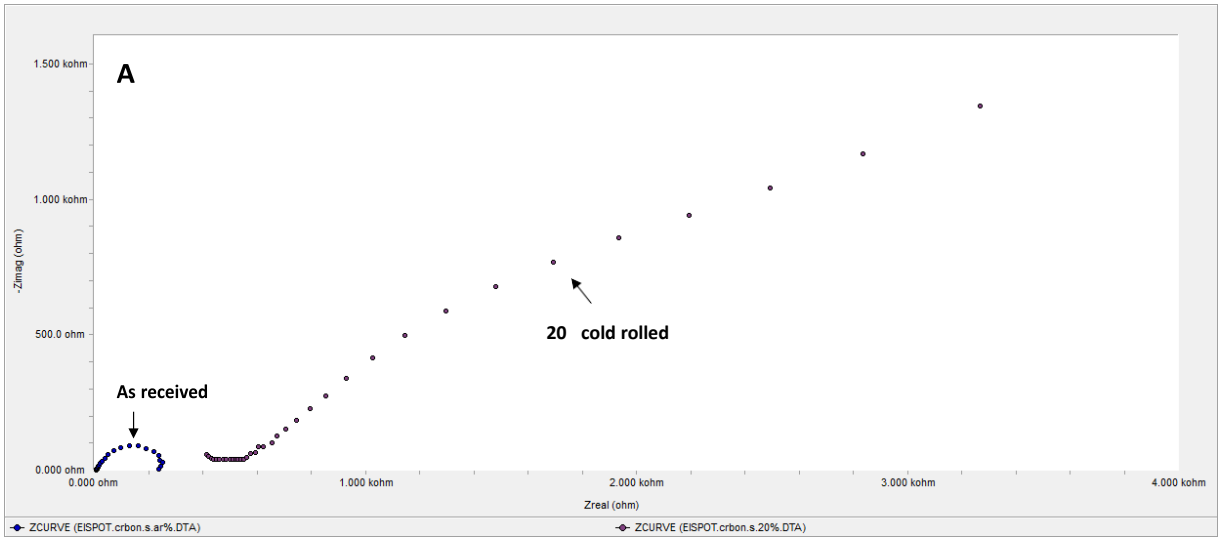

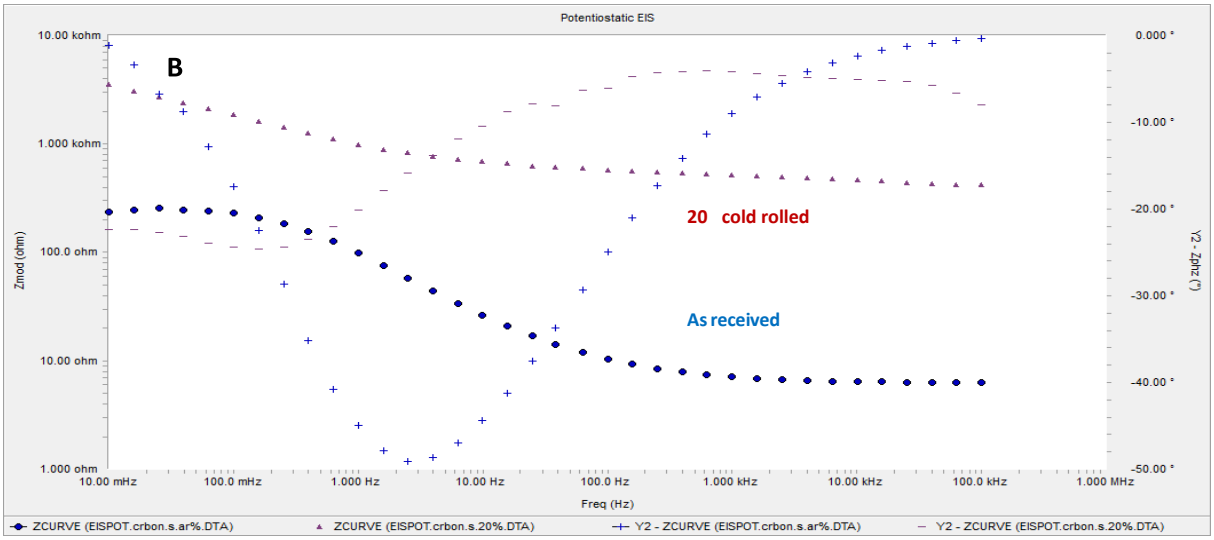

Figure 4. A)- Nyquist plot, B)- Bode plot of the as received and 20% cold rolled carbon steel samples.

SRJMET
Scientific Research Journal for Metal Engineering and Technologies
Volume No.02 Issue No. 01,pp:pp: 16-32
ISSN:399-2017
01. Aug .2021

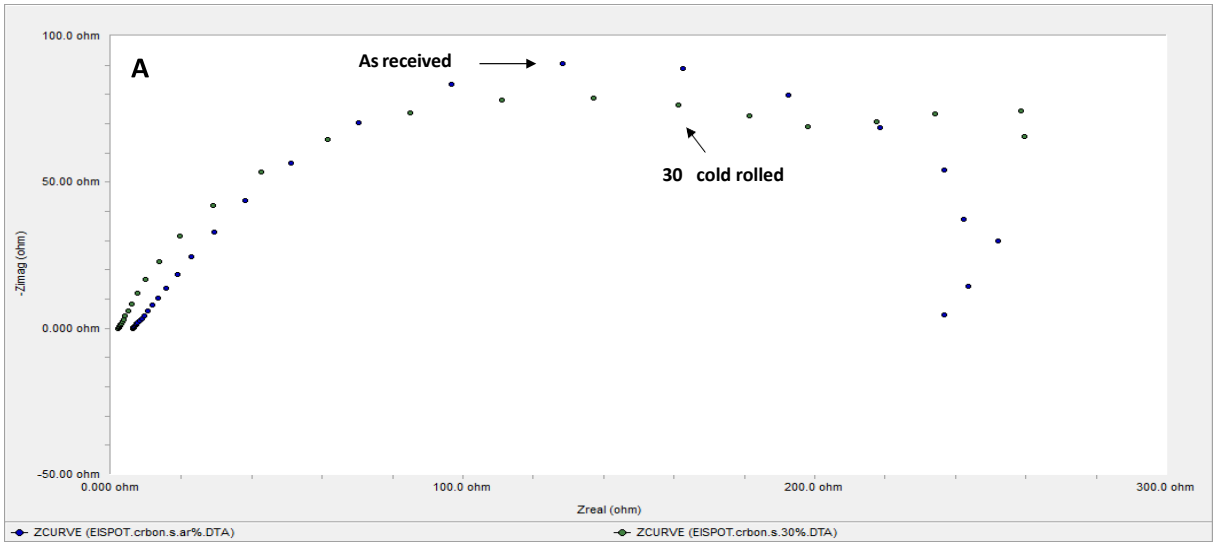

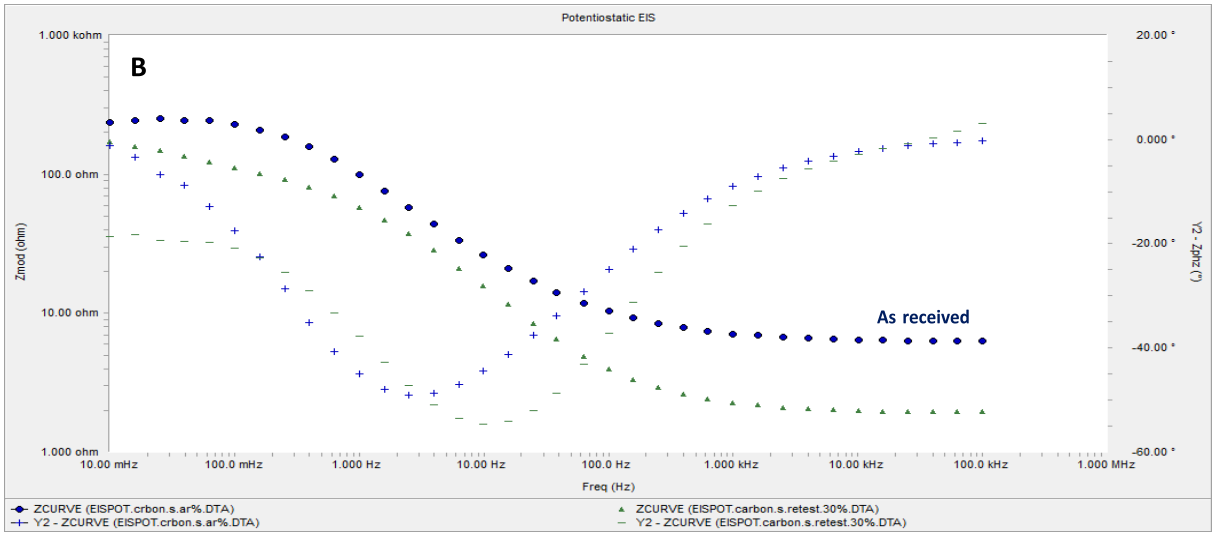

Figure 5. A)- Nyquist plot, B)- Bode plot of the as received and 30% cold rolled carbon steel samples

SRJMET
Scientific Research Journal for Metal Engineering and Technologies
Volume No.02 Issue No. 01,pp:pp: 16-32
ISSN:399-2017
01. Aug .2021

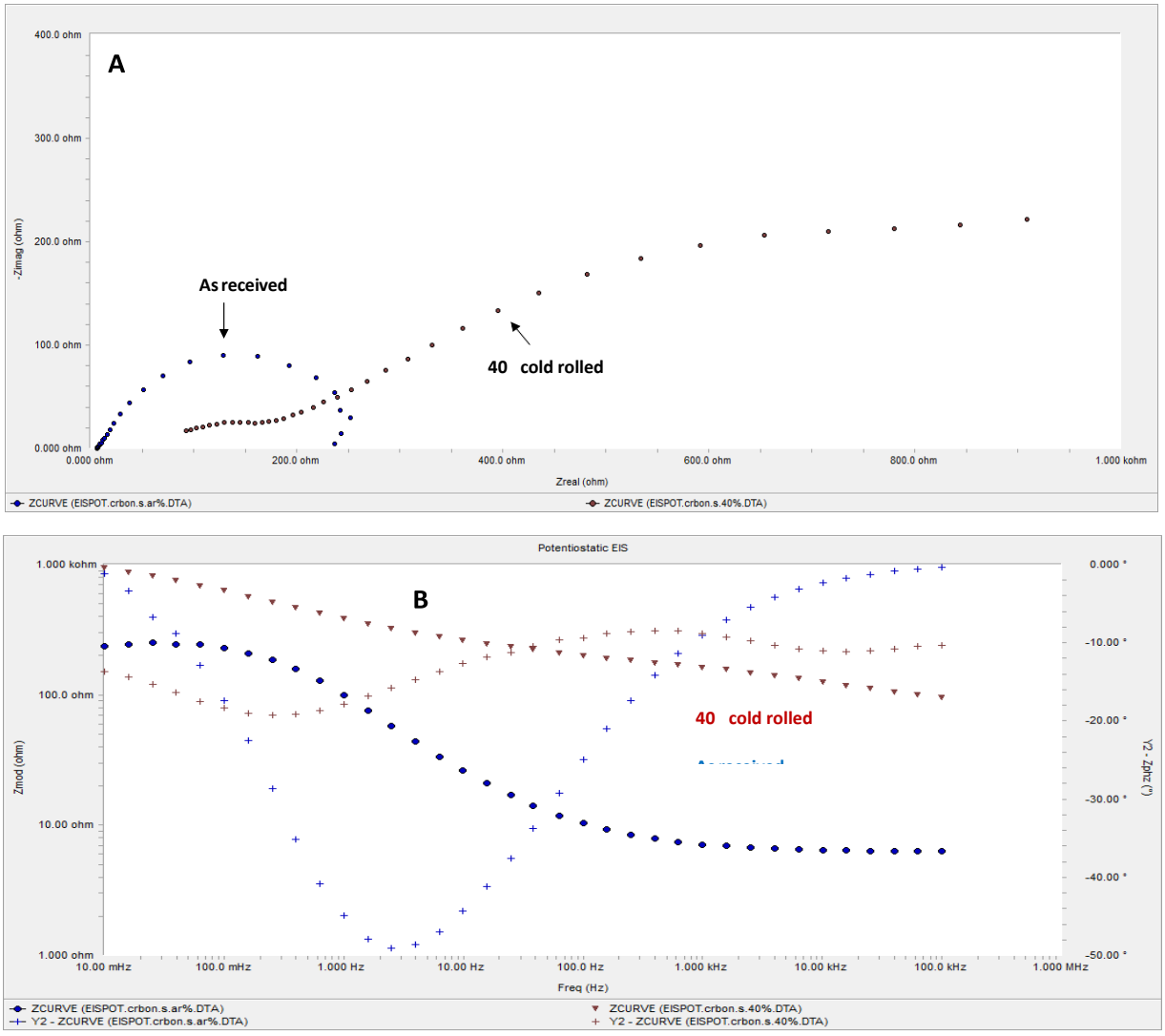

Figure 6. A)- Nyquist plot, B)- Bode plot of the as received and 40% cold rolled carbon steel samples.

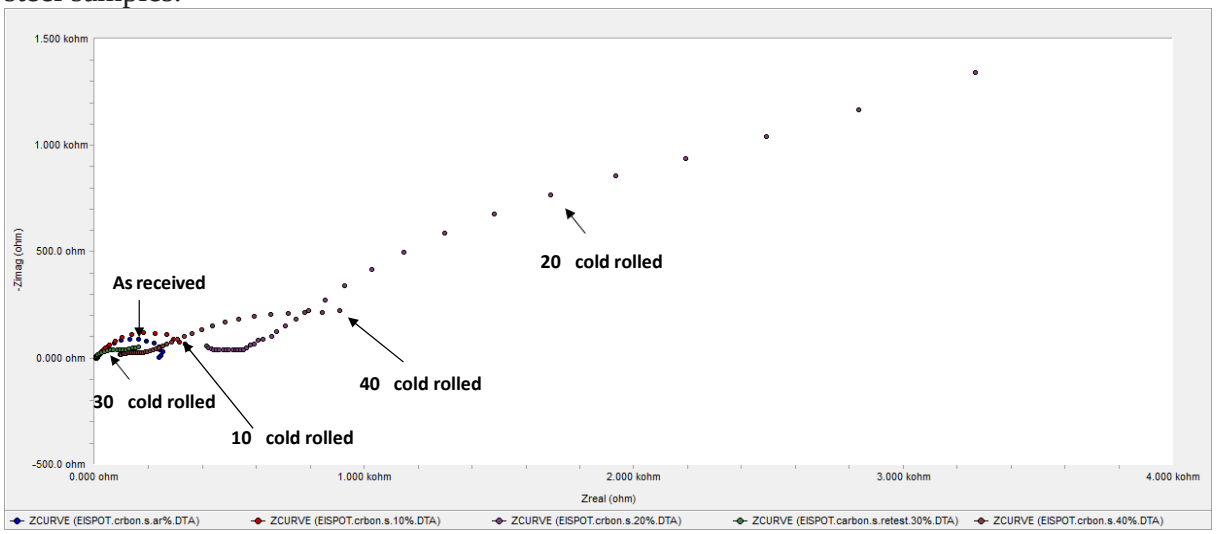

Figure 7. EIS Nyquist plot of the as received and 10, 20, 30, 40 % cold rolled carbon steel samples.

3.3 Polarization Results

The polarization information such as the free corrosion potential E_{corr}, corrosion current I_{corr} and corrosion rate of as received and cold rolled samples are displayed in Figures 8 & 9. The free corrosion potentials of the as received and 10% cold rolling samples are slightly changed from (-600 mV/SCE) to (-610 mV/SCE) respectively. Whereas the corrosion current of as received is 150µA/cm^2 but decreased to 100µA/cm^2 for the 10٪cold rolled sample. The reduction in the corrosion current can be attributed to the changes in the microstructure texture after 10 ٪cold rolling, consequently this microstructure delayed the corrosion process better than the microstructure of the as received sample.

The sample of 20 ٪cold rolling provided better corrosion resistance than the as received and the 10 ٪cold rolled samples. This improvement can be recognized from the corrosion current value decreased to around 8µA/cm^2 and the free corrosion potential value shifted to less negative to around - 180mV/SCE. This behaviour is attributed to the new microstructure geometry and to the surface textures caused by 20% cold rolling deformation. This new surface textures are considered to be more dense and there less anodic sites topography for corrosion process to proceed. The nature of surface textures and microstructure at 20 ٪thickness reduction may provide better resistance to the corrosive environment and prevented the corrosive elements to reach the critical concentration to proceed the corrosion process.

Increasing the cold rolling to 30% increased the corrosion current again to 130µA/cm^2 which is less than the corrosion current of the as received sample but higher than the corrosion current of 10٪, and 20 ٪cold rolled samples. The free corrosion potential of this sample decreased to -680mV/SCE. The increase of the corrosion current and the reduction of the free corrosion potential of this sample can be attribute to the impact of the conjunction of the subsurface defects such as the metallic inclusions with other cold rolling defects such as the slip bands and dislocations. Additionally, the cold rolling to 30 ٪caused the subsurface defects in direct contact with the corrosive environment, thus exposed these imperfections to the corrosive environment and created more corrosion preferential sites allowed the corrosion reactions to proceed.

Increasing the cold rolling to 40 ٪improved the corrosion resistance compared to the as received,

10% and 30% cold rolled samples but still less than the corrosion resistance of 20 ٪ cold rolled sample. The free corrosion potential is shifted to around -200mV/SCE and the corrosion current is reduced to around 32µA/cm^2. The improvement of the corrosion performance of this sample is explained by the compact surface texture, ultrafine grain size increased the grains boundaries in its texture geometry. The assumption is, higher deformation produced a microstructure with more flattened grains, closed up microstructure defects, increased compressive stresses and

increased the grain boundaries, therefore less possibility for the autocatalytic corrosion to proceed and hence slow down the corrosion of 40 ٪cold rolled sample compared with as received, 10 ٪and 30% cold rolled samples.

The corrosion data from the impedance as well as from the polarization are tabulated in Table 1 to find out the corrosion rate of the evaluated steels. The corrosion rate from the impedance results show that the 30% cold rolled sample has the highest corrosion rate followed by the as received sample. The corrosion rate decreased after cold rolling to 20%, 40% and 10% respectively. Whereas the corrosion rate from the polarization data shows that the as received samples has the highest corrosion rate followed by the 30% cold rolled samples. As an observationit can be concluded that the two techniques have slightly different corrosion rate values. The effect of cold rolling on corrosion resistance followed the trend of promote or detriment aspects depends on the surface textures obtained after deformation and on the type of evaluation technique. The overall observation from theses experiments indicated that the cold rolling at 30% is more detrimental on the corrosion resistance of the mild steels than the cold rolling at 10, 20 and 40%.

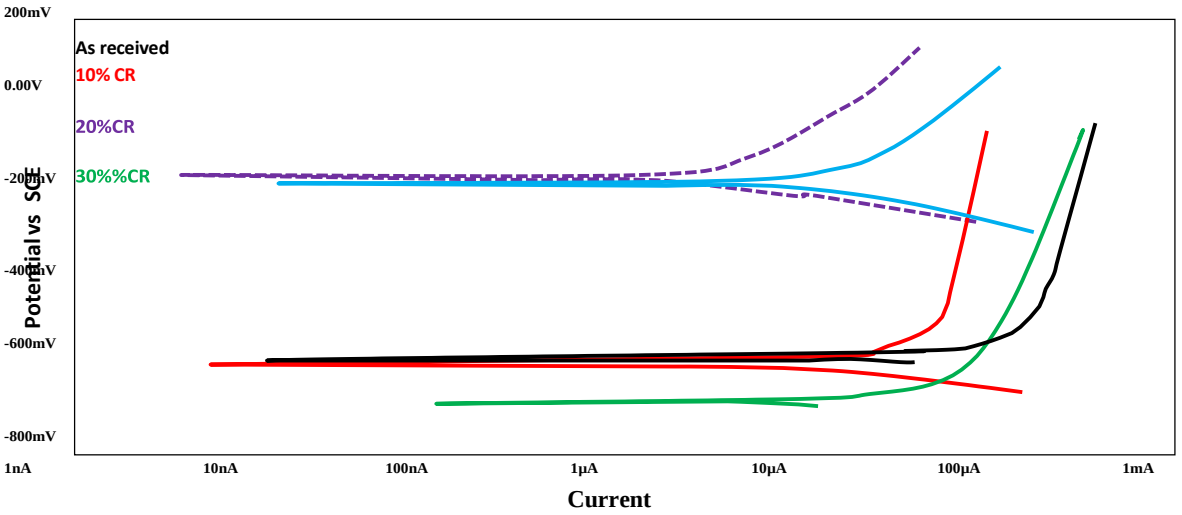

Figure 8. Representation of the polarization behaviour of as received and cold rolled carbon steelsamples.

SRJMET
Scientific Research Journal for Metal Engineering and Technologies
Volume No.02 Issue No. 01,pp:pp: 16-32
ISSN:399-2017
01. Aug .2021

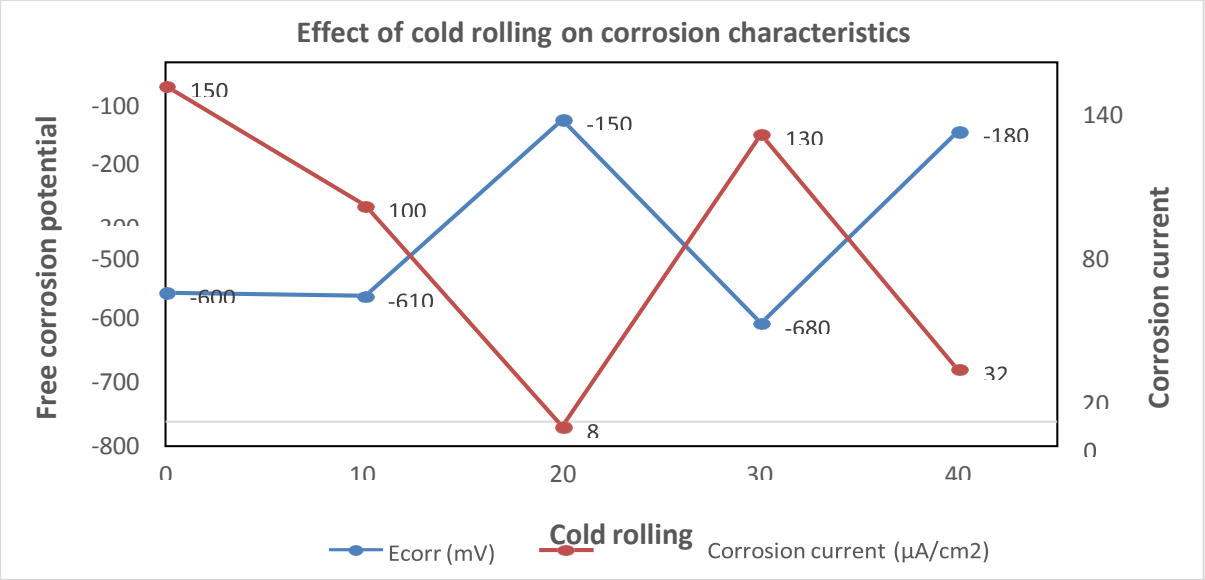

Figure 9. Corrosion data from polarization behaviour of as received with respect to four levels ofcold rolling levels at 10%, 20٪, 30 ٪and 40 ٪of carbon steel samples.

Table 1. Corrosion data from impedance and polarization techniques of cold rolled carbon steelsamples.

Steel condition (%)	EIS		Polarization		Corrosion rate (mm/y)=0.0032I_{corr}(EW)/D	
	R_p (KΩ)	I_{corr} (µA/cm^2)	E_{corr} (mV)	I_{corr} (µA/cm^2)	EIS	Polarization
As received	0.25	104	-600	150	2.36	3.48
10	0.345	75	-610	100	1.71	2.32
20	3.265	7.96	-180	8	0.18	0.18
30	0.180	144.4	-680	130	3.3	3.02
40	1.214	21.4	-180	32	0.48	0.74

3.1 Corrosion Morphology

Figure 10 shows the corrosion morphology of the as received and different levels of cold rolled steel samples after the impedance tests immediately followed by cyclic polarization experiments. The corrosion morphology of the as received and 10 ٪cold rolled steel samples are shown in Figure 10(A&B). It is obviously observed that small size of localized type of corrosion in the as received sample is more dominated on the surface. The size and the quantity of corrosion damage is affected by the degree of the cold deformation. Figure 10(C) shows the corrosion damage of 20 ٪cold rolled

sample, it has wider corrosion damage, this is can be attributed to the surface geometry let the corrosion damage to propagate in shallow shape rather than in deep corrosion shape, the shallow type of corrosion damage can be more rapidly passivated and recovered thus extended the breakdown of the 20% cold rolled sample. Figure 10(D) shows the corrosion morphology of 30 ٪cold rolled sample. It indicates the highest amount of pitting corrosion. The high cluster of pitting corrosion supported the electrochemical behaviour of this sample in the impedance and in the cyclic polarization behaviour because it shows the lowest impedance and lowest free corrosion potential but the highest corrosion current and corrosion rate. Figure 10(E) illustrates the corrosion morphology of 40 ٪cold rolled sample. It shows localized corrosion of moderate size of pitting. The corrosion damage morphology shows variations in the magnitude and size of pitting corrosion of cold worked steels and are in agreement with a number of published results explained that during the different cold working process, residual stresses are significantly introduced on the surface, which affects the localized corrosion resistance by increasing the number of active anodic sites on the surface *(Hossain et al., 2006) and (Hamdy et al., 2006*.

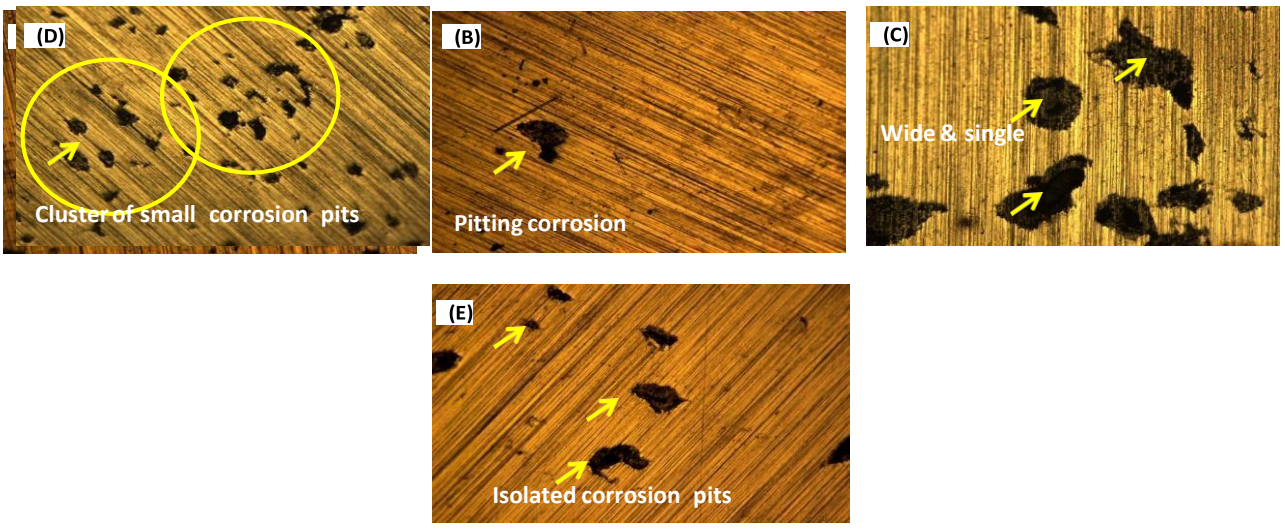

Figure 10. Corrosion morphology 20X; A) as received, B)- 10%, C)- 20٪, D)-30 ٪and E)-40٪ cold rolled carbon steel sample

Corrosion resistance of the cold rolled steel is significantly affected by the surface texture parameters such as shapes and spacing between the irregularities, for example deformation bands and dislocations as well as peaks and valleys of the texture groove.

In this study, the role of the microstructure changes such as grains shape and grains refinement due to the cold deformation on corrosion resistance are obviously observed. The corrosion behaviour versus the various levels of cold deformation of the investigated materials are in agreement with other published works summarized in references *(Renton et al., 2011), (Zhang et al,. 2013), (Wang et al., 2009)*. The surface energy has an important effect on the dissolution and the resistivity of the steel texture. On the other hand, cold plastic deformation of steel deliver additional energy and characteristics orientation of the grains causes reduction of corrosion resistance *(Kurc et al., 2010)*. It is generally accepted that the low energy grain boundaries are highly resistant to grain boundary corrosion *(Schuh et al., 2003), (Michiuchi et al., 2006)*, thus the corrosion rate will decrease as the degree of cold deformation increase.

The dense planes having a lower surface energy than loosely packed surfaces. This led to the anticipation that dense planes will dissolve at a relatively slow rate compared with the low dense planes or high surface energy planes. Although the increase of cold rolling deformation from 10٪, to 20 ٪and 40 % had improved the corrosion resistance of the test samples, this was not the case for 30% cold rolled sample, this sample showed the lowest corrosion rate. The results are in agreement with observations of the cold working of 316L stainless steel where cold rolling up to 20% enhanced the pitting resistance, and thereafter a sudden decrease in pitting resistance at 30% and 40% cold working *(Mudali et al., 2002)*.

The reduction of the corrosion resistance of the 30% cold rolled steel samples was attributedto the impact of the subsurface inclusions. The behaviour of the subsurface inclusions and some other imperfections are schematically presented in Figure 11. It shows the position of the subsurface inclusions before and after the rolling process where subsurface imperfections became as surface imperfections. They offered corrosion sites and decreased the resistance against corrosion. This explanation on the impact of the subsurface inclusions after they became surface inclusions on the corrosion resistance of 30 ٪cold rolled steel samples was also confirmed in the observations reported by *(Ramirez A. H. et al., 2014)* that at certain levels of cold rolling of 30% and 50%, the corrosion resistance of stainless steel decreased due the inclusions fragmentation and voids at the matrix-inclusion interface. The author found the high level of cold deformation at 70% improved the resistance to localized corrosion. The investigated mild steel showed that the deformation above 30% to 40% improved the corrosion resistance because cold rolling to 40% is beyond the depth of inclusions location through the steel thickness and integrated them into the new deformed textures of closely packed and dense microstructure and reduced their effectiveness to corrosion.

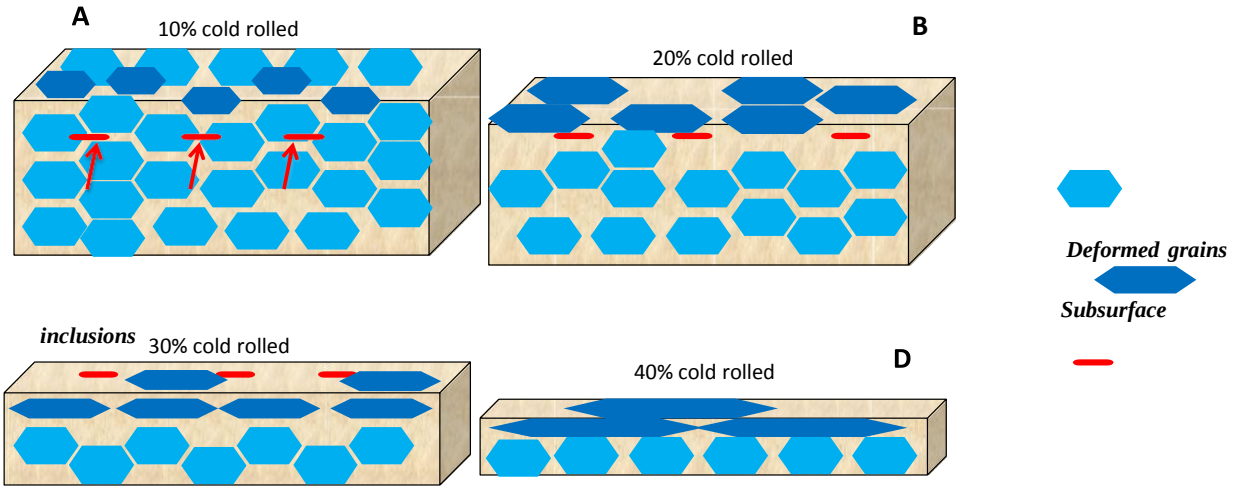

Figure 11. A schematic shows an assumption for the effect of the deformation on the grains and the subsurface inclusions with respect to thickness reduction.

4.CONCLUSIONS

The corrosion resistance of the cold rolled mild steel is influenced by the degree of the cold deformation.

The results of the impedance experiments are in agreement with the polarization results, both techniques showed that cold rolling to 10%, 20% and 40 ٪reduction in thickness improved the corrosion resistance.

The improvement of the corrosion resistance of these samples is explained by the presence of a compact and dense surface texture which delayed the corrosion process and hence delayed the breakdown of the alloy.

On the contrary, cold rolling to 30 ٪was not within this trend because the samples have the highest corrosion rate compared to other cold rolled samples. The high corrosion rate of 30% cold rolled steel samples than the other cold rolled samples is attributed to the detrimental effect of the surface texture and to the subsurface imperfections such inclusions which may converted to surface defects to work as active corrosion sites and reduced the corrosion resistance of 30 ٪cold rolled steel.

The corrosion morphology confirmed the presence of high number of corrosion pits of 30 ٪cold rolled sample than the other cold rolled samples.

References:

1. Alonso C., Andrade, C. & Gonzáles J.A. 1988, 'Relation between concrete resistivity and corrosion rate of the reinforcements in carbonated mortar made with several cement types', Cement and Concrete Research, 18(5), 687-698.

2. Barbucci, A., Cerisola, G. and Cabot, P.L., 2002. Effect of cold-working in the passive behavior of 304 stainless steel in sulfate media. Journal of the Electrochemical Society, 149(12), p.B534.

3. Dwivedi, D., Lepková, K. and Becker, T., 2017. Carbon steel corrosion: a review of key surface properties and characterization methods. RSC advances, 7(8), pp.4580-4610.

4. Hamdy, A.S., El-Shenawy, E. and El-Bitar, T., Electrochemical Impedance Spectroscopy Study of the Corrosion Behavior of Some Niobium Bearing Stainless Steels in 3.5% NaCl, International Journal of Electrochemical Science, Vol. 1, No.4, pp.171–180, 2006.

5. Hossain, S.A. and Almarshad, A.I., 2006. Inhibiting effect of thiosemicarbazide on cold rolled carbon steel. Corrosion engineering, science and technology, 41(1), pp.77-81.

6. Huang, W.H., Yen, H.W. and Lee, Y.L., 2019. Corrosion behavior and surface analysis of 690 MPa-grade offshore steels in chloride media. Journal of Materials Research and Technology, 8(1), pp.1476-1485.

7. Kain, V., Chandra, K., Adhe, K.N. and De, P.K., 2004. Effect of cold work on low-temperature sensitization behaviour of austenitic stainless steels. Journal of nuclear materials, 334(2-3), pp.115-132.

8. Kooliyat, R., Kakkassery, J.T., Raphael, V.P., Cheruvathur, S.V. and Paulson, B.M., 2019. Synthesis, Cyclic Voltammetric, Electrochemical, and Gravimetric Corrosion Inhibition Investigations of Schiff Base Derived from 5, 5- Dimethyl-1, 3-cyclohexanedione and 2-Aminophenol on Mild Steel in 1 M HCl and 0.5 M H2SO4. International Journal of Electrochemistry, 2019.

9. Kurc, A., Kciuk, M. and Basiaga, M., 2010. Influence of cold rolling on the corrosion resistance of austenitic steel. Journal of Achievements in Materials and Manufacturing Engineering, 38(2), pp.154-162.

10. Michiuchi, M., Kokawa, H., Wang, Z.J., Sato, Y.S. and Sakai, K., 2006. Twin-induced grain boundary engineering for 316 austenitic stainless steel. Acta materialia, 54(19), pp.5179-5184.

11. Mudali, U.K., Shankar, P., Ningshen, S., Dayal, R.K., Khatak, H.S. and Raj, B., 2002. On the pitting corrosion resistance of nitrogen alloyed cold worked austenitic stainless steels. Corrosion Science, 44(10), pp.2183-2198.

12. RAMIREZ, A.H., RAMIREZ, C.H. and Costa, I., 2014. Cold rolling effects on the microstructure and pitting resistance of the NBR ISO 5832-1 austenitic stainless steel. International Journal of Electrochemical Science.

13. Renton, N.C., Elhoud, A.M. and Deans, W.F., 2011. Effect of plastic deformation on the corrosion behavior of a super- duplex stainless steel. Journal of Materials Engineering and Performance, 20(3), pp.436-444.

14. Rodríguez J., Ortega L.M., Garcia A.M., Johansson L. & Petterson K. 1995, 'On-site corrosion measurements in concrete structures', Construction Repair, Nov./Dec., 27-30.

15. Saha, R. and Ray, R.K., 2008. Effects of severe cold rolling on the texture and grain boundary character of a Ti–Nb IF steel. Materials Letters, 62(2), pp.222-225.

16. Schuh, C.A., Kumar, M. and King, W.E., 2003. Analysis of grain boundary networks and their evolution during grain boundary engineering. Acta Materialia, 51(3), pp.687-700.

17. Stern M & Geary A.L. 1957, 'Electrochemical polarisation, I. A theoretical analysis of the shape of polarisation curves', J. Electrochem. Soc., 104, 56-63.

18. Takakuwa, O. and Soyama, H., 2014. Effect of residual stress on the corrosion behavior of austenitic stainless steel. Advances in chemical engineering and science, 5(01), p.62.

19. Tewary, N.K., Ghosh, S.K. and Chatterjee, S., 2015. Effect of Annealing on Microstructure and Mechanical Behaviour of Cold Rolled Low C, High Mn TWIP Steel. Int. J. Metall. Engg, 4, pp.12-23.

20. U. Kamachi Mudali, P. Shankar, S. Ningshen, Sanjay Rai and R. K. Dayal, Pitting corrosion studies on cold worked nitrogen-bearing austenitic stainless steels, 7th International symposium on electrochemical methods in corrosion research, EMCR2000, Budapest, Hungary-

21. Wang, Z.F., Li, P.H., Guan, Y., Chen, Q.F. and Pu, S.K., 2009. The corrosion resistance of ultra-low carbon bainitic steel. Corrosion science, 51(5), pp.954-961.

22. Xu, D., Wan, X., Yu, J., Xu, G. and Li, G., 2018. Effect of cold deformation on microstructures and mechanical properties of austenitic stainless steel. Metals, 8(7), p.522.

23. Yu, H., Deng, X., Wang, X., Ji, C. and Zhu, G., 2015. Characteristics of subsurface inclusions in deep-drawing steel slabs at high casting speed. Metallurgical Research & Technology, 112(6), p.608.

24. Zhang, Y., Liang, S., Javed, A. and Guan, D., 2013. Effect of pass deformation on microstructure, corrosion and electrochemical properties of aluminum alloy anodes for alkaline aluminum fuel cell applications. Metals and Materials International, 19(3), pp.555-561.

25. Zidani, M., Hadid, M.D., Messaoudi, S., Dendouga, F., Bessais, L., Baira, F., Bayarassou, M., Helbert, A.L., Mathon,

M.H. and Baudin, T., 2014. The Drawing Process of the Wires of Copper and Aluminium Evolution of the Microstructure and (Mechanical/Electrical) Properties. Publishing in Reult

Thomson.

SRJMET
Scientific Research Journal for Metal Engineering and Technologies
Volume No.02 Issue No. 01,pp:33-42
ISSN:399-2017
01. Aug .2021

Damage Detection in Beams Using Frequency Response Function Measurement

Mohammed Abuqunaydah[1], Mohamed Aljadi[2]
Mohamed Elmkharram[3], Muftah.M.Krer[4]
[1]m_ammar_t@yahoo.co.uk, [2]maljadi251@gmail.com, [3]m.mokharm@hvcc.ly
[4]mu.krer@uot.edu.ly
[1]High Vocational Libyan Centre of Casting ,[2] Advanced occupational centre of welding, High
[3]Vocational Libyan Centre of Casting,[4]University of Tripoli.
Tripoli -Libya

Abstract:

Damage detection in beams has been a vital subject for researchers recently and different techniques were used to detect damage in beams. However, one of the methods which is considered unique because of its feasibility and accuracy is the frequency response function measurement and analysis. In this researchGalrkin finite element model is established for a hollow circular beam and natural frequencies as well as modes were predicted. Experimental model analysis is used for validating the finite element model, results of finite element analysis agreed well with the experiments specially for the fundamental mode as higher modes showed some deviation due to different factors such as damping effect and hammer tip stiffness .Other experiments were carried out on damaged beam and compared to results of undamaged one. The first three frequencies showed deviation in frequency between the damaged and intact beam this happens due to decrease beam stiffness.

Keywords: Finite element model, Frequency response function, experimental modal analysis**.**

1. Introduction

Damages are generally the main reason of sudden structural failures during machine operations. The interest is in the ability to monitor a structure and detect damage at the earliest possible stage is pervasive throughout the mechanical, civil, and aerospace engineering communities. They may cause serious damage or injury; Damage to structure may be caused as a result of normal operations, accidents, temperature, corrosive deterioration or severe natural events such as earthquake and storms. Therefore, detecting damage in structural component at the earliest possible stage has become an important aspect in today's engineering. There are various techniques for damage detection. One of techniques in non-destruction detection and locating of

damage is the use of vibration response of structures. Damage identification methods are classified according to the type of measured data and technique to gather that data. They are mainly based upon the shifts in natural frequencies or dynamically measured flexibilities and changes in mode shapes. The importance of an early detection of cracks appear to be crucial for both safety and economic reasons because fatigue cracks are potential source of catastrophic Structural failure.

Damage identification methods are mainly based upon the shifts in natural frequencies or changes in mode. It is well known that when damage develops in a component it leads to changes in its vibration parameters, e.g. a reduction in the Stiffness and increase in the damping and a reduction in the natural frequency. Ratcliffe et al [1]. used non destructive vibration based techniques for locating delamination damage in a composite beam. Here the method makes use of the displacement eigenvector and converts it into a curvature mode shape. A damage detection index locates the delamination, irrespective of its position along the beam or depth within the beam. Wang et al [2]. developed a detection algorithm that uses frequency response function data measured prior and posterior to structural damage. From this data, a damage vector was extracted indicating both magnitude and location of damage. In order to account for model incompleteness an iterative version of the algorithm was introduced. Owolabi et al [3]. used natural frequency as the basic criterion for crack detection in simply supported and fixed-fixed beams. The method suggested has been extended to cantilever beams to check the capability and efficiency. Jai Kumar Sharma et al [4]. in the his work for cantilever beam, the natural frequencies and mode shapes were obtained through experimental, analytical and numerical method. The natural frequencies through experiments were determined using a laser vibrometer, for which the beam was fixed at one end and the free vibrations of the beam were excited using impact hammer. Thus obtained natural frequencies and mode shapes are compared with the results obtained through finite element modeling using ANSYS composite beam. Here the method makes use of the displacement eigenvector and converts it into a curvature mode shape. A damage detection index locates the delamination, irrespective of its position along the beam or depth within the beam. Neffati M. Werfalli and Mohamed Abugheneda [5]. focused in their work on the influence of structural damping on the natural frequencies of rectangular plates. The research extended previous work by testing rectangular plates with different boundary conditions

and comparing them with finite element analysis. Plots of mode shapes were compared and natural frequencies were tabulated in order to see the correlation between testing and analysis. They showed that fixation of clamped boundaries effects the resultant natural frequencies and modes in rectangular plates.

In this work damage in beams will be detected by the shift in natural frequencies extracted from frequency response function (FRF).

2- Mathematical Modelling.

Consider the assembly of two adjacent elements. As shown in figure (1) .The, beam's mass and stiffness are distributed evenly along the length of the longitdinal axis.

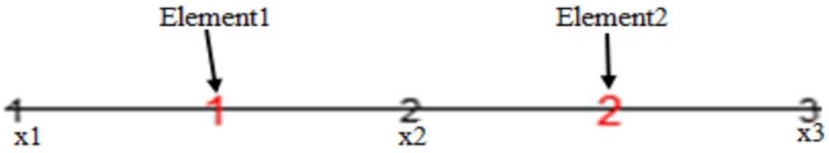

Figure (1) Free-body diagram of free beam.

In order to properly describe the behavior of the beam, a discrete system will be used. The consistent mass approach is based on beam theory

$\frac{d^2}{dx^2}\left(EI\frac{d^2w}{dx^2}\right) = f(x)$For 0<x<L

The element equation could be expressed as

$[K]\{a\} = \{F\}$

Where

$[K]$ Stiffness or property matrix.

$\{a\}$ Nodal displacement vector.

$\{F\}$ Nodal force vector.

L length of beam

EI is the modulus of rigidity of the beam.

Expressions for Kij could be determined for the beam element

$$K = \frac{EI}{l^3}\begin{bmatrix} 12 & 6l & -12 & 6l \\ 6l & 4l^2 & -6l & 2l^2 \\ -12 & -6l & 12 & -6l \\ 6l & 2l^2 & -6l & 4l^2 \end{bmatrix}$$

Using this vector and the definition of kinetic energy, the mass matrix for an element of the beam can be defined as.

$$M = \frac{ml}{420}\begin{bmatrix} 156 & 22l & 54 & -13l \\ 22l & 4l^2 & 13l & -3l^2 \\ 54 & 13l & 156 & -22l \\ -13l & -3l^2 & -22l & 4l^2 \end{bmatrix}$$

Where
M is the mass matrix.
m is mass per unit length.
The model that is developed consists of four elements with five nodes. Global matrices representing the system's mass and stiffness are 10 by 10 symmetric matrices, as shown in Figure (2).

Figure (2):Free-free beam

3-Experimental Work:

Test setup consists of an impact hammer that provides the excitation while the accelerometer records the response and transfers it to the signal conditioner which in turn sends data to Pulse software where data could be presented on time or frequency domain as requested. Data post processing was performed using Icats software and results were plotted for comparison.

Figure (3): Typical modal test set up.

Beam properties were tabulated in table (1)

Table 1: Physical properties for the beam

Beam property				
Young's modulus of elasticity(E) (N/m^2) $207 * 10^9$	Beam length(cm) 100	Internal diameter(mm) 38	Outer diameter(mm) 42	Density (ρ) (kg/m^3) 7850

3-1 Damage Scenarios

Damage in the beams consisted of a transverse crack on the surface of the steel beam. The crack was made with a vertical milling machine. The damage is located halfway of the beam (point 3) figure 4.

Figure (4): Beam with transverse damage.

4-Results and Discussion

Based on GALERKIN THEORY, the mass and stiffness matrices of model are constructed, and their parameters are show in matrix form.

$$\omega^2 = 10^{10}\begin{bmatrix} -.000 & 0 & 0 & 0 & 0 & 0 & 0 & 0 & 0 & 0 \\ 0 & .000 & 0 & 0 & 0 & 0 & 0 & 0 & 0 & 0 \\ 0 & 0 & .0003 & 0 & 0 & 0 & 0 & 0 & 0 & 0 \\ 0 & 0 & 0 & .0021 & 0 & 0 & 0 & 0 & 0 & 0 \\ 0 & 0 & 0 & 0 & .008 & 0 & 0 & 0 & 0 & 0 \\ 0 & 0 & 0 & 0 & 0 & .3635 & 0 & 0 & 0 & 0 \\ 0 & 0 & 0 & 0 & 0 & 0 & .8527 & 0 & 0 & 0 \\ 0 & 0 & 0 & 0 & 0 & 0 & 0 & 2.3668 & 0 & 0 \\ 0 & 0 & 0 & 0 & 0 & 0 & 0 & 0 & 8.2496 & 0 \\ 0 & 0 & 0 & 0 & 0 & 0 & 0 & 0 & 0 & 9.9123 \end{bmatrix} \quad M = \begin{bmatrix} .1832 & .0065 & .0634 & -.0038 & 0 & 0 & 0 & 0 & 0 & 0 \\ .0065 & .0003 & .0038 & -.0002 & 0 & 0 & 0 & 0 & 0 & 0 \\ .00634 & .0038 & .3664 & 0 & .0634 & -.0038 & 0 & 0 & 0 & 0 \\ -.0038 & -.0002 & 0 & .0006 & .0038 & -.0002 & 0 & 0 & 0 & 0 \\ 0 & 0 & .0634 & .0038 & .3664 & 0 & .0634 & -.0038 & 0 & 0 \\ 0 & 0 & -.0038 & -.0002 & 0 & .0006 & .0038 & -.0002 & 0 & 0 \\ 0 & 0 & 0 & 0 & .0634 & .0038 & .3664 & 0 & .0634 & -.0038 \\ 0 & 0 & 0 & 0 & -.0038 & -.0002 & 0 & .0006 & .0038 & -.0002 \\ 0 & 0 & 0 & 0 & 0 & 0 & .0634 & .0038 & .1832 & -.0065 \\ 0 & 0 & 0 & 0 & 0 & 0 & -.0038 & -.0002 & -.0065 & .0003 \end{bmatrix}$$

$$K = 10^7\begin{bmatrix} .8011 & .4005 & -.8011 & .4005 & 0 & 0 & 0 & 0 & 0 & 0 \\ .4005 & .2670 & -.4005 & .1335 & 0 & 0 & 0 & 0 & 0 & 0 \\ -.8011 & -.4005 & 1.6022 & 0 & -.8011 & .4005 & 0 & 0 & 0 & 0 \\ .4005 & .1335 & 0 & .5341 & -.4005 & .1335 & 0 & 0 & 0 & 0 \\ 0 & 0 & -.8011 & -.4005 & 1.6022 & 0 & -.8011 & .4005 & 0 & 0 \\ 0 & 0 & .4005 & .1335 & 0 & .5341 & -.4005 & .1335 & 0 & 0 \\ 0 & 0 & 0 & 0 & -.8011 & -.4005 & 1.6022 & 0 & -.8011 & .4005 \\ 0 & 0 & 0 & 0 & .4005 & .1335 & 0 & .5341 & -.4005 & .1335 \\ 0 & 0 & 0 & 0 & 0 & 0 & -.8011 & -.4005 & .8011 & -.4005 \\ 0 & 0 & 0 & 0 & 0 & 0 & .4005 & .1335 & -.4005 & .2670 \end{bmatrix} \quad \phi = \begin{bmatrix} .0345 & -1.4126 & 1.3836 & -1.2763 & .8946 & -1.0195 & 1.4960 & -1.6324 & 2.9154 & -2.7013 \\ -.3203 & .5195 & -1.7237 & 3.0394 & -3.3454 & 14.6060 & -27.9619 & 41.9605 & -106.7749 & 103.3223 \\ -.2857 & -.8931 & -.2016 & .9988 & -.9817 & .2709 & .1903 & -.6440 & .5441 & -.3113 \\ -.3203 & .5195 & -1.2926 & .6871 & 1.1102 & -17.9927 & 27.3986 & -18.9790 & -30.0350 & 38.5679 \\ -.6060 & -.3736 & -.9085 & -.000 & 1.2081 & -.000 & -.7116 & -.000 & .4453 & .000 \\ -.3203 & .5195 & -.000 & -1.8780 & -.000 & 20.9449 & -.000 & -43.2429 & -.000 & 29.2935 \\ -.9263 & .1458 & -.2016 & -.9988 & -.9817 & -.2709 & .1903 & .6440 & .5441 & .3113 \\ -.3203 & .5195 & 1.2926 & .6871 & -1.1102 & -17.9927 & -27.3986 & -18.9790 & 30.0350 & 38.5679 \\ -1.2466 & .6653 & 1.3836 & 1.2763 & .8946 & 1.0195 & 1.4960 & 1.6324 & 2.9154 & 2.7013 \\ -.3203 & .5195 & 1.7237 & 3.0394 & 3.3454 & 14.6060 & 27.9619 & 41.9605 & 106.7749 & 103.3223 \end{bmatrix}$$

According to the above results, analytical model based on modal analysis approach were utilized to evaluate the structural dynamic response of undamaged beam. This work have been done by writing MATLAB code program. It can be seen from all plots that the analytical and experimental (FRF) are identical with taking into consideration that the experimental work deals with real structure while in theoretical analysis deals with structure as ideal. The frequency response functions (FRF) of theoretical analysis is shown in figures (5) to (9) beside the experimental (FRF) results, and the values of natural frequencies are tabulated. These results are compared with finite element analysis, the error percentage is calculated using the following formula: -

$$e\% = \frac{f_{exp} - f_{theo}}{f_{exp}} * 100$$

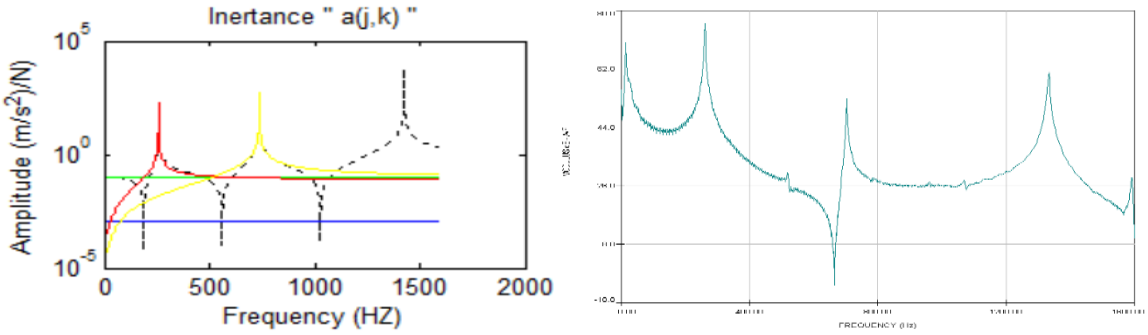

(a) Analytical FRF (b)Experimental FRF

Figure (5): Plot of analytical and experimental FRF at A_{31}

Table (2): Theoretical and experimental results of the undamaged beam of A_{31}

Natural frequencies (HZ)	Theoretically	Experimentally	*e* %
1st Natural frequency	258.5	260	0.5769
2nd Natural frequency	737.8	702	5.0997
3rd Natural frequency	1425.2	1330	7.1578

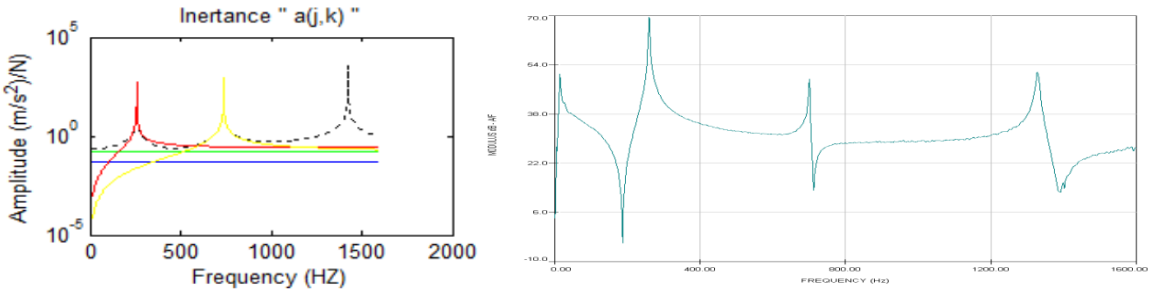

a) analytical FRF (b)Experimental FRF

Figure (6) Plot of analytical and experimental FRF at A_{32}

Table (3): Theoretical and experimental results of the undamaged beam of A_{32}

Natural frequencies (HZ)	Theoretically	Experimentally	e %
1st Natural frequency	258.5	259	0.1931
2nd Natural frequency	737.8	700	5.4
3rd Natural frequency	1425.2	1330	7.1578

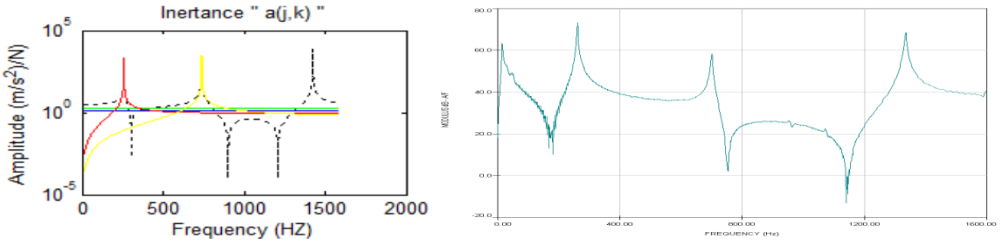

(a) Analytical FRF (b) Experimental FRF

Figure (7):Plot of analytical and experimental FRF at A_{33}

Table (4): Theoretical and experimental results of the undamaged beam of A_{33}

Natural frequencies (HZ)	Theoretically	Experimentally	e %
1st Natural frequency	258.5	260	0.5769
2nd Natural frequency	737.8	700	5.4
3rd Natural frequency	1425.2	1334	6.8365

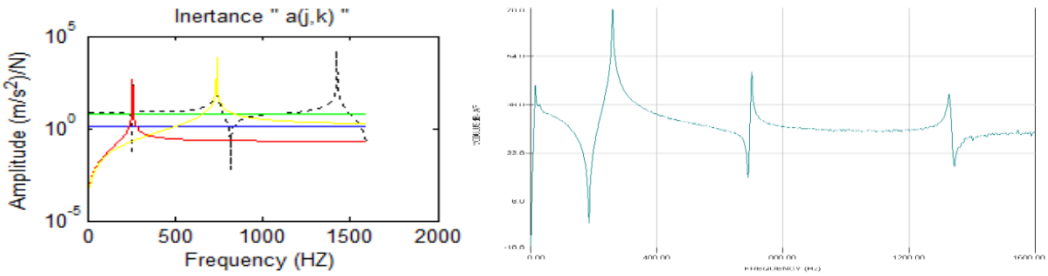

a) Analytical FRF (b) Experimental FRF

Figure (8): Plot of analytical and experimental FRF at A_{34}

Table (5): Theoretical and experimental results of the undamaged beam of A_{34}

Natural frequencies (HZ)	Theoretically	Experimentally	e %
1st Natural frequency	258.5	259	0.1931
2nd Natural frequency	737.8	700	5.4
3rd Natural frequency	1425.2	1330	7.1578

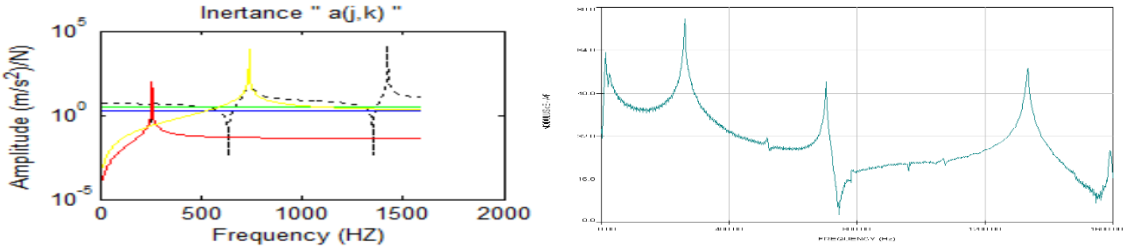

a) Analytical FRF (b) Experimental FRF

Figure (9): Plot of analytical and experimental FRF at A_{35}.

Table (6): Theoretical and experimental results of the undamaged beam of A_{35}

Natural frequencies (HZ)	Theoretically	Experimentally	e %
1st Natural frequency	258.5	260	0.5769
2nd Natural frequency	737.8	702	5.0997
3rd Natural frequency	1425.2	1330	7.1578

4-1 Beam With Damage:

Transverse damage was induced in the beam by making partial cut across the beam axis at location of point 3. Experiments were executed on transverse damaged beam, and the resulted (FRF) are plotted and merged with the (FRF) of undamaged beam. These plots are shown below in figures (10), (11), (12), (13) and (14).Objective function used in this researchpaper is based on the changes in experimental natural frequency.

$$\Delta f\% = \left| \frac{f_{undamage} - f_{damage}}{f_{undamage}} \right| * 100$$

The natural frequencies of the two conditions are summarized in tables (7) to (11).

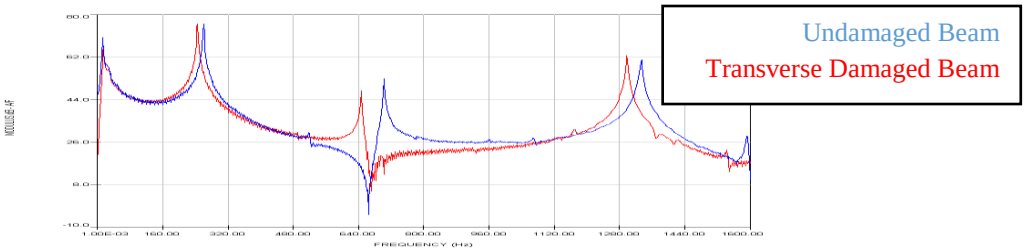

Figure (10): Experimental FRF of undamaged and transverse damage at A_{31}

Table (7): Experimental results of undamaged and transverse damaged beam at A_{31}

Natural frequencies (HZ)	Undamaged	Damage	Δf %
1st Natural frequency	260	244	6.1538
2nd Natural frequency	702	646	7.9772
3rd Natural frequency	1330	1300	2.2556

SRJMET
Scientific Research Journal for Metal Engineering and Technologies
Volume No.02 Issue No. 01,pp:33-42
ISSN:399-2017
01. Aug .2021

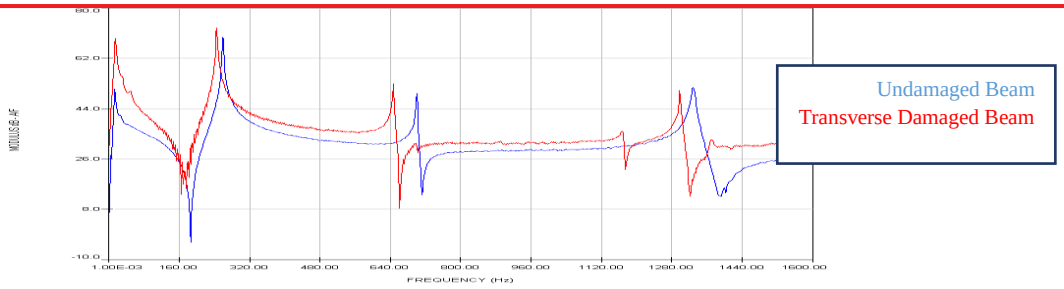

Figure (11): Experimental FRF of undamaged and transverse damage at A_{32}

Table (8): Experimental results of undamaged and transverse damaged beam at A_{32}

Natural frequencies (HZ)	Undamaged	Damage	Δf %
1st Natural frequency	259	244	5.7915
2nd Natural frequency	700	646	7.7142
3rd Natural frequency	1330	1300	2.2556

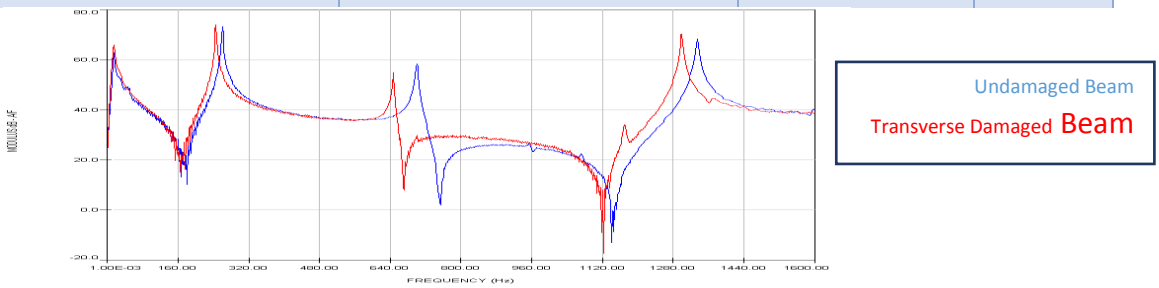

Figure (12) :Experimental FRF of undamaged and transverse damage at A_{33}

Table (9): Experimental results of undamaged and transverse damaged beam at A_{33}

Natural frequencies (HZ)	Undamaged	Damage	Δf %
1st Natural frequency	260	244	6.1538
2nd Natural frequency	700	646	7.7142
3rd Natural frequency	1334	1300	2.5487

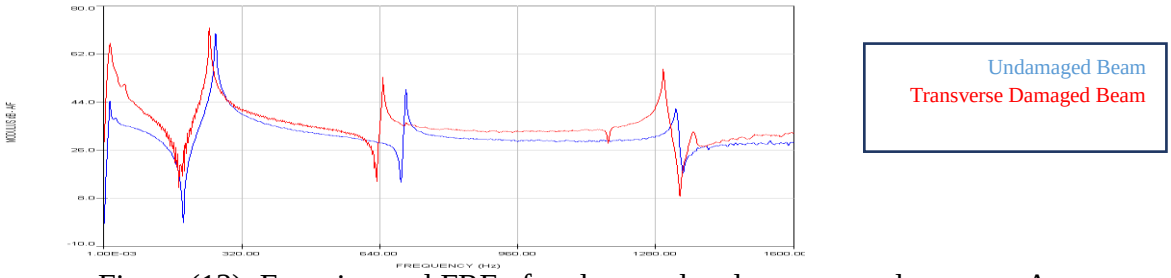

Figure (13): Experimental FRF of undamaged and transverse damage at A_{34}

Table (10): Experimental results of undamaged and transverse damaged beam at A_{34}

Natural frequencies (HZ)	Undamaged	Damage	Δf %
1st Natural frequency	259	246	5.0193
2nd Natural frequency	700	646	7.7142
3rd Natural frequency	1330	1300	2.2556

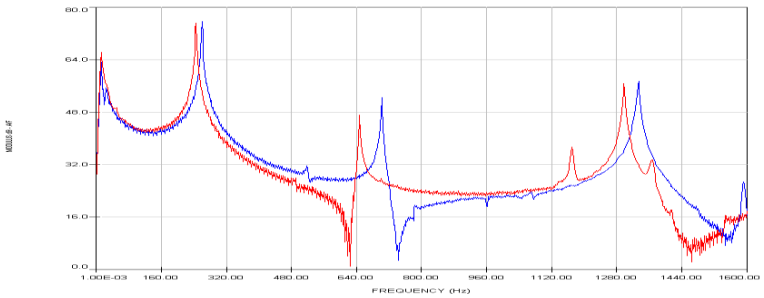

Figure (14) Experimental FRF of undamaged and transverse damage at A_{35}

Table (11): Experimental results of undamaged and transverse damaged beam at A_{35}

Natural frequencies (HZ)	Undamaged	Damage	Δf %
1st Natural frequency	260	246	6.1538
2nd Natural frequency	702	646	7.9772
3rd Natural frequency	1330	1300	2.2556

5- Conclusion

The following conclusions were draw from this study as follows:

- Finite element model for free-free beam is developed using Galrkin approach is validated by modal testing, where the results are compared and proved a very well agreement between the analytical and experimental work.
- There is a significant change (shift) in FRF for the damaged beam compared to the FRF for the intact beam due to decrease in beam bending stiffness.
- Change in spatial parameters of a structure due to a damage can be deducedby the shift in natural frequency and structure response.

References:

1. Ratcliffe, C. and Bagaria, W. (1998). Vibration Technique for Locating Delamination on a composite Beam. AIAA Journal, VOL.36, No. 6: PP. 1074-1077.
2. Wang, Z., Lin, R. M. and Lim, M. K. (1997). Structural Damage Detection Using Measured FRF Data. Computer Methods in Applied Mechanics and Engineering, VOL. 147:PP. 187-197.
3. G. M. Owolabi, A. S. J. Seamidas, R. Seshadri. (2003). Crack Detection in Beam Using Change in Frequencies and Amplitudes of Frequency Response Function, Journal of Sound and Vibration , VOL. 265,No.1:PP. 1-22.
4. Jai Kumar Sharma, Sandeep Kumar Parashar (2016). Experimental investigation using vibrometer and modal analysis of cantilever beam. International Journal of Innovative Research in Science and Engineering. VOL. 2. No: 04.
5. Neffat M. Werfalli and Mohamed Abugheneda. (2013). The effect of structural damping on natural frequencies of rectangular plates. Master thesis University of Tripoli.

SRJMET
Scientific Research Journal for Metal Engineering and Technologies
Volume No.02 Issue No. 01,pp:43-54
ISSN:399-2017
01. Aug .2021

Mechanisms of Corrosion Related Sulphate-Reducing-Bacteria and its Impact on Steel Structure

Osama Terfas[1], Rayan Tarek[2]

Department of Marine and Offshore Engineering, University of Tripoli

[1]O.Terfas@uot.edu.ly

Abstract:

Steel structure of oil tanks is one of engineering components susceptible to biocorrosion phenomenon associated with the microbiological activities that induced corrosion known as Microbiological induced corrosion (MIC). The bacteria most frequently associated with corrosion failure of steel are those generate sulphides and these are commonly called Sulphate-Reducing-Bacteria (SRB). The forms of corrosion promoted by the SRB are pitting, crevice, stress corrosion cracking, enhancement of corrosion fatigue, and hydrogen embrittlement. Consequently, corrosion progressing can deteriorate engineering materials and cause structure complete failure. Therefore, this paper discusses the mechanisms of biocorrosion in terms of SRB, and its effect on steel structures of oil storage tanks. To understand the causing of SRB, several mechanisms, causes, and effects on the steel structure are described. The study shows that environmental conditions preferred by SRB include zero dissolved oxygen, water and presence of soluble organic nutrients are available in oil content which assist the corrosion process to develop. It is shown that most cases of corrosion related to SRB are associated with a severe localized pitting attack, particularly on the bottom shell of oil storage tanks. This is due to the combined sulfate reduced with hydrogen resulting in chemical compounds such as hydrogen sulphide (H_2S) that react with the steel surface producing corrosion products such as ferrous sulphides or ferrous hydroxides, eventually causing metal loss in the form of pitting corrosion.

Keywords: biocorrosion, microbiological induced corrosion, sulphate-reducing-bacteria.

1. Introduction.

A wide range of bacteria can exist in all areas of oil production and storage facilities including the production plant, pipelines, water injection plant, reservoirs, and oil cargo tanks. Microorganisms tend to attach themselves to solid surfaces, colonize, proliferate, and form biofilms which may in turn produce an environment at the biofilm-metal interface radically different from the bulk environment in terms of pH, dissolved oxygen, organic and inorganic species. Since the biofilm tends to create nonuniform surface conditions, localized attack might start at some points on the surface leading to localized corrosion, usually in the form of pitting [1]. When microorganisms are involved in the corrosion of metals, the situation is complicated because microorganisms not only modify the near-surface environmental chemistry via microbial metabolism but also may interfere with the electrochemical processes occurring at the metal–environment interface [2].

Biocorrosion is an electrochemical process of metal dissolution initiated and accelerated by bacteria and other microorganisms through their metabolic activities [3]. The interaction of bacteria with the metal surface results in the formation of biofilms, which severely affects the kinetics of cathodic and anodic reactions in an electrochemical process [4]. Moreover, a synergistic interaction of microorganisms may occur, resulting in biofilms and metabolic products that enhance corrosion processes [5].

Microbiological induced corrosion (MIC) is an electrochemical mode of corrosion that results from microbes that react with the metal surface and lead to corrosion or influence other corrosion processes of metallic materials [6]. MIC is a form of corrosion produced by living organisms such as bacteria, algae or fungi. MIC encourages the increase in the corrosion rates of a preexisting surface corrosion due to the presence of bacteria that accelerate the rates of the anodic and cathodic corrosion reaction. The typical electrochemical corrosion depends on material, and corrosive medium, however, in MIC a third element that is the microorganisms in the biofilm form are involved[7].

The bacteria most frequently associated with corrosion of steel in oil, gas, shipping, and refineries are those generate sulphides called sulphate-reducing-bacteria (SRB) [8]. Under favorable conditions these bacteria can produce prodigious quantities of sulphide which can precipitate out as metal sulphides, dissolved sulphide or hydrogen sulphide. The SRB are particularly aggressive, generally causing pitting corrosion in the metal thickness, which results in high corrosion rates and costs [9]. In all cases, iron sulfides are characterized by strong cathodic effects on the hydrogen reduction reaction, causing an indirect increase in the corrosion rate. Thus, the biocorrosion process will be related to the breakdown of steel passivity by corrosive metabolic products generated by SRB. The biogenic sulfide production consequences include health, safety problems, environmental hazards, and the corrosion of structure.

The role of SRB in pitting corrosion of various metals and their alloys in both aquatic and terrestrial environments, under anoxic as well as oxygenated conditions,

has been confirmed [10]. Carbon steel and stainless steel are the most commonly exploited materials in the petroleum industry which are known to undergo from SRB-MIC. Several models have been proposed to explain the mechanisms by which SRB can influence the corrosion of steel.
reported extensive pitting of mild steel when ferrous and sulfide ions were being formed concurrently. When only sulfide was produced, corrosion rates first increased and then declined due to the formation of a protective FeS film. High levels of soluble iron prevented the formation of such protective layers. Demonstrated that high soluble iron levels could lead to high corrosion rates of piling grade carbon steel, and this was shown to be linked to a decrease in pH [13]. The hydrogenase of biofilm has been shown to be regulated by ferrous ions availability, offering yet another mechanism whereby corrosion may be affected, as assessed by [14]. Thus the influence of iron ions on SRB-influenced corrosion is a complex phenomenon; as mentioned in [15]. This complex interaction exists in carbon steel in a corrosive medium such as seawater and crude oil when the effects taking place among inorganic corrosion products and biofilms in a biologically conditioned interface. In the presence of sulfur species (either biogenic or abiotic), carbon steel firstly develops a film that later changes through several chemical and electrochemical paths to more stable iron sulfides [16]. Therefore, this paper aims to discuss several mechanisms of one of the most common type of microbiological corrosion encountered in oil industry, that is sulphate-reducing-bacteria (SRB), as well as its impact on steel structures of crude oil tanks.

2. Mechanisms of Sulphate-Reducing-Bacteria.

The biofilm formation is an essential step in the Microbiological induced corrosion (MIC). The formation of the biofilm begins with the adherence of bacteria to a metal surface by the extracellular polymeric substances (EPS), which made of polysaccharides and proteins[17]. Figure 1 shows steps of biofilm formation. Once a mature biofilm has been established on a surface, it actively propagates and eventually covers the entire surface. The mechanisms of propagation in mature biofilms are more complex than those of initial attachment. Microorganisms such as SRB and products of their metabolic activities including enzymes, exopolymers, organic and inorganic acids, as well as volatile compounds such as ammonia or hydrogen sulfide are responsible for biocorrosion processes that occur on metal surfaces. Thus, affecting the cathodic and anodic reactions, and altering electrochemistry at the biofilm-metal interface.

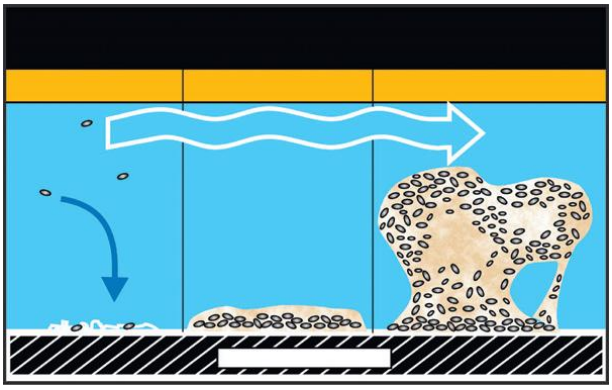

Figure 1: Steps of biofilm formation[17].

There are a number of mechanisms associated with this form of corrosion. However, most of them take the form of pits that form underneath colonies of living organic matter and mineral and biodeposits. The mechanism of biofilm creates a protective environment where conditions can become quite corrosive and corrosion is accelerated. Biofilms mediate interactions between metal surfaces and the liquid environment, leading to major modifications of the metal–solution interface by drastically changing the types and concentrations of ions, pH, and oxygen levels. The importance of biofilm is driven from the fact that it represents the predominant form of life of bacteria in natural environment[18]. In other words, the biofilm is the consequence of the development of microbial communities on submerged surfaces in aqueous environments. They usually grow as a general phenomenon that can be observed in almost all media, and at a temperature range between 25°C to 60°C and in almost all ranges of PH from 4 to 9.5.

One mechanism considers oxygen depletion where differential aeration cells are formed as shown in Fig. 2. In this mechanism, non-uniform colonies of biofilm result in the formation of differential aeration cells where areas under respiring colonies are depleted of oxygen relative to surrounding noncolonized areas. Having different oxygen concentrations at two locations on a metal surface causes a difference in electrical potential, where the areas under the respiring colonies become anodic and the surrounding areas become cathodic[19]-[20]. This accelerates the electrochemical process, consequently results pitting corrosion. Features of SRB-influenced corrosion are hydrogen sulfide (rotten egg smell), blackening of waters, and black deposits.

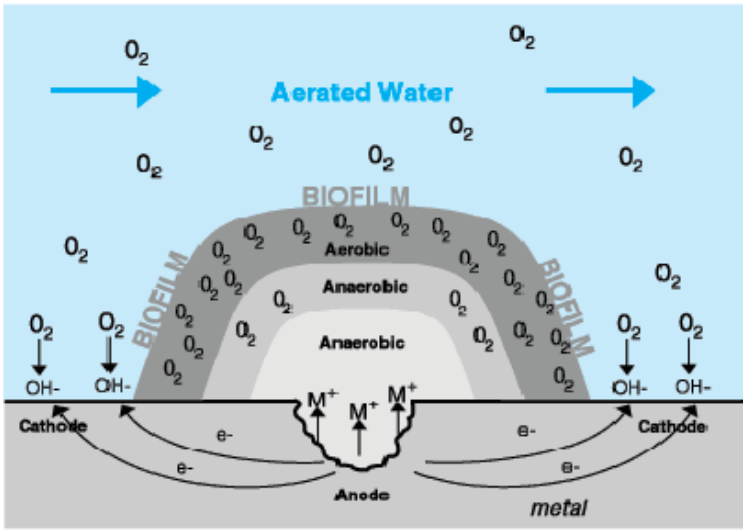

Figure 2: Pitting initiation on the metal surface beneath the biofilm[19].

SRJMET
Scientific Research Journal for Metal Engineering and Technologies
Volume No.02 Issue No. 01,pp:43-54
ISSN:399-2017
01. Aug .2021

The well-known cathodic polarization theory is the most applicable explanation whereby protons may act as an electron acceptor at the cathode in the absence of oxygen. The typical reactions of this theory are[21]:

1. Metal: Anodic reaction $4Fe \rightarrow 4Fe^{2+} + 8e^-$
2. Solution: Cathodic reaction $8H^+ + 8e^- \rightarrow 8H+4H_2$
3. Cathodic Reaction: water dissociation $8H_2O \rightarrow 8H^+ + 8OH^-$
4. Micro-Organism:$SO_4^{2-} + 4H_2 \rightarrow H_2S- + 2H_2O+2OH^-$ (Microbial Depolarization).
5. $Fe^{2+} + H_2S \rightarrow FeS$ (Corrosion Products) $+ 2H^+$
6. $3Fe^{2+} + 6OH^- \rightarrow 3Fe(OH)_2$ (Corrosion Products)
7. $4Fe + SO_4^{2-} + 4H_2O \rightarrow 3Fe(OH)_2 + FeS + 2OH^-$ (Overall Reaction).

The schematic process of corrosion of ferrous metal due to SRB by the cathodic depolarization theory is shown in Fig 3. At the cathodic site, reducing agents designated as [H] from the iron flow to the bacteria and are used for reduction of sulfate $(So_4)^{2-}$ to sulfide (H_2S). At the anodic site, only one fourth of the dissolved Fe^{2+} reacts with H_2S to form FeS. In the presence of CO_2 and bicarbonate as common in marine environments, the remaining Fe precipitates $FeCO_3$, in the absence of bicarbonate the more soluble $Fe(OH)_2$ is formed, the total reaction of corrosion is as follows:

$$4Fe + SO_4^{2-} + 3HCO_3^- + 5H^+ \Rightarrow FeS + 3FeCO_3 + 4H_2O$$

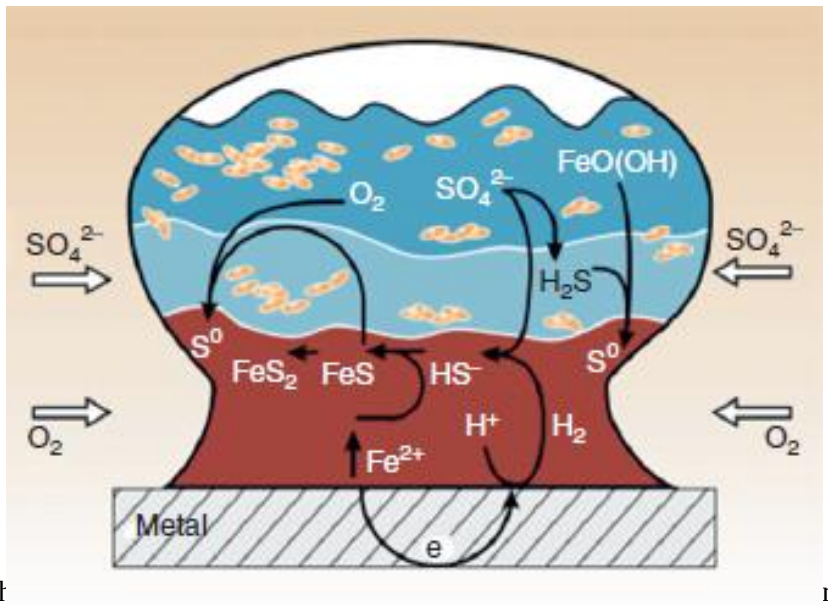

Figure 3: Th rrosion based on cathodic depolarization theory[22].

Another biocorrosion mechanism is based on the products of bacterial metabolism. In this process, the sulfate-reducing bacteria (SRB) derive their energy by oxidizing organic nutrients or molecular hydrogen (H_2) reducing (SO_4) to (H_2S). SRB's fundamentally are anaerobic microorganisms generally found in anoxic environments, such as soil sediment, oil fields and the anaerobic reactors used in wastewater treatment [20]. This means that these bacteria do not require oxygen for growth and activity, instead they use Sulfate to proceed the reduction process. The main characteristic of SRB is the use of a sulphate ion as the final electron acceptor in their bioenergetic process. The sulphate ions reduced to sulphide ions may present in three forms: H_2S (soluble), HS^- and $S2^-$, depending on the pH of the environment. Bacteria can produce aggressive metabolites, such as organic or inorganic acids. An alternative mechanism considers the formation of an iron/iron sulphide galvanic cell, in which the iron sulphides formed by the precipitation of the biogenic sulphide with ferrous ions act as sites for the reduction of H+ ions to molecular hydrogen, enhancing the corrosion [23, 24].

The SRB can act as a catalyst in the reduction reaction of sulfate to sulfide. It means they are able to make severe corrosion of metals in a water system by producing enzymes, which can accelerate the reduction of sulphate compounds to H2S. However, to occur this reduction, three components namely SRB, sulphates, free electrons as an external energy source must be present and the water temperature must be less than approximately 65°C. Acids produced by bacteria accelerate corrosion by dissolving oxides (the passive film) from the metal surface and accelerating the cathodic reaction rate.

3.Impact of SRB on Steel Structure

Biofilm detachment might facilitate the removal of inorganic passive layers, resulting in a patchy distribution of the biofilm. Stalked ciliates observed as the predominant biofouling species can facilitate passive layer detachment. Most cases of SRB-corrosion are observed to be associated with localized pitting, and changes in metal surface characteristics of mild steel [23], as shown in Figures 4 and 5, respectively.

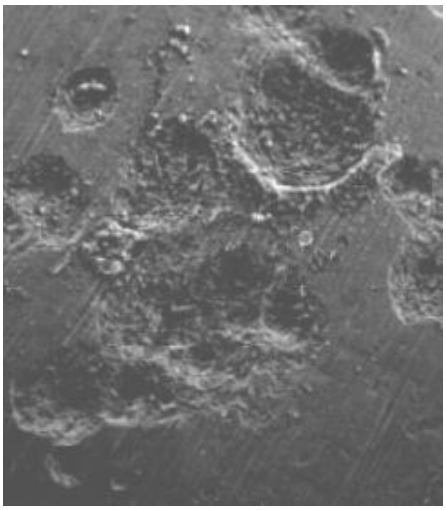

Figure 4: SEM graph of mild steel surface attacked by pitting corrosion due to SRB [23].

Figure 5: Scanning electron micrograph for mild-steel after the removal of the biofilm of SRB[23].

Figure 6 shows the scanning electron micrograph of a steel surface covered by sulfate-reducing biofilm and corrosion products, and discontinuity that possibly leads to pit formation due to the action of microorganisms embedded in the biofilm. Figure 7 shows a localized pitting corrosion with size of 20 μm approximately for carbon steel coupon exposed to the SRB. Figure 8 shows pitting corrosion on API 5L X-70 steel coupon after exposure to SRB activity, which proves the SRB could have a catastrophic effect on metallic structures [26].

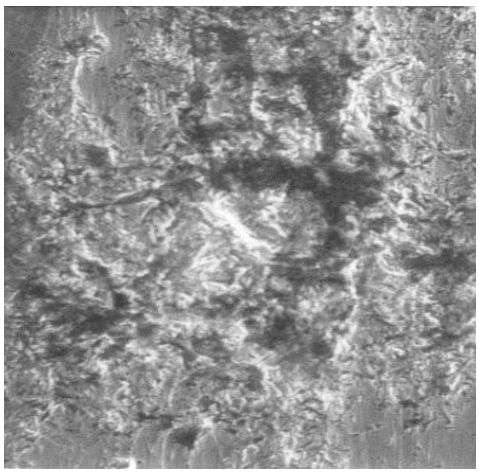

Figure 6: Biofilm and corrosion products over a steel surface[20].

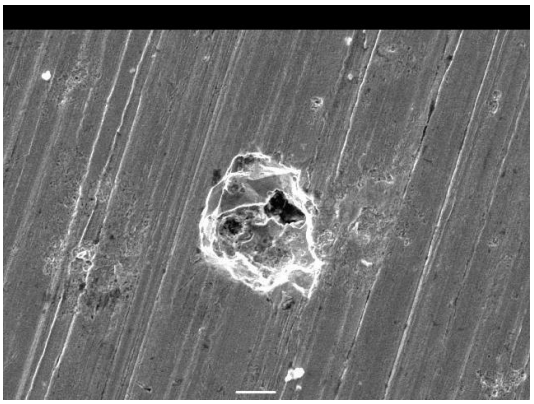

Figure 7: SEM micrograph of the morphology of the corrosion for SRB[25] .

SRJMET
Scientific Research Journal for Metal Engineering and Technologies
Volume No.02 Issue No. 01,pp:43-54
ISSN:399-2017
01. Aug .2021

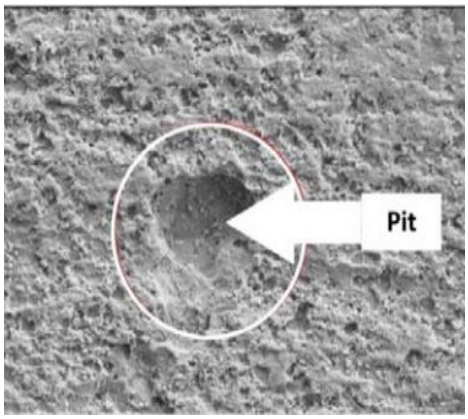

Figure 8: Pitting corrosion on API 5L X-70 steel coupon after exposure to SRB activity.

The environmental conditions preferred by SRB include zero dissolved oxygen, water and presence of soluble organic nutrients exist in oil tanks assist the corrosion pit to develop. Pitting corrosion in crude oil tanks contaminated with sulphate reducing bacteria (SRB) is caused when substantial populations of microorganisms inhabit the tank and create the conditions necessary for SRB proliferation. Aerobic micro-organisms use up oxygen and the oxygen deficient zone formed is anodic in relation to adjacent relatively oxygen rich zones thus causing anodic corrosion pits to develop. Temperatures above ambient suit most SRB and they are known to inhabit seawater and the produced water associated with crude oil from reservoirs where the necessary nutrients for their growth may be found.

Figure 9 shows blistering and coating failure on the bottom steel plate as the initiation process for the SRB corrosion to occur in a floating crude oil tank. Due to the presence of the SRB activity taking place on the exposed metal surface at sites where bottom plate coating failure became in direct contact with oil, and residual water, the SRB-metal interactions process began leading to corrosion as shown in Figure 10. Underneath blisters, oxidation process occurred and steel get rusted and become brown. The evidence of the presence of hydrogen sulphide is associated with the black deposit of iron sulfide, the brown color and rotten eggs smells.

Figure 9: Blistering and coating failure.

SRJMET
Scientific Research Journal for Metal Engineering and Technologies
Volume No.02 Issue No. 01,pp:43-54
ISSN:399-2017
01. Aug .2021

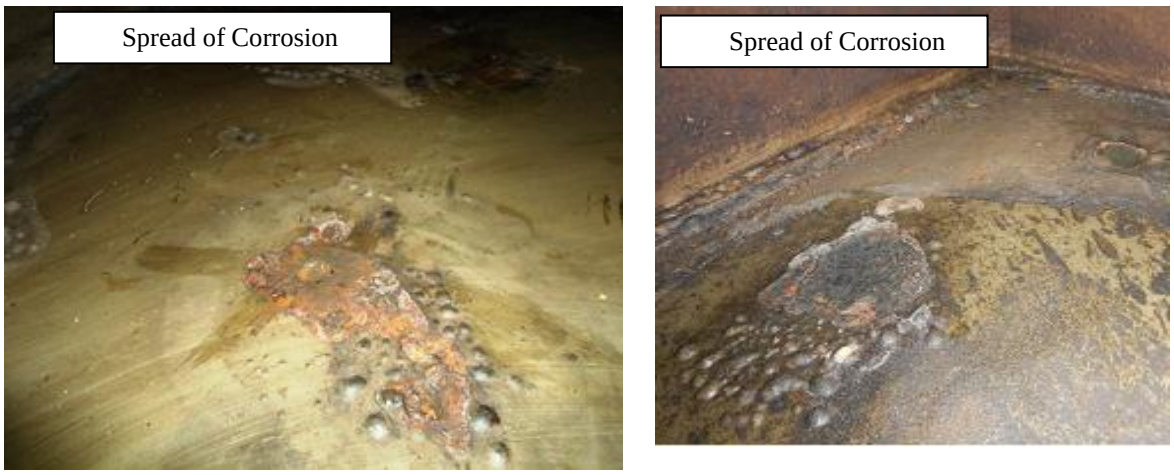

Figure 10: Corroded area of the bottom steel plate of the floating oil storage tank.

A localized pitting corrosion due to the SRB was occurred under the deposits of organisms that shield the metal surface. The damage occurred is characterized by pits in carbon steel as in Figures 11 and 12. The figures show the initiation of pitting corrosion blistering precedes the coating failure and initiation of pitting corrosion. This blistering occurred as a result of deficiency of coating binding to the tank surface which allows the crude oil contents to react or enter in the coating-surface interface at weak positions of the coating. The presence of the SRB that produces sulfate can be the cause which reacts hydrogen leading to chemical compounds as H_2S that react with the steel to produce ferrous sulphides or ferrous hydroxide, eventually causing metal loss in the form of pitting corrosion which vary in depth. Furthermore, these pittings can act as stress corrosion cracking (SCC) initiator; because the "roots" of pits act as "stress concentration" so that the applied stress becomes multiplied several times, resulting stresses much larger than the tensile yield strength, thus causing failure.

Figure 11: Initiation of pitting corrosion.

Scientific Research Journal for Metal Engineering and Technologies
Volume No.02 Issue No. 01,pp:43-54
ISSN:399-2017
01. Aug .2021

Figure 12: Pitting corrosion on the bottom plate of the tank.

The presence of the SRB that use sulfate in the crude oil to consume hydrogen on metal surface leading to chemical compounds that react with the steel causing metal loss in the form of pitting corrosion. Higher tank temperatures preferred by SRB, coupled with residual water in the crude oil tanks can also offer favourable conditions for SRB to grow, and activate the formation of corrosive cells on the surface of the bottom plate. Water exists on the surface of the bottom tank plates can also accelerate the chemical reaction process producing ferrous oxides that destroy the metal surface. In addition, the large coating thickness observed and rapid curing time of the coating may be the cause of coating failure. This causes the solvents to remain inside the coating materials, thus, the solvent evaporates afterwards causing material loss, contraction and stress inside the coating. The stress may result in cracking, or cause the coating to loosen from concave shaped surfaces.

4. Conclusion

Various possible mechanisms of SRB corrosion in steel-oil/water interface were discussed. Depending on the environmental and medium condition, such as concentration of ions, pH and oxygen content, one mechanism or a combination of several mechanisms can occur. Thus, mechanisms of Sulfate-Reduced-Bacteria (SRB) has to be well understood in order to get better result in corrosion inhibition. It was shown that corrosion defects in the form of pitting corrosion was observed in bottom steel plates of the floating crude oil tanks due to the presence of SRB as a result of the hydrocarbon content of the crude and residuals of water. The process of failure could possibly begin with blistering and coating failure at less density areas, then bare steel becomes exposed to crude oil where the metabolic of SRB progresses and produces hydrogen sulphide that interacts with the steel shell of the tank causing metal loss in the form of localized pitting corrosion.

References:

1. AL-DARBI M. M., AGHA K., ISLAM M. R. "Modeling and simulation of the pitting microbiologically influenced corrosion in different industrial systems". In: Corrosion. Houston, NACE International, 2005.
2. PIERRE R. ROBERGE "Corrosion Engineering: Principles and Practice", McGraw-Hill Companies, Inc. 2008.
3. MIRANDA E., BETHENCOURT M., BOTANA J. "Biocorrosion of carbon steel alloys by an hydrogenotrophic sulfate-reducing bacterium", Corrosion Science, v. 48, n. 9, pp. 2417-2431, Sep. 2006.
4. XU C., ZHANG Y., CHENG G. "Localized corrosion behavior of 316L stainless steel in the presence of sulfate-reducing and iron-oxidizing bacteria", Materials Science and Engineering, v. 443, n. 1, 235 - 241, 2007.
5. ABBAS F.M., WILLIAMSON C., BHOLA S.M. "Influence of sulfate reducing bacterial biofilm on corrosion behavior of low-alloy, high-strength steel (API-5L X80)" International Biodeterioration and Biodegradation, v.78, n. 1, 34-42, 2013.
6. USHER K.M., A. H. K., Cole I. D. "Microbially influenced corrosion of buried carbon steel pipes" International Biodeterioration and Biodegradation: 23, 2014.
7. GAYOSSO M. H., OLIVARES J.Z., ORDAZ N. R., RAMIREZ C.J., ESQUIVEL R.G., VIVEROS A.P. "Microbial consortium influence upon steel corrosion rate, using polarisation resistance and electrochemical noise techniques", Electrochimica Acta, v. 49, n. 25, pp. 4295-4301, 2004.
8. MANSFELD F. "The interaction of bacteria and metal surfaces", Electrochimica Acta, 52, 7670–7680, 2007.
9. ALZUHAIR S., ELNAAS M. H., ALHASSANI, H. "Sulfate inhibition effect on sulfate reducing bacteria", Journal of Biochemistry Technology, v. 1, n. 2, 39-44, 2008.
10. HAMILTON, W.A. "Metabolic interaction and environmental microniches: implications for the modeling of biofilm process" Biofouling and Biocorrosion in Industrial Water Systems, 2nd edition, CRC Press Inc., Boca Raton, FL, pp. 27-36.1994
11. OBUEKWE C.O., WESTLAKE D.W.S., PLAMBECK J.A., Cook, F.D. "Corrosion of mild steel in cultures of ferric iron reducing bacterium isolated from crude oil I. polarization characteristics", Corrosion, 37 (8): 461-467, 1981.
12. MOULIN J. M., MARSH E., CHAO V., KARIUS R., BEECH I. B., GUBNER R., RAHARINAIVO A. "Prevention of Accelerated Low- Water Corrosion on Steel Piling Structures due to Microbiologically Influenced Corrosion Mechanisms", ECSC final draft report,1998.
13. GUBNER R. J., BREAKSPEAR S., BEECH I. B. "The effect of iron and dissolved oxygen level on the biocorrosion of piling grade carbon steel" The British Phycological Society, UK, 1998.

14. CHEUNG W.S., BEECH I.B. "The use of biocides to control sulphate-reducing bacteria in biofilms on mild steel surfaces" Biofouling, 9: 231-249, 1996.
15. VIDELA H.A., SWORDS C.L., DE MELE M., EDYVEAN R.G., WATKINS P., BEECH, I.B. "The role of iron in SRB-influenced corrosion of mild steel" Corrosion, NACE, Houston, Tx., 1998.
16. VIDELA H.A "An overview of mechanisms by which sulphate-reducing bacteria influence corrosion of steel in marine environments". Biofouling: The Journal of Bioadhesion and Biofilm research, 15:37-41. 2000.
17. ZBIGNIEW LEWANDOWSKI, JOSHUA BOLTZ "Biofilms in Water and Wastewater Treatment" Montana State University, Bozeman, MT, USA, Elsevier. 2011.
18. JAVAHERDASHTI R. "Impact of sulphate-reducing bacteria on the performance of engineering materials" Applied Microbiology and Biotechnology, v. 91, n. 6, pp. 1507-1517, Sep. 2011.
19. BORENSTEIN S.B. "Microbiologically Influenced Corrosion Handbook". New York: Industrial Press, 1994.
20. PATRIZIA PEREGO, BRUNO FABIANO "Microbiological Induced Corrosion and Inhibition" John Wiley and Sons Inc., 2009.
21. YASSER S. ALSUBHI "Microbially influenced corrosion (SRB) attack in oil/gas refining industries: An overview" International Journal of Science: Basic and applied research, 2016.
22. LEWANDOWSKI Z, DICKINSON W, and LEE W. "Electrochemical interactions of biofilms with metal surfaces" Water Science and Technology 36: 295--302. 1997.
23. SAEID KAKOOEI, MOKHTAR ISMAIL, BAMBANG ARIWAHJOEDI, "Mechanisms of Microbially influenced corrosion: Review" World Applied Sciences Journal. 2012.
24. IWONA B. BEECH, CHRISTINE C. GAYLARDE, "Recent Advances in the Study of Biocorrosion: An Overview" Revista de Microbiologia 30:177-190. 1999.
25. ARMAN ABDULLAH, NORDIN YAHAYA, NORHAZILAN MD. NOOR, and ROSILAWATI MOHD RASOL, "Microbial Corrosion of API 5L X-70 Carbon Steel by ATCC 7757 and Consortium of Sulfate-Reducing Bacteria" Journal of Chemistry. 2014.
26. MUHAMMAD ALI, NORDIN YAHAYA, AKRIMA ABU BAKAR, MARDHIAH ISMAIL, LIBRIATI ZARDASTI and NORHAZILAN MD. NOOR "Corrosion of X-70 Carbon Steel Pipeline Subject to Sulfate Reducing Bacteria" ARPN Journal of Engineering and Applied Sciences, V. 11, No. 21, 2016.

SRJMET
Scientific Research Journal for Metal Engineering and Technologies
Volume No.02 Issue No. 01,pp:55-62
ISSN:399-2017
01. Aug .2021

Loader bucket hard facing using stick welding technique

Azaldin Alhaj Kozam [1], Mustafa I. Elshbo [2] and Khaled Gewa[3] and Hesham Eshabani[4] and Mohamed Saraj[5]

Advanced Occupational Center for Welding Technologies, Tripoli, Libya

*Corresponding author email: ezdeen_khzam@yahoo.com

[1]ezdeen_khzam@yahoo.com, [2]els1972@yahoo.com,[3] khaledgewa@gmail.com, [4]eshabani2010@gmail.com , [5]mohamedssct@gmail.com

Abstract:

Improvements in the field of earth moving machines which are operating continuously require a new way to increase wear resistance of these equipment that operating in various types of sand and rock structures in resistance- field environments. Impact and abrasion actions are the main effects that cause wear of earth moving machinery. The aim of this study is to investigate and enhance the useful operating life of the excavator bucket teeth that fail due to abrasive wear and impact action. DIN 8555: E6-UM-60-GP hard-facing electrode type was selected and deposited by manual metal arc welding process. The hard facing process was applied on two teeth; in the first one the deposition was applied directly while for the second tooth the hard facing was applied on the top of a Nickle based alloy as buffer layer. Hard faced and non-hard-faced teeth were tested for 850 hours of working in field and the results were compared. The hard-faced tooth without using a buffer layer showed the greatest resistance to abrasive wear and the working life of the tooth had extended by 28 %, followed by the tooth with the hard-faced layers and Nickle based alloy as buffer layer while the non-hard-faced tooth showed the lowest wear resistance.

Keywords: wear, hard facing, bucket teeth, earth moving machinery.

1. Introduction

A bucket tooth is an attachment for heavy equipment that is designed to be used in excavation work on construction fields. It is a bulk material handling element and is available in different sizes and shapes. Excavator buckets are produced from medium carbon steel and teeth are sticking out from the bucket, to break up rigid material and avoid wear-and-tear of the bucket. Therefore, excavator buckets are made from steel and bucket teeth are attached and has to be tough and extremely well-made and durable. The excavator bucket teeth need to bear weighty loads of materials like wet soil and rock and additionally subjected to abrasion wear and impact due to the abrasive nature of soil particles once teeth acting to interrupt up material because the bucket are dragged through it. Therefore, the teeth of excavator bucket may suffer from breaking and wear tear takes place. Hard-facing is employed to extend the life of components against abrasive wear [1]. Wear in earthmoving machineries are mostly taken place at the outer surface which are the most exposed to contact during service. The teeth are suffered from wear and weight loss and as result of that effect is the replacing of worn parts which lead to cost more and cause downtime on the equipment. The surface properties of technical materials have a significant effect on the usability and life of a part. Therefore, it cannot be neglected in the design. Outer services of extraction Machinery components are early subjected to failure result of abrasive wear [2].

2. Back ground

Hard-facing is the deposition of a surface layer by various welding processes that is harder than the base material. [3] the aim of hard-facing is to reduce costs - Hard surfacing a worn metal part to like new condition is usually 25 - 75% of the cost of a replacement part, prolong equipment life depends on the application, as compared to that of a non-surfaced part, reduce downtime - because parts last longer, fewer shutdowns are required to replace them and reduce inventory of spare parts - There is no need to keep numerous spare parts when worn parts can be rebuilt. One or more layers of weld metal can be applied during hard-facing. Some types are designed to be applied in one layer only, while others can be applied without limit. [4]. The proper application of hard facing could extend the service life of used parts by two to four times compared with installation of new parts.[5] Mentioned that, based on the knowledge gained in practice and from the previous studies, a criterion for a worn tooth replacement was established, stating that teeth should be replaced after two seasons of operation or when the mass loss is about 20%. It is clear from the literature that most of the companies nowadays make effective use of hard-facing parts as it is helpful in minimizing costs and saves time. The best way to hard-facing is to use parts in the best possible ways. Rebuilding of damaged parts of automobiles is highly appreciated in companies as they take the working parts and, after testing, make them available for customers at reasonably low prices [6].

3. Methodology

Initially three samples of Hyundai 210 excavator bucket teeth are prepared, cleaned from any scale present and coating paint is removed as shown in Figure 1.

SRJMET
Scientific Research Journal for Metal Engineering and Technologies
Volume No.02 Issue No. 01,pp:55-62
ISSN:399-2017
01. Aug .2021

Chemical analysis was carried out on the teeth material and the chemical composition is as shown in Table 1.

Figure (1-a) New loader bucket tooth

Figure (1-b) New loader bucket tooth after cleaning

One of the teeth designated as (W2) was hard faced by two layers; the first layer was Nickel based alloy type ENiCrFe-2 as a buffer layer to enhance the resistance of the teeth to the impact. The second layer was the hard-facing layer using the electrode type DIN 8555: E6-UM-60-GP. The chemical compositions of the filler material are shown in Table 2. The other tooth was hard faced by the same hard facing electrode without buffering and designated as (W1) as shown in Figure 2.

Figure (2) The teeth after hard facing

Both hard faced teeth were compared with non-hard-faced tooth designated as (W3) to investigate the effect of hard facing on the work life of excavator bucket teeth. Manual metal arc welding process was the method of welding. Hard-faced layers were deposited at the edges of teeth from the front and back along all sides. All deposited lines width was from 10 mm to 13 mm and the height was approximately from 3 to 4 mm. The weight of the three samples were measured using Digital Scale before testing. After that, the non-hard-faced tooth installed onto the second place from the right side of the bucket as shown in Figure 3 where abrasive action is expected to be less than at the sides and the hard-faced teeth were mounted onto both sides of the bucket. Field tests are performed for both hard faced samples and the non-hard faced sample. The teeth were tested for 850 hours divided into five equal intervals of 170 h each. At the end of each interval, teeth were dismounted and the weight is measured with a digital scale.

SRJMET
Scientific Research Journal for Metal Engineering and Technologies
Volume No.02 Issue No. 01,pp:55-62
ISSN:399-2017
01. Aug .2021

Figure 3- The teeth after installation onto the bucket.

Table 1. Nominal chemical composition of the bucket teeth

C %	Si %	Mn %	Cr %	Ni %	P %	S %	Cu %	Fe
0.37- 0.44	0.17-0.37	0.5-0.80	0.80-1.10	0.30	0.035	0.35	0.030	Bal.

Table 2. Nominal chemical composition of the filler materials

	Hard facing alloy	Percentage of chemical compositions										
		C	Mn	Si	S	P	Cr	Ni	Mo	Nb&Ta	Fe	Cu
1	DIN 8555: E6-UM-60-GP EN ISO EN 14700: E Z Fe8	0.50	0.40	0.45			7.0				Bal.	
2	SFA/AWS A5.11:ENiCrFe-2,	0.022	1.80	0.24		0.001	15.2	73.9	0.80	1.1	6.70	< 0.001

4. Results & Discussion

The initial measured weights of the three samples and the weight loss after each interval are shown in Table 3 and shown graphically in Figure 5.

Table 3. The accumulative percentage of weight loss after each interval

Sample	Initial weight (grams)	Weight loss after 170 hrs	Weight loss after 340 hrs	Weight loss after 510 h	Weight loss after 680 hrs	Weight of loss after 850 hrs	Percentage of extended life
W1	6605	375	605	931	1193	1498	27.98
W2	6740	380	780	1167	1562	1952	6.153
W3	6330	390	830	1237	1666	2080	-

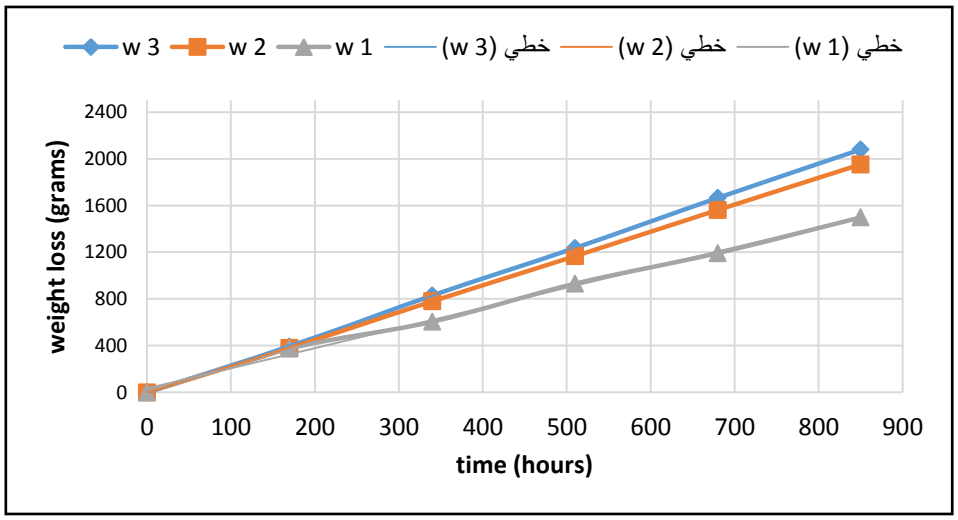

Figure 5. The weight loss versus testing time

These results showed that sample W1 exhibits the lowest weight loss at all test intervals. The weight loss measured from sample W2 was slightly lower than W3. Table 4 presents the percentage of in accumulative weight loss and shown graphically in Figure 6.

Table 4. The mass losses for the three tested teeth.

Sample	Percentage of weight loss after 170 hrs	Percentage of weight loss after 340 hrs	Percentage of weight loss after 510 hrs	Percentage of weight loss after 680 hrs	Percentage of weight loss after 850 hrs
W1	5.68 %	9.2 %	14.1 %	18.1 %	22.7 %
W2	5.64 %	11.57 %	17.31 %	23.2 %	28.96 %
W3	6.2 %	13.11 %	19.54 %	26.31 %	32.9 %

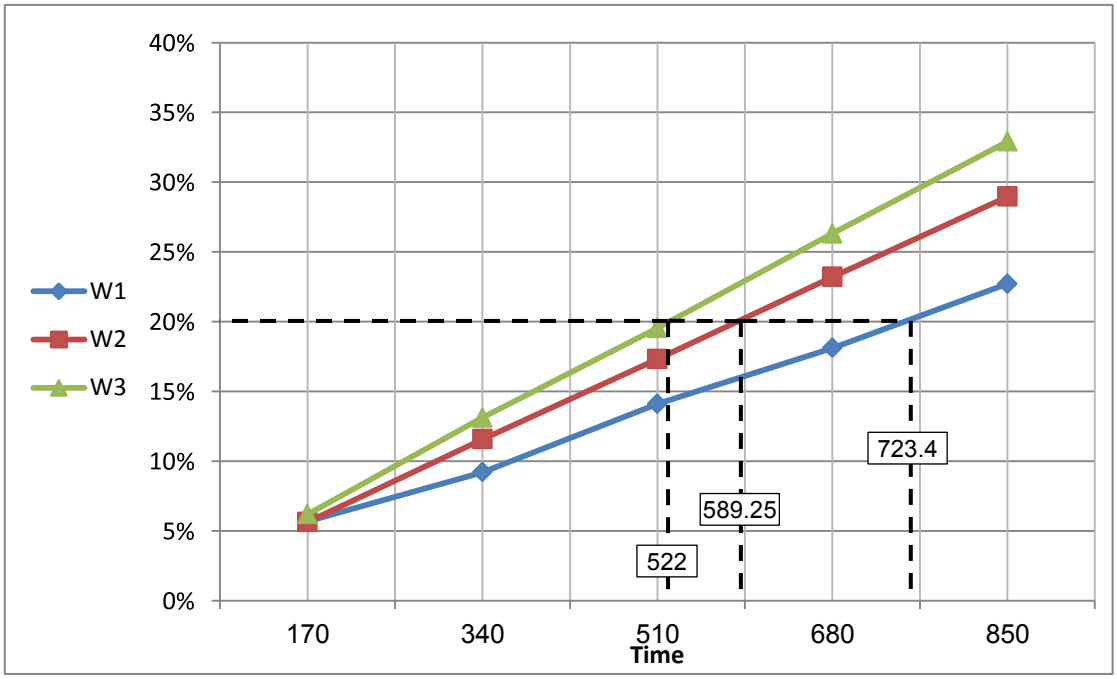

Figure 6 the replacing required

When applying the replacement criterion based on 20% weight loss Figure 6 indicates the gain in working hours obtained by the hard facing compared with non hard facing. After the evaluation and measurement process, we observed that the upper surface areas had worn more than the lower surface areas as shown in Figure 4. This is due to the friction of the upper surfaces touching with the abrasive material. The resistance to abrasive wear for the tooth hard-faced layers (EN ISO EN 14700: E Z Fe8) without buffer layer was higher than the tooth with the hard-faced layers and Nickle based alloy as buffer deposited layer while the non-hard-faced tooth showed the lowest wear resistance. The results showed that the buffering process had improved the working life by only about 6 % while the hard facing process without buffering had increased the working life by about 28 %. Thus, the buffering process was not an affective technique to be used in extending the life of hard faced components

Table 3 and from the initial weight we saw that the hard facing had added 275 gm of deposited material. This added material cost about 13 % of the purchasing cost of a new tooth. Meanwhile this extra cost by the hard facing had extended the working life of the tooth by 28 % as mentioned above (the gain is about 201.4 hours). Thus, the process of hard facing is recommended to be carried out to extend the working life of loader bucket teeth.

Table 5. The rate of weight loss after each interval

sample	Rate of loss after 170 hrs (g/h)	Rate of loss after 340 h (g/h)	Rate of loss after 510 h (g/h)	Rate of loss after 680 h (g/h)	Rate of loss after 850 h (g/h)	Average rate of loss
W1	2.21	1.78	1.83	1.75	1.76	1.866
W2	2.24	2.29	2.29	2.29	2.29	2.28
W3	2.29	2.44	2.42	2.45	2.44	2.408

Figure 4. Excavator teeth condition after 850 work hours

5. CONCLUSION

Based on the stated criterion of 20 % weight loss for teeth replacement, we concluded that

1) The DIN 8555: E6-UM-60-GP is an effective type of electrode for hard facing processes which has the lowest average rate of weight loss of about 1.86 g/h compared with 2.4 g/h of W3 sample. .
2) The conducted experiments showed that an extension of about 28 % of the working life as a result of 13 % additional price relative to the original cost of the of the loader bucket teeth was obtained.
3) The buffering process was not effective to enhance the working life of the hard-faced tooth (component)

References

1. S. I. P. 3. A. K. 4. Neeraj Chandrakar1, “Analysis of Excavator Bucket Teeth Using FEM,” International Journal of Innovative Research in Science, Engineering and Technology, 4 April 2017.
2. A. S. K. a. J. S. G. Shivali Singla1, "Enhancing Wear Resistance of Low Alloy Steel Applicable on Excavator Bucket Teeth Via Hardfacing," *ARME*, July - December 2012.
3. *. K. V. P. a. B.Venkatesha, "Wear characteristics of hardfacing alloys: state-of-the-art," ScienceDirect, (2015).
4. A. S. R. R. N. M. M. Vuki} Lazi}1, “SELECTION OF THE MOST APPROPRIATE WELDING,” 15 01 2014.
5. V. L. M. M. D. A. M. Jovanovi}, “Selection of optimal technology for reparatory hard facing of bucket teeth, Welding and welded structures,” 2005.
6. R. H. Karuna Subramaniam, "Remanufacturing for the automative aftermarket-strategic factores," journal of cleaner production, 2009.

SRJMET
Scientific Research Journal for Metal Engineering and Technologies
Volume No.02 Issue No. 01,pp:63-68
ISSN:399-2017
01. Aug .2021

The Influence of Laser Surface Nitriding On The Microstructure And Hardness of Carbon Steel Specimens

[1]Abdlkarim A. Elalem , [2]Amged A. El hames

[1]Plasma Research Laboratories, Authority of National Science and Technology
[2]Physics Department, Factuality of Science, Misurata University

elalemkareem@gmail.com, mosa213@yahoo.com

Abstract:

nitriding is a common method for improving the hardness , mechanical properties, wear and corrosion resistance of metals. Laser nitriding of metals is an efficient process, where the irradiation of surfaces in nitrogen atmosphere leads to the fast take-up of nitrogen in the irradiated surfaces. In this paper laser surface nitriding of carbon steel carried out by melting the surface of substrate using high power CW CO_2 laser with nitrogen as shrouding environment. Laser tracks were arranged as single tracks with the use of various laser powers ranging from 0.8kW to 2.0 KW , and laser scanning rates from 120mm/min to 200 mm/min. The influence of laser beam power and laser scanning rates on the microstructure and hardness profiles analysed. The laser nitride layer studied using optical microscope, and scanning electron microscope. The laser surface nitriding of carbon steel led to refinement in the microstructure and the diffusion of nitrogen caused the formation of $\varepsilon + \gamma'$iron nitrides on the surface. The micro hardness of the nitride surface improved to a maximum of 400HV in the present set of laser processing conditions as compared to 150HV of as received substrate as a result of the appearance of marten site in the melted pool and heat effect zones.

key words: laser surface nitriding, carbon steel, hardness, microstructure.

1.Introduction.

Laser intruding is an efficient process where the irradiation of iron and other metals with pulsed or continuous lasers in nitrogen atmosphere leads to huge take-up of nitrogen in the irradiated surfaces [1-2] .The advantages of laser assisted surface treatment over conventional diffusion-aided include the ability to deliver a large power density $(10^3 - 10^5 W/cm^2)$, high heating /cooling rate $(10^3 - 10^5 K/s)$, and solidification velocities $(1 - 30 m/s)$ [3,12].The basic mechanisms of the laser nitriding process however, are still rather poorly understood, as they are closely related to the laser-induced plasma above the sample and to the complicated laser-plasma material interactions[10]. As a result of Laser surface nitrided the grain refined and the substructures such as dislocations are increased. The formed high volume interfaces locate in intergranular which provides an ideal channel for diffusion of elements [11]. In this paper laser surface nitrided carried out on carbon steel. The influence of laser processing parameters on the surface microstructure and hardness are described.

2.Experimental Procedure.

The carbon steel specimens for laser surface nitriding of dimensions of$3cm \times 2cm \times 1cm$ were chosen as substrates. The chemical composition of this steel was 0.18%C, 0.5%Cr, 0.74%Mn, 0.04%Mo, 0.19%Si, 0.006%Al, 0.25%Nb, and the rest Fe. The laser nitriding of the carbon steel specimens was performed by using high power CW CO_2 laser. The maximum power of the laser system is 9kW, wave length 10.6μm, the focal length of laser system lens is 200mm, and the maximum scanning velocity is 5000mm/min. Laser melting tracks carried out on the surface of ten carbon steel specimens during nitrogen gas flowing normally on the melting layer at rate of 1500ml/hr. The laser nitriding process carried out using (0.8kW, 1.0kW, 1.8kW, 2.0kW) laser power and (120mm/min, 140mm/min, 180mm/min, 200mm/min) scanning rate parameters. The polished cross-section of the specimens surfaces analysed using optical and scanning electron microscope.. The Vickers method was applied for micro hardness measurements. A load of 300gm was applied for 10 seconds and a 0.5mm distance between each indentation.

3.Results and discussions.

The presence of nitrogen in the melting pool MP and the heat affected zones HAZ was observed in the white nitride layer in depth of about $800\mu m$.The laser nitriding process produced ε in the MP and $\varepsilon + \gamma'$ iron nitrides phases in the HAZ [9,11] as shown Figure (1) a , b.

SRJMET
Scientific Research Journal for Metal Engineering and Technologies
Volume No.02 Issue No. 01,pp:63-68
ISSN:399-2017
01. Aug .2021

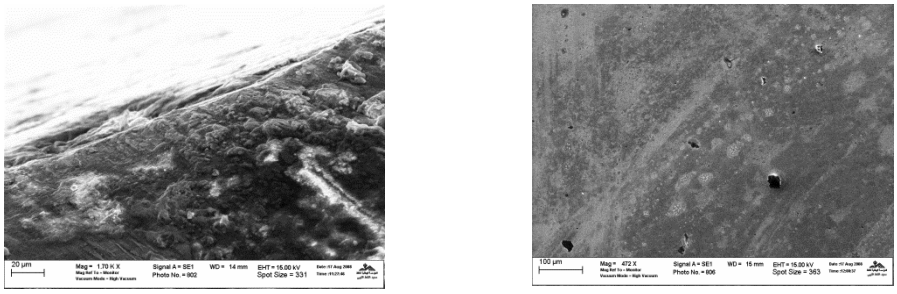

(a) (b)

Figure 1: Microstructure of MP (a) and HAZ (b) of the laser nitrided layer of carbon steel

(a) 120mm/min (b) 180mm/min (c) 200mm/min

Figure 2:Influence of laser scanning rate on the microstructure of laser surface nitrided crbon steel

The influence of the scanning rate on the microstructure is clearly observed in the MP and HAZ as shown in the images figure (2) (a) and (b). In figure(2)c specimens processed using scanning rate of 200mm/min and laser power 2.00kW has finer microstructure than those processed with the same power and at lower scanning rate (b) and (c). This is due to the fact that the higher the scanning rate was the less interaction time and higher quenching rates and hence finer microstructure.

(a) 0.8kW (b) 1.0kW (c) 1.8kW

Figure 3: The influence of the laser beam power on the microstructure of laser surface nitrided carbon steel.

The laser processing power is having observable effect on the microstructure and depth [5] of MP and HAZ as in fig.(3). Deeper processed layers were obtained as laser power increased from 0.8kW to 1.8kW. The carbon specimens processed using higher laser

power produced finer microstructure as a result of the high quenching rate of the rapidly melted layer by high laser power density.

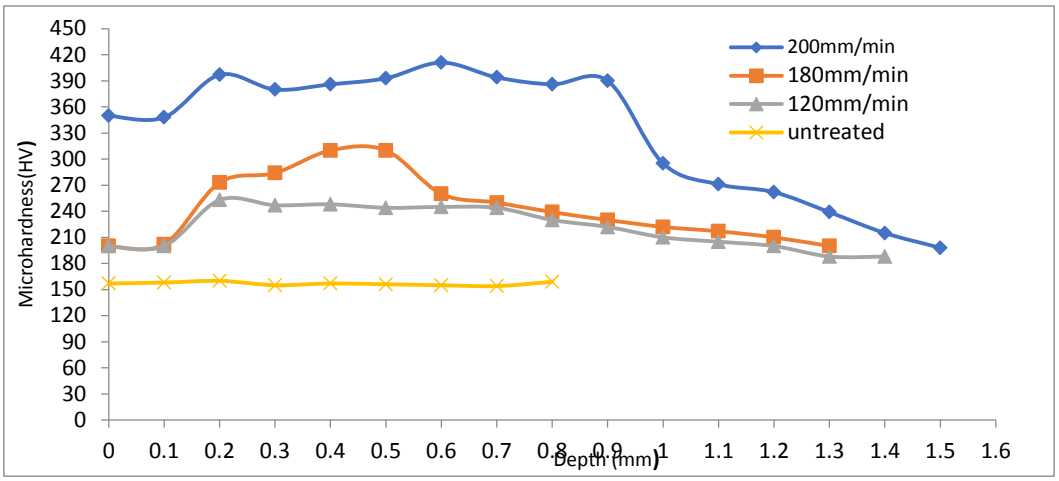

Figure 4: The influence of laser scanning rate on microhardness profiles of laser nitrided

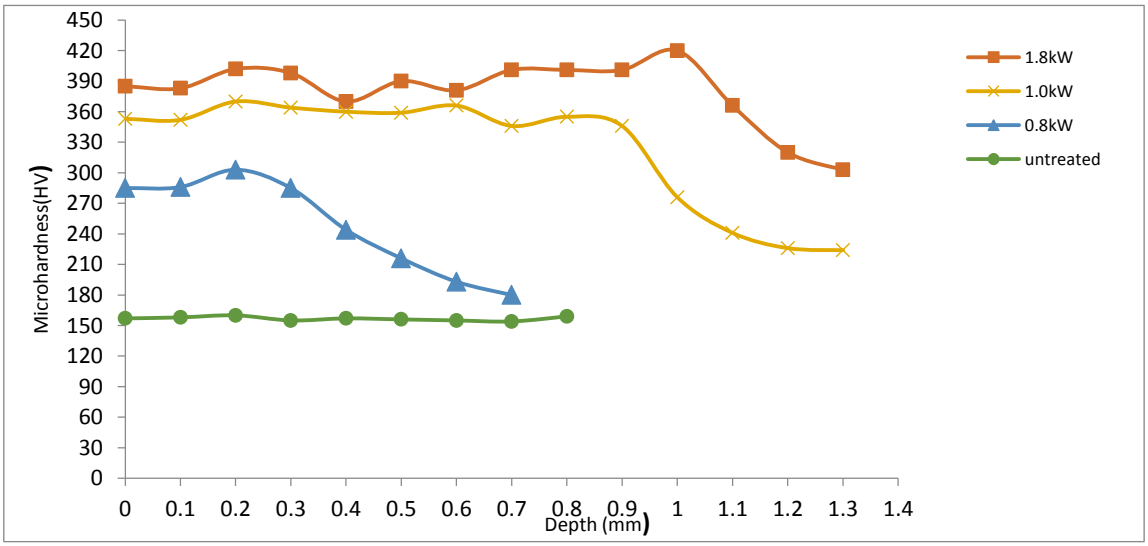

Figure 5: The influence of laser processing power on microhardness profiles of laser nitrided carbon steel.

The microhardness profiles of the laser nitrided layers processed with different scanning rates are shown in figure 4 The maximal hardness of the laser nitrided carbon steel layers was obtained in the melting pool zone (411HV) using laser power of 2.00kW and scanning rate of 200mm/min. This maximal hardness reduced gradually to (386 - 264HV) as the laser scanning rates decreased from 180 to 120mm/min. The rise in scanning rate led to rapid re-solidification of the melted layer of carbon steel and hence its hardenability improved[5,6]. The improvement in microhardness with the use of higher laser processing power is observed [5,7]as in microhardness profile figure

5.The hardness of laser nitrided layers of carbon steel was improved from 300HV to more than 400HV as laser processing power increased from 0.8kW to 1.8kW with 200mm/min scanning rate.

The increased in microhadness was caused by a changed microstructure, especially by the present of martensite in hardened layer (MP and HAZ). Additionally nitrogen dissolved in austenite caused increase in hardenability[4-8]. The diminished hardness close to the surface could result from the lower cooling rate in this area. In HAZ microhardness decreased gradually due to reducing the percentage of martensite within a distance from the surface.

4. Conclusions.

The laser surface nitrided carbon steel produced a modified layer on the substrate surface. The laser treated layer of carbon steel consisted of three zone: The melting pool MP, the heat-affected zone HAZ , and substrate. The diffusion of nitrogen in the melting pool and heat affected zone caused the formation of ε and $\varepsilon + \gamma'$ nitrides. The laser rapid melting and quenching rates refined the microstructure. The maximal hardness measured in the melting pool decreased gradually toward the heat affected zone. The increase in hardness in the laser treated layer because of the formation of martensite in the MP and partially in the HAZ, in addition to the dissolved iron nitrides in austenite. Laser processing parameters such as laser power and scanning rates have observable influence on the microstructure and hardness. The influence of rapid melt/solidification on the refinement of the microstructure and the improvement of carbon steel hardness increased with higher laser beam power and higher scanning rates. The maximal hardness observed at powers greater than 0.8kW and scanning rates greater than 120mm/min.

. **References:**

1. Xi Shoumou, Zhang Jianguo Sun Xiaoyan et al. Laser quenching + nitride compounds treatments of 38CrMoAIA steels[J]. Chinese Journal of Lasers, 2004, 31 (6) : 761 – 764.
2. Carpene E., Schaaf P. , Laser nitriding of iron and aluminum, Applied Surface Science, 2000, vol. 186, s. 100 – 104.
3. J. Kusinski, S. Kac, O. Kopia, et al. Laser modification of materials surface layer, Bulletin of Polish Academy of Sciences, ,2012, No. 4,vol.60, 711-724
4. Zhong Minlin, Liu Wenjin, Leading areas and hot topics on global laser materials processing research [J]. Chinese journal of lasers, :2008 35(11) 1653 – 1659.
5. DominikaPanfil, PiotrWach,Michal Kulka, Jerzy Michalski, The influence of laser re-melting on the microstructure and hardness of gas nitride steel, Archive of mechanical technology and materials, 2016,vol.36, 18-22.
6. Pengyu Lin, Zhihui Zhang, Hong Zhou, LuquanRen, The mechanical properties of medium carbon steel processed by biomimetic laser technique, Elsevier publisher, Materials Science & Engineering, (2013), A 560, 627-632.
7. Shin H.J., Yoo Y.T., Ahn D.G., Im K., Laser surface hardening of S45C medium carbon steel using ND YAGlaser with continuous wave, Journal of Materials Technology, (2007), 187-188,467-470.
8. Yan M.F., Wang Y.X., Chen X.T.,Guo L.X., Zhang C.S., You Y., Bai B., Long Z., Li R.W., Laser quenching of plasma nitrided 30CrMnSiA steel, Materials and Design, 2014, vol.58,s.,154-160.
9. Kulka M., Michalski J., Panfil D., Wach P., Laser heat treatment of gas nitrided layer produced on 42CrMo4 steel, Inzynieria Materials, 5(207) (2015) 301-305.
10. Peter S., Felix L., Meng H., Pettore C., Klaus-P.L., Laser nitriding of iron, stainless steel, and plain carbon steel investigated by Mossbauer spectroscopy, Hyperfine Interaction 2002, 139/140:, 307-314.
11. Cheng Y., Wang C., Chen Z., NiuY.,The influence on brittle of microstructure of laser quenching/nitriding layer, Advanced Materials Research online;2012, ISSN:1662-8985, vol. 549, 548-552.
12. Amit Biswas, Lin Li, U.K. Chatterjee, I. Manna, Diode laser assisted surface niriding of Ti-6Al-4V:properties of nitided surface, Metallurgical and materials transactions A,2009, vol.40A, 3031-3037.

SRJMET
Scientific Research Journal for Metal Engineering and Technologies
Volume No.02 Issue No. 01,pp:69-78
ISSN:399-2017
01. Aug .2021

Failure investigation of 500 tons cement silo

K.I.Azzabi [1], A.A.Marwan [2],W.A. Allafi [3]

1) College of engineering technology-janzour
2) College of renewable energies-tajoura
3) High Vocational Libyan Center of Casting

[1] Email, azzabikh@gmail.com_, [2] Email , azez.mrwan@gmail.com

[3] Email, waleedallafy@gmail.com

Abstract:

Silo structures are utilized in many industries (e.g. energy, mining, cement) throughout the world to store granular bulk solids such as a wheat coal, cement, raw materials, and mineral ores among many others. Every year the news headlines about structural failures are alarming and, in many cases, not only economic loss is involved but also loss of human life. These failures usually occur due to inadequate design and over load. In this paper investigation of 500-ton cement silo is performed using SOLIDWORKS simulation to solve problem failure cement silo. A systematic approach is followed, where possible a theoretical calculation is performed to check the results and to serve as guide for investigation. The analysis is performed in progressive steps, the load distribution and members loading are considered individually to assess the strength of various members and understand its behavior before performing the full model analysis. It is concluded that reinforcement will improve the results, but it will not solve the problem; the load carrying capacity of the frame is over estimated, from the investigation. The results showed excessive deflection at the mid-span of the base ring caused localized stresses on the attached cone and the cylindrical ring. It is recommended to strengthen the ring by either welding curved beam to the existing one, or redistributing the trusses in order to provide a support to the mid-span. Further analysis should include dynamic loading due wind, seismic and filling/discharging of cement.

Key words: cement silo, Solidworks, finite elements,

Introduction.

Silo structures are used all around the world to store granular bulk solids (e.g. grains, coal, cement, plastic pellets, raw materials, mineral ores) that are a critical part of the production and fabrication of many products that we commonly utilize in our daily life such as food, electricity, highways and roads, clothing, electronics, etc. Silos are some of the most critical pieces of equipment in industrial facilities, yet they fail with a frequency which is much higher than almost any other industrial building or equipment. Failures can range from small deformations and cracks to catastrophic rupture and complete collapse of the silo structure. Failures in silos are costly as replacement and repairs of the storage structure are required, and personnel may be injured or even killed. Additionally, the downtime during this period translates into lost production as well as potential litigation [1,2]. This failure is due to design defects, lack of periodic inspection and maintenance, or overload.

The design of silo structures requires specialized knowledge. This includes not only understanding the structural analysis and design of these types of structures, but also bulk solids flow behavior, their loading patterns as well as operation practices used for the specific silo. The designer must first establish the material's flow properties [3], and then consider such items as flow channel geometry, flow and static pressure development, and dynamic effects. Non-uniform loads, thermal loads, and the effects of non-standard fabrication details must be considered as well. Once the design criteria have been established, a competent design has to follow. Here the engineer in charge of the design must have a full understanding of load combinations, load paths, primary and secondary effects on structural elements as well as the relative flexibility of the elements [4,5].

1. Methodology.

1.2. Description of model.

The real cement silo was modeled by using solidworks program. 3_D model was developed as shown in figure 1. The diameter of silo is 5580 mm, thickness of shell is 5 mm with height 2.357 m. The half angle of cone is 40 deg, the area was determined as well as the uniform loading which are used in the calculations. Roark's Formulas for Stress and Strain was used in this study to investigate the failure [6]. Figure 2 and 3 present some of calculation procedure of Roark's formulas that used in the calculations.

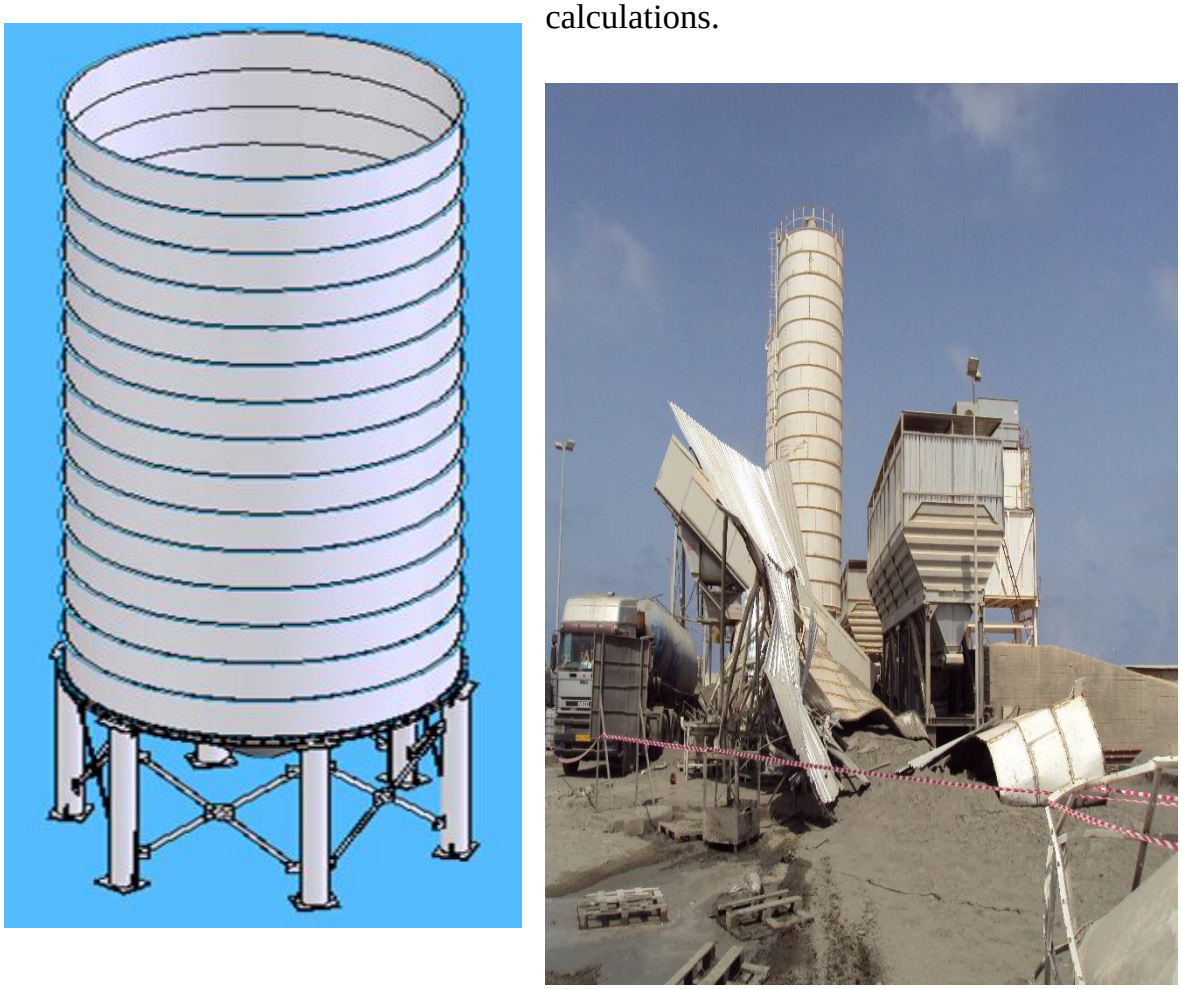

Figure 1. Conical Shell (Model and real failure cement silo)

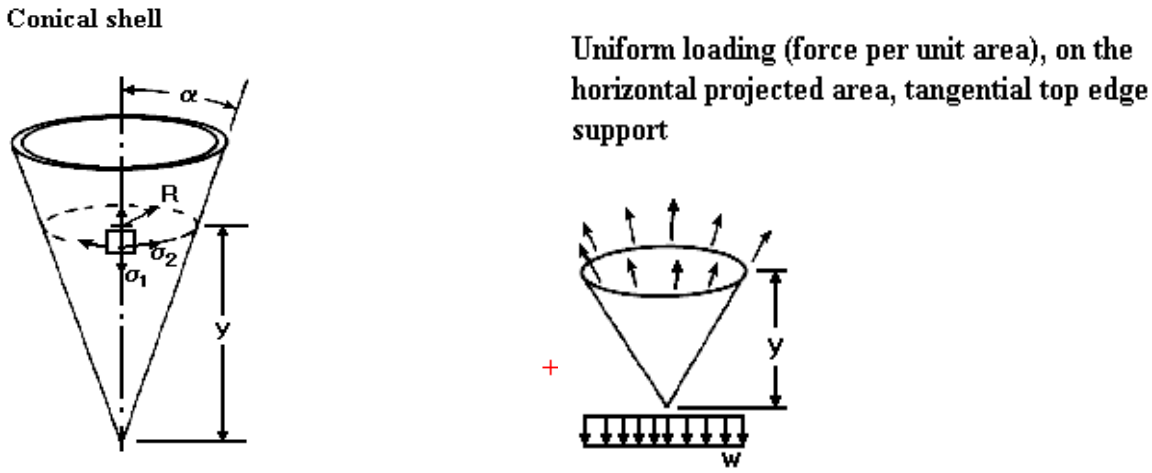

Figure 2. Uniform loading on horizontal projected area.

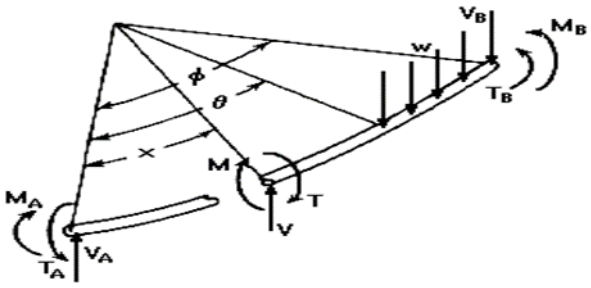

Figure 3. Roark's Formulas for Stress and Strain.

2.1. Investigation process.

During the failure investigation process, the first step is a visit to the incident site to gather facts and evidence relevant to the failure and to document the appearance of the site. (Information shall be provided by you) Once the evidence is obtained and examined, the developing potential failure scenarios was beginning. To further evaluate potential failure theories, engineering **analysis & modeling** is generally performed.

The types of engineering analyses used in this failure investigations include:

- Stress analysis (linear and nonlinear)

Special loading conditions evaluated in these analyses include:

- Gravitational.

- Thermal.
- Pressure.
- Wind.

Initial analyses often employ closed form, hand calculation methods to approximate structure behavior. This approach serves as a check on the validation of the models, and expensive, computer models (finite element).

The failed item is simulated on a computer using “finite element” software. Parametric models are built in order to investigate the effects of various component changes on the integrity of the structure. Parameters used in these models include: geometry, material properties, loading conditions, repairs, and fabrication defects.

3. Results and discussion

3.1 Theoretical calculations

The main ring is supported by six evenly distributed legs the load is transferred from the silo to the main ring. The ring has to support the full load including the dead weight. Roark's Formulas for Stress and Strain was used in this study to investigate the failure [6]. Mathcad is used to find the theoretical solution of displacement as shown in Figure 4. A distributed load of 500 tons were used in this case which is the capacity of cement silo. The unit load per unit length is calculated to be 179.8 kN/m.

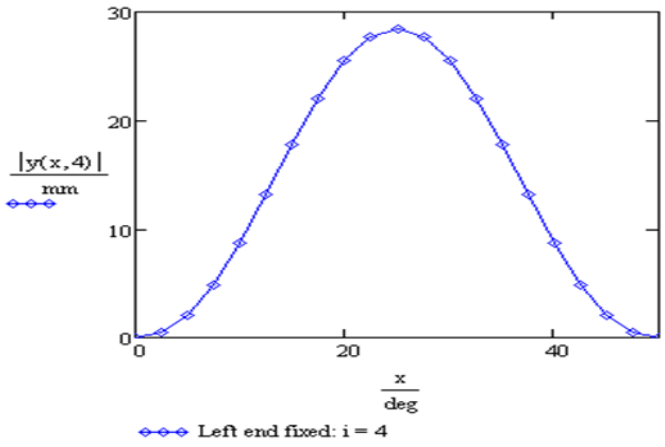

Figure 4. Displacement of the main ring theoretically

3.2 FE calculation

The main ring is supported by the legs and a distributed load is applied. The mass acting on the ring is the same one used in the theoretical calculation. The model solved using solid elements and beam elements.

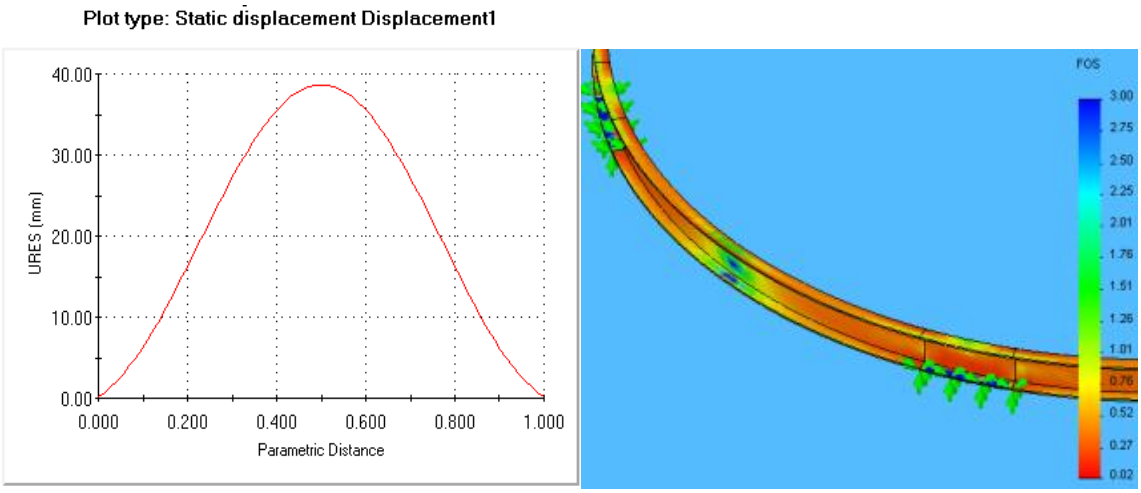

Figure 5. The static displacement of the main ring.

As shown in Figure 5. The deflection is large which is approximately 40 mm. Where the beam should be supported in order to withstand the acting load. Rectangular Stiffeners are suggested to increase bear rigidity. The rectangular stiffeners distributed on the ring as presented in the Figure 6. The results show some improvement; lateral support should be applied to improve the stiffens. The displacement decreased to become around 32mm.

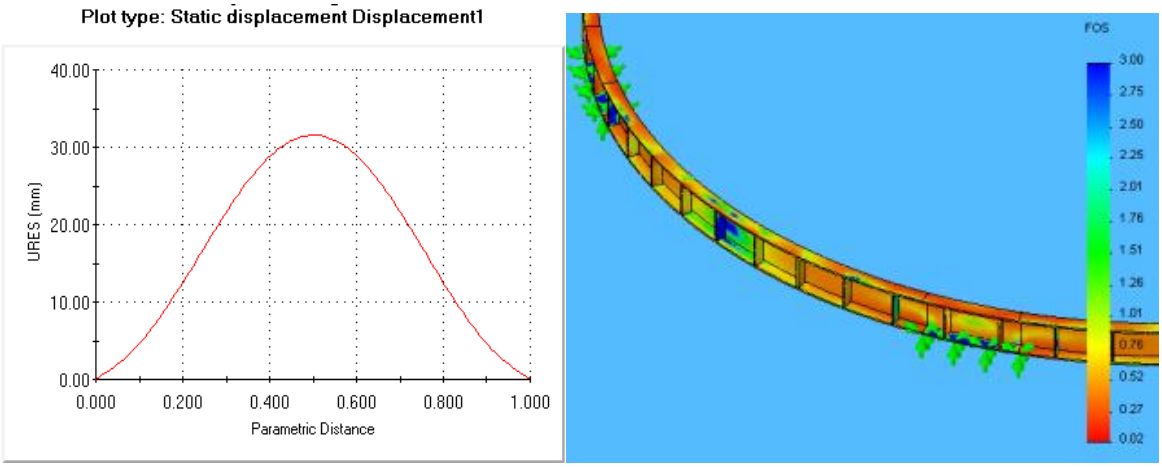

Figure 6. The displacement after rectangular stiffeners.

3.3 Ring and cone.

The second Phase of analysis is to consider the cone as part of the model. The cone will transfer the load to the Ring and will also stiffen the ring. Mixed elements are used to reduce the calculation time, shell elements are used for the cone and solid dements are used for the ring.

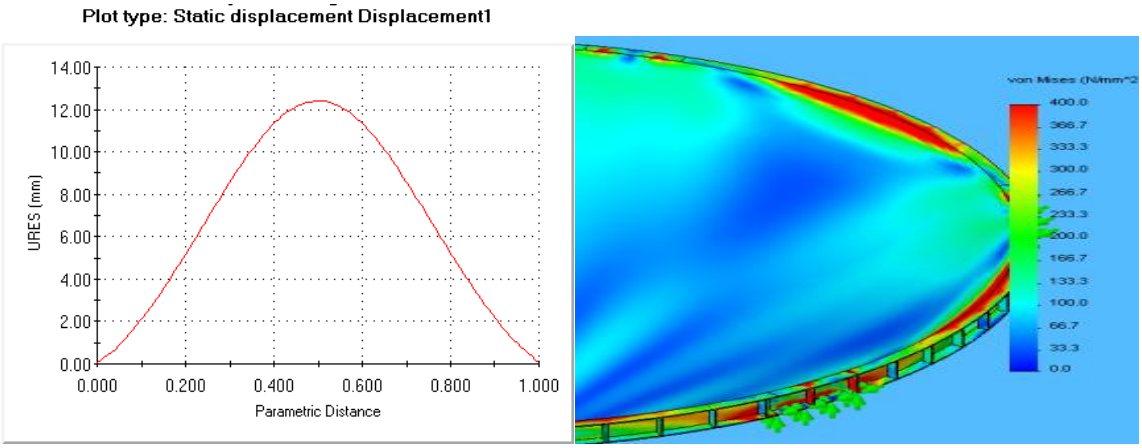

Figure 7. Static displacement for ring and cone included rectangular stiffeners.

3.4 Ring reinforcement.

The ring is supported with a C- section beam along the span between the legs. This will act as extra loading member and should be welded to the ring and the ends welded to the legs. Figure 8 presents the static displacement of the ring without the reinforcement. The displacement was around 15mm.

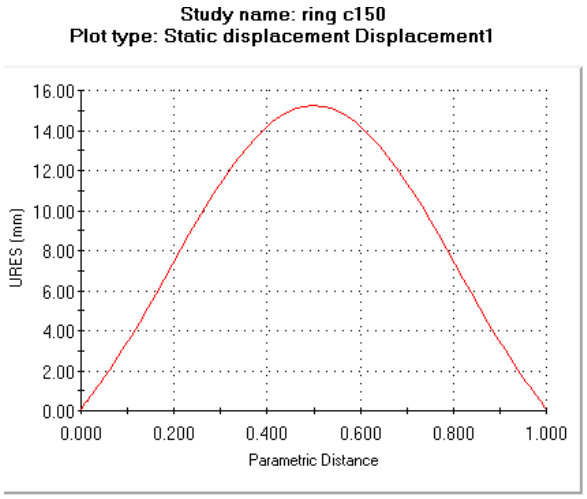

Figure 8. Static displacement of ring without reinforcement.

After the reinforcement was added to the ring. The improvement was noted in the displacement which is reduced to 12 mm approximately as shown in figure 9.

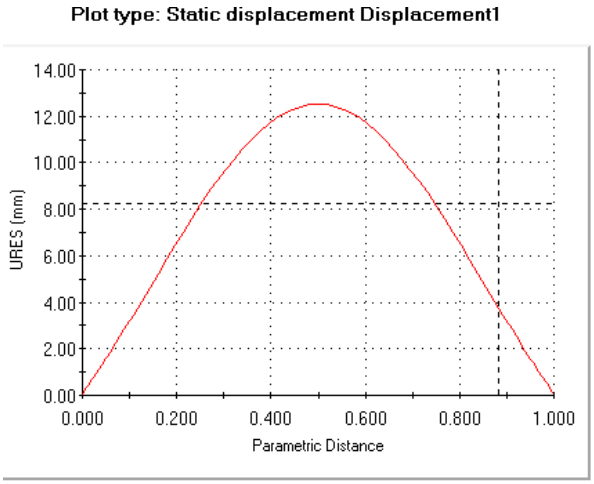

Figure 9. Static displacement of ring with reinforcement.

3.5 Full Silo.

Only the lower part is need to be investigated, being the section where the maximum deflection will cause and cause the highest stresses in the structure. The results showed an area of stress concentration at the upper part of the beam.

Close up on the area is shown below.

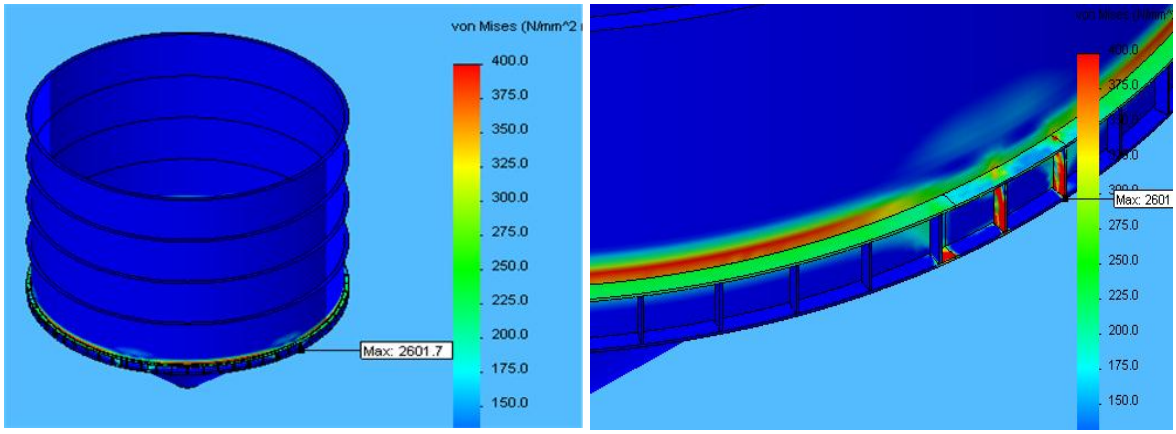

Figure 10. The highest stress on the full silo.

4. Conclusion

This paper presents the failure investigation of 500 tons cement silo. 3_D model of solidworks program was solved. The displacement of the ring and cone were obtained via finite elements and compared with the theoretical solution. The results show that there is a deflection in the ring which is may occur the failure of the silo. Some of highlight points were concluded on this study:

- The load carrying capacity of the frame is over estimated, reducing the capacity of silo to 300 ton was recommended and applying rectangular stiffeners on the ring.
- Reinforcements needed to be added to the other silos.
- All welding lines should be inspected and rectified.
- A periodic examination should be carried out in a timely manner to correct the problem before it occurs

Acknowledgments

The authors would like to thank everyone who assist in this work to be provided in the best form.

References:

1. Sagarnaga, J. C. (2018). Concrete Silo Failures Due to Design Errors. In *Forensic Engineering 2018: Forging Forensic Frontiers* (pp. 696-706). Reston, VA: American Society of Civil Engineers.
2. Maj, M. (2017). Some causes of reinforced concrete silos failure. *Procedia Engineering*, *172*, 685-691.
3. Jenike, A.W.: Storage and Flow of Solids, University of Utah Engineering Experiment Station, Bulletin No. 123, Nov. 1964.
4. Jenike, A.W.: Effect of Solids Flow Properties and Hopper Configuration on Silo Loads, In Unit and Bulk Materials Handling (Loeffler, F.J., and C.R. Proctor, eds.), ASME, 1980, pp 97-106.

5. Carson, J.W. and Jenkyn, R. T.: Load Development and Structural Considerations in Silo Design, Presented at Reliable Flow of Particulate Solids II, Oslo, Norway, August 1993.
6. Roark, R. J., Young, W. C., & Plunkett, R. (1976). Formulas for stress and strain.

SRJMET
Scientific Research Journal for Metal Engineering and Technologies
Volume No.02 Issue No. 01,pp:79-90
ISSN:399-2017
01. Aug .2021

Comparison Between Chemical Vapor Deposition CVD and Physical Vapor Deposition PVD Coating Techniques: A Review Paper

[1]Ali Musbah, [2]Wafa Eljaafari, [3]Enas Fessatwi, [4] Yusra Elsahli

1. Department of Mechanical Engineering, Bani Waleed University, Bani Waleed Libya.
2. The Higher technical center for training and production, Tripoli-Libya.
3. Advances center of Technology, Tripoli-Libya.
4. Department of Materials and Metallurgical Engineering, University of Tripoli, Tripoli, Libya.

[1] aaammm198088@gmail.com,[2] Wafaaljaafari@yahoo.com,

[3]e.fessatwi@yahoo.com, [4]y.elsahli@uot.edu.ly

Abstract:

Due to the rapid and continuous development of surface engineering technologies, especially thin films. Vapor deposition coating techniques are the preferred processes for it. Both types Chemical and physical vapor deposition processes have been used to improve the surface properties of engineering materials by depositing a very thin layer of metallic, non-metallic, organic and inorganic materials. The diversity of sedimentary materials in both techniques has led to a great variety of surface properties obtained, improving their quality and increasing their ability to withstand the conditions of work within the design limits. In this present review article, the research and progress in comparison between chemical and physical vapor deposition techniques focusing on their respective types, features, advantages, disadvantages, applications, and the last thig the two technologies have achieved.

الملخص:

نتيجة للتطور السريع والمستمر لتقنيات هندسة الأسطح خاصة ما يُعرف بطلاء الطبقات الرقيقة لذلك تعتبر تقنيات الطلاء بالترسيب من أفضل هذه التقنيات المستخدمة لطلاء المعادن والمواد الهندسية. تستخدم تقنيتا الترسيب الكيميائي و الفيزيائي لتحسين الخصائص السطحية للمواد الهندسية عن طريق ترسيب طبقة رقيقة جدًا من المواد المعدنية وغير المعدنية والعضوية وغير العضوية. أدى تنوع المواد التي يمكن ترسيبها كطلاء على أسطح المعدات بواسطة كلا التقنيتين إلى تحسين الخصائص الميكانيكية، وتحسين جودتها وزيادة قدرتها على تحمل ظروف العمل. في هذه الورقة البحثية تم إجراء مقارنة بين تقنيات الترسيب الكيميائي والفيزيائي مع التركيز على أنواعها ومميزاتها وعيوبها وتطبيقاتها واخر ما توصلت اليه التقنيتين.

Keywords: chemical vapor deposition, physical vapor deposition,surface coating technique

SRJMET
Scientific Research Journal for Metal Engineering and Technologies
Volume No.02 Issue No. 01,pp:79-90
ISSN:399-2017
01. Aug .2021

1. Introduction.

Though many developments of human needs and the increase in the use of new and modified materials, the need to develop and techniques to improve the performance of these materials has become urgent, especially at the surface. Surface engineering science deals with the techniques and methods used to study and improve the surface properties of engineering materials, and the most important of these methods is coating. A general classification of surface engineering techniques is shown in figure(1) .

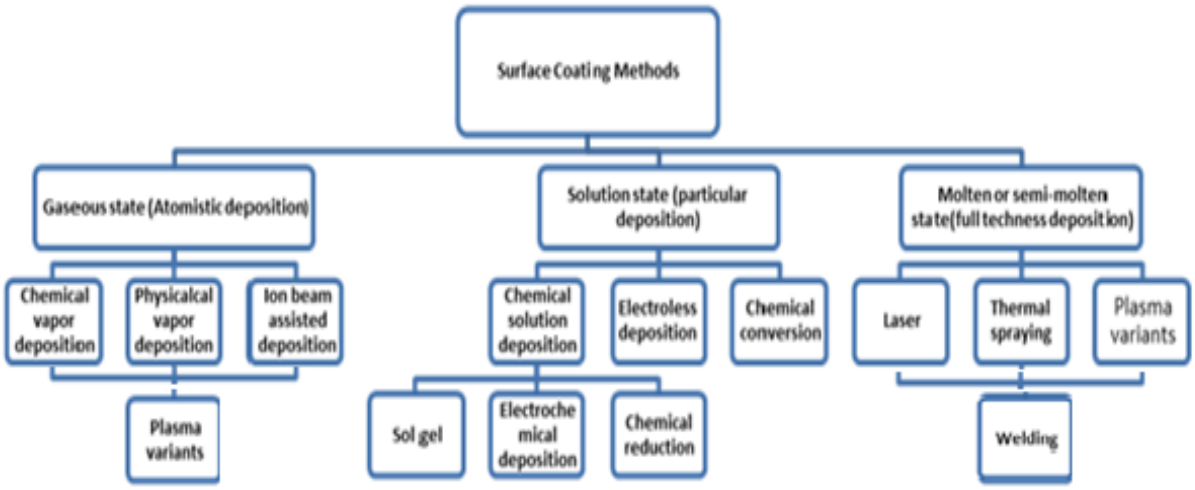

Figure 1: A General Classification of Surface Engineering Techniques[1].

2. Literature review

The surface coating technique requires the deposition of thin film layers on the surface, there by altering the properties of the surface. Examples of surface coating techniques are vapor phase processes deposition (chemical and physical vapor deposition)[2]. In CVD, as in PVD, vapor supersaturation affects the nucleation rate of the film whereas substrate temperature influences the rate of film growth. These two factors together influence the extent of epitaxy, grain size, grain shape and texture. Low gas supersaturation and high substrate temperatures promote the growth of single crystal films on substrates. High gas supersaturation and low substrate temperatures result in the growth of less coherent, and possibly amorphous, films [3].

3. Chemical Vapor Deposition CVD

3.1 CVD Definition and Types.

There are several definition of CVD in the published literature. A practical and common definition of CVD is that it is a complex of depositing solid material and form a thin film from gaseous phase material. At a high temperature as a result of a chemical reaction. It is used to produce high purity, specialized thin coatings. CVD involves mixing the source material as a carrier device[4,5,6]. Different types of CVD for different materials, precursors, growth rates, substrates as shown in table (1)[7], table (2) show Some typical materials deposited by CVD and some common precursors utilized to achieve deposition by CVD[8]. Table (3) illustrate Comparison of deposition properties of CVD[9].

Table1: Show different types for CVD[7].

Type	Symbol
Plasma Enhanced	PE-CVD
Micro wave Plasma assisted	MP-CVD
Remote plasma assisted	PRE -CVD
Metal Organic	MO-CVD
Aerosol assisted	AA-CVD
Direct Liquid Injection	DL- ICVD
Lower Pressure	LP- CVD
Ultrahigh vacuum	UH-CVD.

Table2: Some typical materials deposited by CVD and some common precursors utilized to achieve deposition by CVD[8].

Film type	Representative materials	Ex: of common precursors
Group IV Semiconductors	Si, SiGe, Ge	SiH4, SiH2Cl2, GeH4
Compound semiconductors	GaAs, GaAlAs	MR3,M=Ga, As, Al, In
Dielectrics	SiO2, Si3N4,SiOxny	SiH4, SiH2Cl2, Si(OR)4
High-k dielectrics	Al2O3, Ta2O5. TiO2, ZrO2	M(OR)4, M(NR2)4
Ferroelectrics	SrTiO3, BaSrTiO3, SrBi2Ta2O9	M(thd)2, M=Sr, Ba, Pb

Table3: Comparison of deposition properties of CVD[9].

Deposition conditions	CVD
Vacuum requirement	10-2 – 10-3 Torr
Deposition thickness range	10nm->3µm
Uniformity control	nm
Deposition rate	10-1000nm/min
Conformality	0%-100% at 4:1 aspect ratio
Contamination/Particles	Particles can exist due to gas phase reactions

3.2 CVD Process conditions and mechanisms.

CVD was the first of the vacuum based technique to be used widely for ceramic deposition particularly for tool coating. In this process a stream of gas containing volatile compounds of the element or elements to be deposited is introduced into a

reaction chamber. The conditions within the chamber are controlled to enable an appropriate chemical reaction to take place which leads to the formation of a coating on the substrate surface. The volatile reaction products are removed from the chamber during the process. CVD can take place at normal atmospheric pressure or at low pressure < 100 Mpa but generally requires high temperatures > 900C^{o} for the necessary reactions to take place. This has caused difficulties in the coating of temperature sensitive materials[10].as shown in figure (2) [11].

CVD reactors are typically classified in the several ways, a.b.c.d and e replaced word of by the number of wafers processed simultaneously (batch versus single wafer), a.b.c.d and e replaced word of by the wafer arrangement (stacked versus planar), a.b.c.d and e replaced word of by the reactor operating pressure (UHV to atmospheric), a.b.c.d and e replaced word of by the reactor wall temperature (hot wall versus cold wall), and by the method of adding energy to cause deposition (thermal and/or plasma)[8]. As shown figure(3) illustrate the two types of reactors[7].

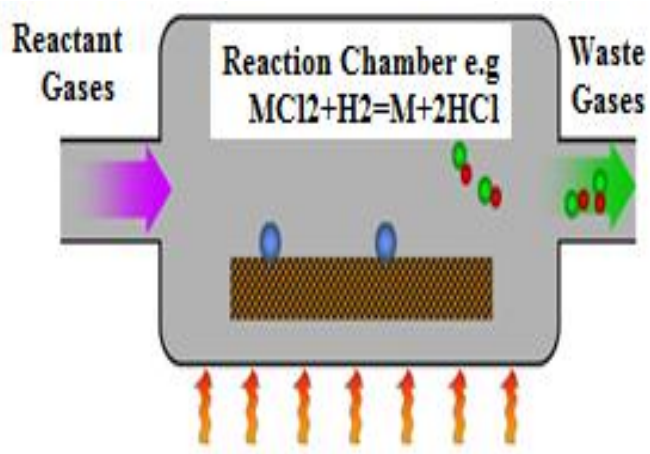

(a)

SRJMET
Scientific Research Journal for Metal Engineering and Technologies
Volume No.02 Issue No. 01,pp:79-90
ISSN:399-2017
01. Aug .2021

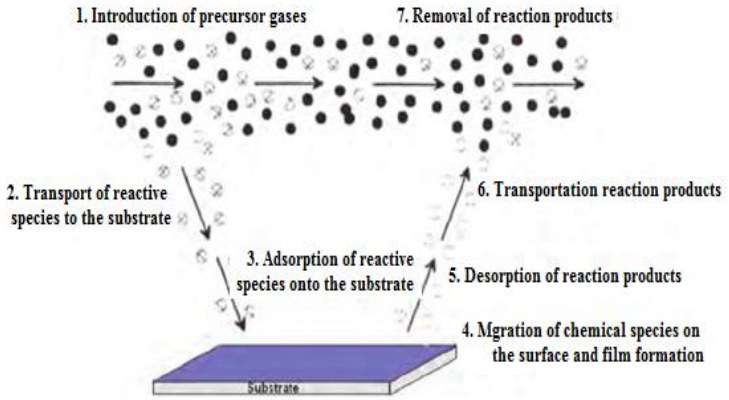

(b)

Figure2: (a) and (b) shows CVD mechanism and steps[11].

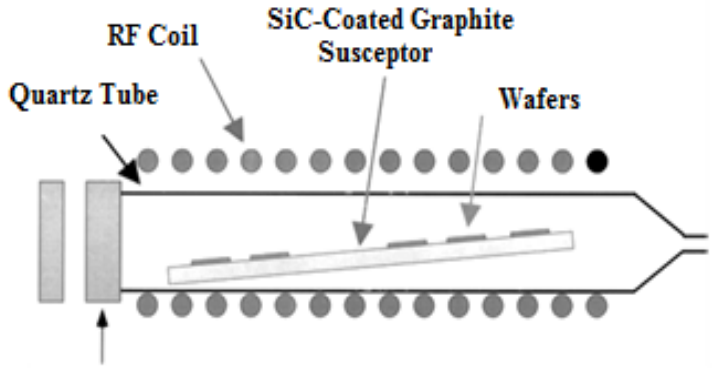

(a)

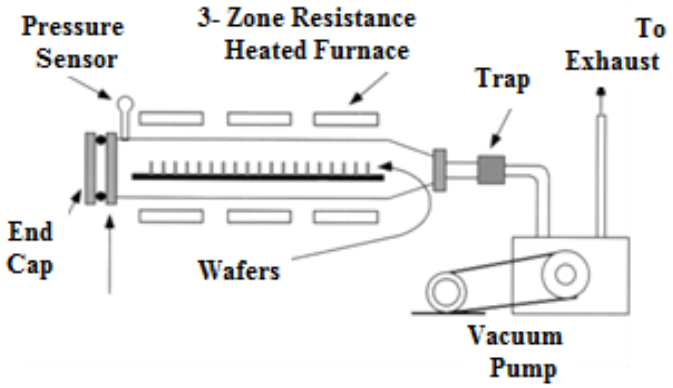

(b)

Figure3: Shows the two types of reactors: a) horizontal, cold wall CVD reactor b) low pressure, hot wall CVD reactor [7].

3.3 CVD advantages and disadvantages.

(a) Adjustable deposition rates allow epitaxial growth as well as high rates of > 10 $\mu m.h^{-1}$.

(b) Highly dense, pure and uniform films.

(c) Conformal deposition (non-line of sight).

(d) Flexibility due to wide range of precursors' (halides, hydrides, metal organic, etc).

(e) Control over crystal structure and morphology.

(f) Good reproduce ability and adhesion to substrate.

(g) Reasonable cost for conventional CVD.

(h) Chemical and safety hazards by the use of toxic, corrosive flammable and/ or explosive precursors.

(i) Difficult to deposit multicomponent films with well controlled stoichiometry due to different evaporation rates of multi-source precursors.

(j) Often high deposition temperatures are needed in conventional CVD systems.

(k) Sophisticated systems (plasma enhanced, low pressure, etc).

(l) Increase cost of fabrication[12].

3.4 CVD Applications.

(a) The application of this thermal energy and the presence of a reducing atmosphere results in the decomposition of the molecules containing the coating element which are subsequently deposited onto the surface of the substrate.

(b) provides an up-to-date introduction to CVD technology for the fabrication of nanomaterials, nanostructured films, and composite coatings.

(c) Discusses processing, structure, functionalization, properties, and use in clean energy, engineering, and biomedical grand challenges.

(d) Covers thin and thick films and composites[13].

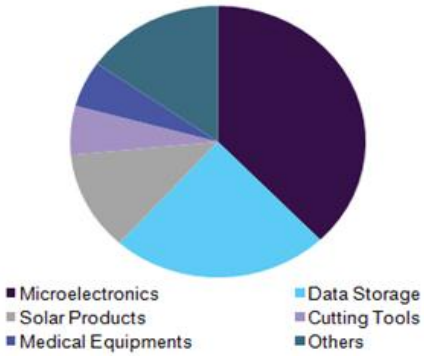

Figure4: Illustrate the application of Chemical Vapor Deposition[14].

4. Physical vapor deposition PVD

4.1 PVD Definition and types

If the vapor is created by physical means without a chemical reaction, the process is classified as PVD[3]. Physical vapor deposition is fundamentally a vaporization coating technique , involving transfer of material on an atomic level .It is an alternative process to electroplating. PVD is a well-known technology that is widely used for the deposition of thin films regarding many demands, namely tribological behavior improvement, optical enhancement, visual/esthetic upgrading, and many other fields, with a wide range of applications already being perfectly established [15,16].

The different types of PVD represent to :

(a) Cathodic arc deposition : in which a high –power electric arc discharged at the target material blasts away some of the material into a highly ionized vapor to be deposited onto the work piece.

(b) Electron beam physical vapor deposition : in which the material to be deposited is heated to a high vapor pressure by electron bombardment in a high vacuum and is transported by diffusion to be deposited by condensation on the cooler work pieces.

(c) Evaporative deposition: in which the material to be deposited is heated to a high vapor pressure by electrically resistive heating in a low vacuum.

(d) Pulsed laser deposition: in which a high power laser ablates material from the target into a vapor.

(e) Sputter deposition: in which a glow plasma discharge bombards the material, sputtering some away as vapor for subsequent deposition [17,18].

(f)

4.2 PVD Process condition and mechanism.

Physical Vapor Deposition PVD processes (often just called thin film processes) are atomistic deposition processes in which material is transported in the form of a vapor through a vacuum or low pressure gaseous or plasma environment to the substrate where it condenses. Typical PVD deposition rates 10- 100 A_o (1- 10 nanometers) per second. PVD processes can be to deposit films of elements and alloys as well as compounds using reactive deposition processes. Three basic process of PVD are vacuum or thermal evaporation, ion plating and sputtering. During the evaporation process, thermal effect causes injection of atoms from the source , whereas, for ion plating process, the growing film is exposed to can current ion bombardment. While during sputtering, the atoms are ejected from the surface of the solid target the impact of gaseous and then deposited on the surface of the substrate[3,18,14]. Figure (5) shows PVD process[18], and table (4) shows Comparison of deposition properties for PVD[9].

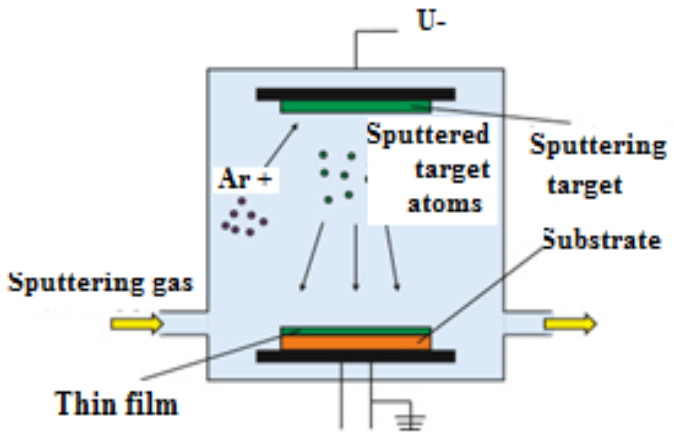

Figure 5: Schematic illustration of the physical vapor deposition process[18].

Table 4: Comparison of deposition properties for PVD[9].

Deposition conditions	PVD
Vacuum requirement	<10-2 Torr
Deposition thickness range	5nm- >10µm
Uniformity control	nm
Deposition rate	10-1000nm/min
Conformality	15% at 4:1 aspect ratio
Contamination/Particles	Indirectly only (flaking)

4.3 PVD Advantage and Disadvantage

(a) is only one of the methods used to coat surfaces.

(b) is safer than those methods.

(c) Also, it can be used on almost any type of inorganic material.

(d) is used as the deposition method to produce an extremely hard, corrosion resistant coating.

(e) Thin films made with PVD have a high temperature tolerance and superior ablation resistance.

(f) PVD is also considered an environmentally – friendly process.

(g) Is higher costs, due in part to the intense heating and cooling that is required.

(h) The process requires complex machines that need skilled operators.

(i) Also, the rate at which coating PVD operates is relatively slow.

(j) PVD is also (line of sight) technique, which means it is not ideal for coating non- visible surface[5,19].

4.4P VD applications.

PVD technology is very versatile, enabling one to deposit virtually every type of inorganic material, such as metals, alloys, compounds and mixtures, as well as some organic materials. PVD coating are general used to improve hardness, wear resistance and oxidation resistance. So, such coating are used in a wide range of applications such as : aerospace, automotive, surgical/ medical, dyes and molds for all manner of material processing, cutting tools, firearms, optics, watches, thin films and in the textile industry[18,19]. Figure(5) shows the applications of PVD [20].

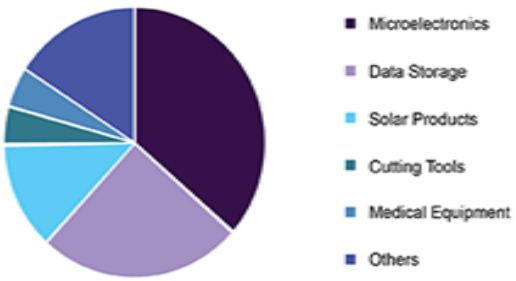

Figure6: Shows types of application of Physical vapor deposition[20].

5. Assistant view across future expected Of CVD and PVD

Based on above, the future will open the wide areas and give a real promises to develop an advance techniques of CVD and PVD processes. This confidence comes from the reality of continuously development on manufacturing world. Many applications of engineering materials needs to specific properties with a different degrees of complexity. That means, new materials/properties "substrate or precursor", new application, low cost, new design, efficient facilities and control system. If the science and technologies dealt with above aspects, then CVD and PVD processes will touch all engineering applications, for example:

(a) Aerospace: to increase wear, thermal resistance.

(b) Nanotechnologies: nano-tubes and nano-rods[21,22].

(c) Robotics: to deposit fine and accurate parts

(d) Health fields: to deposit a hard and white layer of ceramic or other materials to protect human teeth or to produce a "spare tooth" for example.

(e) Environment area: to produce a coatings from an organic materials.

(f) Electronic and electric industries: to deposit macro ad micro- compounds.

In the end, the study will present two models of what the CVD and PVD techniques have achieved, respectively:

Since their discovery, single-walled carbon nanotubes (SWCNTs) have attracted intensive interest in various areas because of their striking structural and electronic properties. SWCNT-based thin films possess a combination of mechanical flexibility, optical transparency, unique electrical properties, ad high surface area, and they show great potential for application I flexile displays, electronic textiles, energy storage and sensors among others. Currently, SWCNT thin films are fabricated mainly either by filtering SWCNT solution or by direct dry fabrication based on floating catalyst chemical vapor deposition (FCCVD) [23].

An effective way of protecting the surface of hot section part of turbine jet engines is the using of Thermal Barrier Coatings (TBCs). The Plasma Spray Physical Vapor Deposition (PS-PVD) was developed as an alternative method to EB-PVD for production of YSZ columnar ceramic layer. Only selected properties of TBCs produced by PS-PVD method were investigated: erosion and oxidation resistance[24].

6. Conclusion.

In CVD, as in PVD, vapor super saturation affects the nucleation rate of the film whereas substrate temperature influences the rate of film growth, both processes are used to deposit wide variety of materials as a coatings. CVD processes are generally more complex than those involving while PVD friendly process but it is higher costs and relativity slow.

References:

1. K. Holmberg, A. Matthews," casting Tribology properties, Mechanism's, Techniques and applications in surface engineering", 2009.
2. Y. Deng ,K. Tong," Physical vapor deposition technology for coated cutting tools: A review, 2020.
3. L.B. Freund," Thin film materials, stress, defect formation and surface evolution",2003.
4. K. Wang, Chemical Vapor Deposition of large – area high- quality grapheme films for electronic applications, 2014.
5. B. Smith, The difference between physical vapor deposition and chemical vapor deposition , 2018.
6. V. pahade, P.S. Chavan, V.P. Baisane" A review paper on vapor deposition coating",2016.
7. J.E. Crowell," Chemical methods of thin film deposition: chemical vapor deposition, atomic layer deposition, and related technologies",2003.
8. P.T. Hagerty, "chemical vapor deposition of materials for flexible two dimensional electronic devices,2016.
9. P.M. Marthin," Handbook of deposition technologies for films and coatings: science, applications and technology", 2010.
10. H.O. Pierson, " Handbook of chemical vapor deposition CVD principles, Technology, and application.
11. Dr. Ing." Advanced chemical vapor deposition methods for All solids state, conversion- Type and 3D Li- Ion Battery concepts", 2018..
12. D.M. Mobkin, M.K. Zuraw,"Principles of chemical vapor deposition",2003.
13. V. panka, S. Chavan, V. Baisane, A review paper on vapor deposition coating, 2016.
14. http://www.grandview research.com/ industry-analysis/ chemical-vapor. deposition. Cvd .market.
15. A. Baptista, Francisco silva, Jacobo Portiero, Jose Miguez, Sputtering physical vapor deposition coating ,2018.

16. A. Baptista, Francisco silva, Jacobo Portiero, Jose Miguez, Sputtering physical vapor deposition coating ,2018.
17. S. Shahidi, Sheila, Moazzenchi, Bahareh, Ghoranneviss, Mahmood, A review application of physical vapor deposition PVD and related methods in the textile industry,2015,p2.
18. N.Selvakumar, H.C.Barshilia, Review of physical vapor deposited PVD spectrally selective coatings for mid-and high temperature solar thermal applications,2012.
19. D. Mattox, Hand book of physical vapor deposition processing ,2010,p.29.
20. www. grandviewresearch.com.
21. Xiaobin Niu, Stephen P. Stagon, Hanchen Huang, J. Kevin Baldwin and Amit Misra, The Smallest Metallic Nanorods Using Physical Vapor Deposition, www.researchgate.net
22. Sheng-Joue Young, Yi-Hsing Liu, Zheng-Dong Lin, Kumkum Ahmed, MD Nahin, Islam Shiblee, Sean Romanuik, Praveen Kumar Sekhar, Thomas Thundat, Larry Nagahara, Sandeep Arya, Rafiq Ahmed, Hidemitsu Furukawa, and Ajit Khosla, Multi-Walled Carbon Nanotubes Decorated with Silver Nanoparticles for Acetone Gas Sensing at Room Temperature, Journal of The Electrochemical Society, 2020.
23. Aqeel Hussain , Yongping Liao , Qiang Zhang , Er-Xiong Ding , Patrik Laiho , Saeed Ahmad , Nan Wei , Ying Tian, Hua Jiang , Esko. Kauppinen, Floating Catalyst CVD Synthesis of Single Walled Carbon Nanotubes from Ethylene for High Performance Transparent ElectrodesMarek, Nanoscale, 2018, DOI: 10.1039/C8NR00716K.
24. Góral, Radosław Swadźba, Tadeusz Kubaszek, TEM investigations of TGO formation during cyclic oxidation in two- and three-layered Thermal Barrier Coatings produced using LPPS, CVD and PSPVD methods , Surface & Coatings Technology journal, Accepted 1 May 2020

SRJMET
Scientific Research Journal for Metal Engineering and Technologies
Volume No.02 Issue No. 01,pp:91-99
ISSN:399-2017
01. Aug .2021

The relationship Between Silicon Carbide Percent and the Mechanical Properties of Aluminum Powders

Yala Salam Elhaj [1], Mohamed H. Alaalam[2] ,

1)Department of Mechanical Engineering, Higher Institute of Engineering Technologies, Libya.

2) Department of Mechanical Engineering, College of Engineering, Elmergib University, Libya

[a] yalaalhaj@gmail.com, [b] 11mala22@gmail.com

*Corresponding author email: yalaalhaj@gmail.com

Abstract:

Powder metallurgy is a highly developed method of manufacturing reliable aluminum silicon carbide composites in different structural applications. Production of a homogenous, high strength and net shape structural components made from aluminum-silicon carbide composites can be achieved using this technology.

The effects of Sintering Temperature and Silicon Carbide Percent on the mechanical Properties of the aluminum silicon carbide produced by powder metallurgy are studied by using the heat treatment of the composite. This method produce a local fusing and welding of the aluminum particles while using aluminum powder with thick oxide layer surrounding the particles prevents the all melting of the composite.

After cold compaction the sintering temperatures between 500 and 850 °C were applied on samples containing (0%, 5%, 10%, 15%, 20%, 25% 30% and 35%) of silicon carbide powder then the specimens examined to investigate the mechanical behavior of aluminum powders. Generally , The results illustrate that the mechanical properties of the samples increases with increasing the silicon carbide percent and sintering temperature. Also, to obtain good mechanical properties the sintering temperature are found to be 600°C for the aluminum with no silicon carbide content, 700°C for composite containing both 5% SiC, 750°C for composite containing 15% SiC, 800°C for composite containing 20% ,25% SiC.

Keyword: Powder Metallurgy, silicon carbide, composites, sintering temperature, compaction technique, heat treatment, compression and mechanical properties.

1-Introduction.

In powder metallurgy compaction is an important step which can be done at room temperature (cold pressing), or elevated temperature (hot pressing). The important processes in cold compaction include powder rearrangement, plastic deformation and fragmentation [1].

Powder metallurgy (P/M) is a process of making components from metallic powders. Initially, it was used to replace castings for metals which were difficult to melt because of high melting point. The development of technique made it possible to produce a product economically, and today it occupies an important place in the field of metal process, it consist of pressing a powder to desired shape, followed by heating at an elevated temperature below its milting point[2,3].

The addition of high strength, high modulus refractory particles to a ductile metal matrix produces a material whose mechanical properties are intermediate between the matrix alloy and the ceramic reinforcement. The ceramic particle additions make it possible to increase the specific elastic modulus of aluminum and improve aluminum thermal properties as well as improve another mechanical properties [4].

Powder metallurgical processing has been applied to reinforce ductile metal (aluminum) powder with high strength high modulus refractory (Sic) particles, with this addition, produces a material whose mechanical properties are intermediate between the Matrix alloy and the ceramic reinforcement [5].

Previous work by W. M. Khairaldien et al [6]. illustrates that bad sintering at low temperature of aluminum composite was solved by increasing the sintering temperature above the melting temperature of aluminum (660°C).This study will demonstrate the effect of increasing the Sintering Temperature and Silicon Carbide Percent on the mechanical Properties of Production of Aluminum-Silicon Carbide Composites.

2-Experimental Procedures.

Samples dimensions shown in figure1 where X is variable depending on the sample weight were produced, containing 0%, 5%, 10%, 15%, 20%, 25% ,30% and 35% weight percent silicon carbide respectively as shown in figure 2 to study the effect of silicon carbide percentage and sintering temperature on the mechanical properties of the composite. The mixtures were weighted and blended without any pre-

processing operation to decrease cost of production; the aluminum powder used in this work was a flake type having percent of aluminum oxide surrounding it. The aluminum powder has no uniform particles shape and the particles size between 200-300 meshes show in figure 3. The mixtures were cold compressed in the die under applied pressure 24 ton, to enhance the composite density distribution, and then the Samples sintered at five different temperatures for one hour.

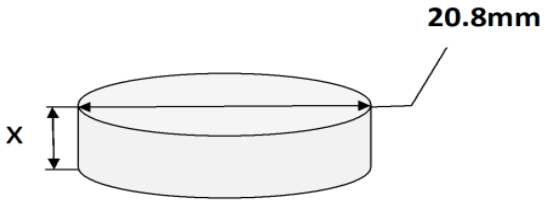

Figure 1: Aluminum composition sample dimensions.

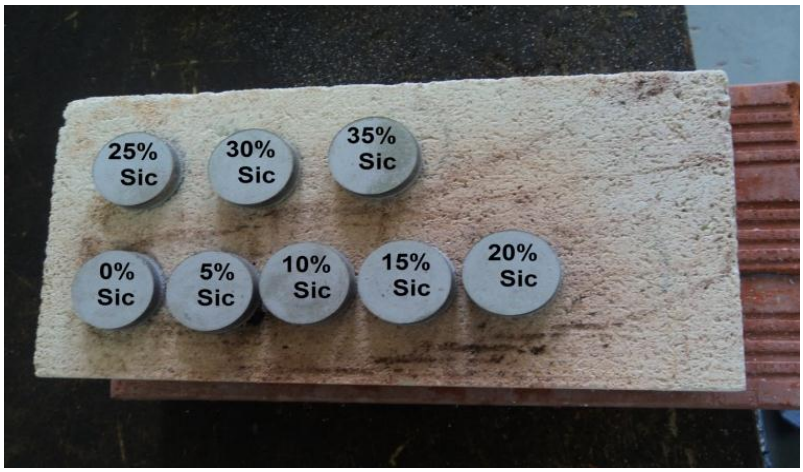

Figure 2: Aluminum samples before sintering contain (from 0% to 35%) of Silicon Carbide.

Hydraulic universal testing machine was used in this research to determine the compression properties (model 1190, Instron Ltd., High Wycomebe, U.K.) fitted with a manual with maximum load 400,000 pounds, also the maximum movement to the ram is 30 cm.

Microhardness Vickers test was achieves by using microhardness tester indenter and 50 g indenting load for 15 sec. The hardness values are the average of minimum three reading on each sample.

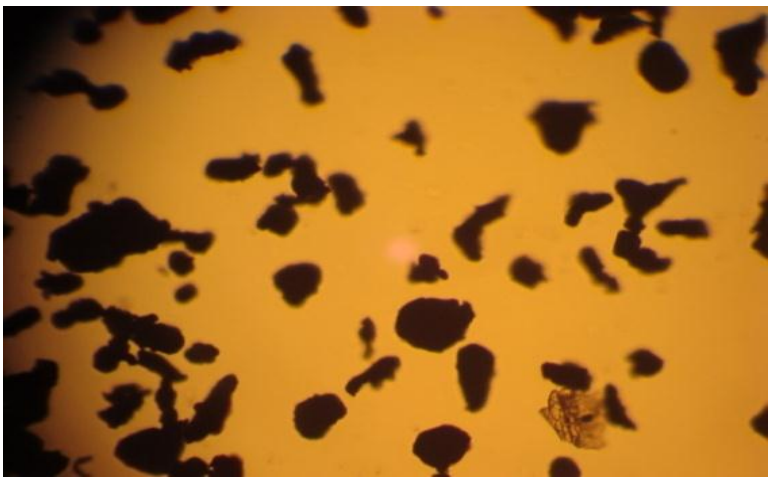

Figure 3: As received aluminum powder under the optical microscope[7]

3-Results and Discussion.

The hardness values were determined on polished samples using load (50g) for 15 sec on Vickers micro-harness tester. The micro-hardness values are reported in HV (Kg/mm²) unit As can be seen from figure 4 the hardness of the samples increases with increasing the percent of silicon carbide and raising the sintering temperature. The pure aluminum samples given in figure 5 show slightly increase in hardness with increasing sintering temperature. In the 5% weight silicon carbide, the effect of silicon carbide starts as soon as the presence of these particles become a hinder for the aluminum particles contact. To bypass these obstacles, the sintering temperature can be increased. In this percent, the hardness increases slightly from the pure aluminum at 500°C sintering temperature whereas an abruptly increase happen in the 600°C in the hardness for the samples with sintering temperature rising. The 10% weight silicon carbide increases the properties of the silicon carbide in the composite where the silicon carbide particle contacts have bond badly with each other so require to raising the sintering temperature. However, It can be seen in figure 4 the 10% weight Sic was not enough to do a proper changes in the composite properties, but still gives better results than the 5% weight Sic. The strength and hardness can be enhanced by using 15% weight Sic instead of 10% weight Sic. In 20% and 25% weight Sic, the hardness is increased and become more clear. The same

thing happen for the samples contain 30% and 35% weight silicon carbide where they have nearly the same behaviour as before (i.e. the hardness increases with increasing the percent of silicon carbide and sintering temperature).

The maximum hardness value of the composite under investigation can be obtained with 30% weight silicon carbide and 850°C sintering temperature.

Although the cycle of heat treatment is different, this result is agreement with other result carried out by W. M. Khairaldien, A.A. Khalil and M. R. Bayoumi [6].

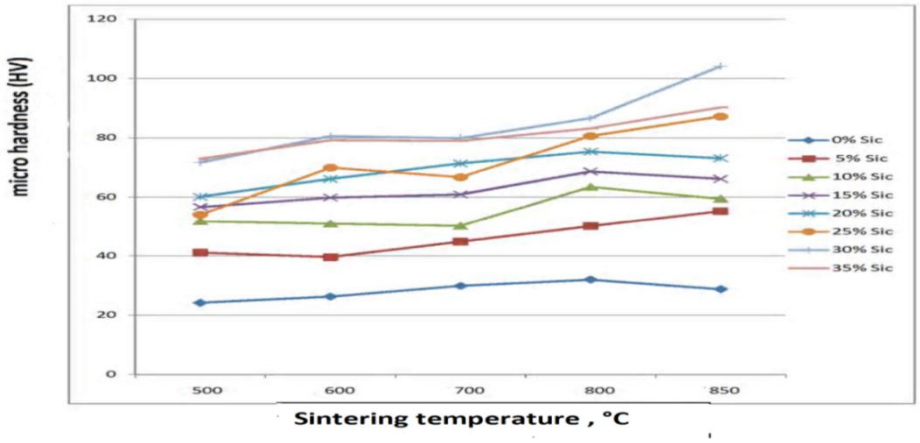

Figure 4: Effect of sintering temperature and silicon carbide on the hardness values.

The problem of the silicon carbide and aluminum particles may be greater in grain size than the indenter. Also the indenter may land on a hidden void or on a cluster of silicon carbide particles. These are the reasons for taking many readings for the same sample. So the micro-hardness test needs a confirmation. There for the compression test is the best choice since it needs small size specimen and very little machining process to prepare the samples.

Fig. 5 shows the stress diagram for the aluminum specimens with no silicon carbide contents and it shows a clear ductile behavior for the specimens at different sintering temperatures. In the case of 5% weight silicon carbide, Fig. 6 depicts the relation between the maximum stress and the sintering temperatures. In the beginning of compression test at 500, 600, and 700°C sintering temperature, the samples has a ductile behavior to some extent, but after that the samples cracked in similar manner to green sample, because the sintering process was not complete. However, if we rise the

sintering temperature, the samples become more brittle. In general, the samples (the one with no or low silicon carbide content) show a complete ductile behavior. The 15% and 20% weight silicon carbide are explained in figures 8 and 9. It shows the samples become brittle at 600 °C and 700 °C compared to the case of 5% which has a ductile behavior at these temperature. So with increasing both the percent of silicon carbide and the sintering temperature, the samples become brittle. This is because the aluminum particles contact with each other and with the particles of silicon carbide when this process is accelerated with increasing the percent of silicon carbide and raising the sintering temperature so the samples become more brittle. The specimens that contain 25% weight silicon carbide gives more brittle behavior as shown in Fig. 10 The 30% and 35% weight silicon carbide gives more a clear brittle behavior .

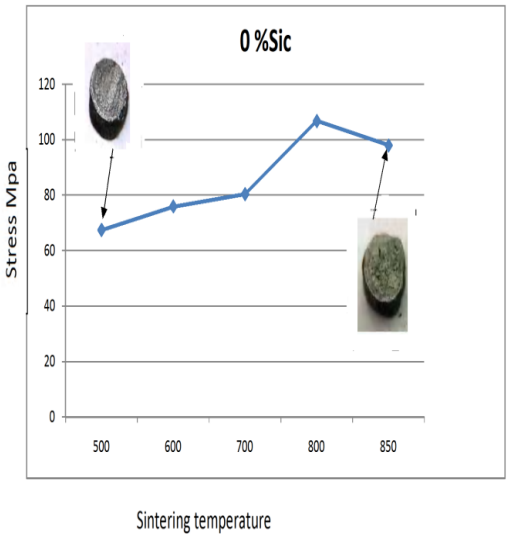

Figure 5: Effect of sintering temperature on the Compression strength for the specimens contain (100%Al, 0%Sic).

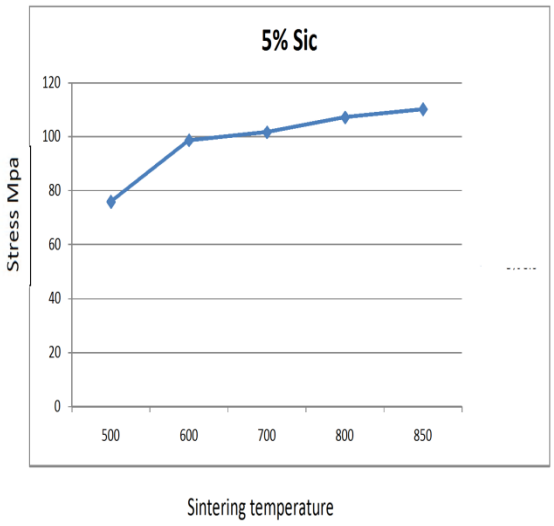

Figure 6: Effect of sintering temperature on the Compression strength for the specimens contain (95%Al, 5%Sic).

SRJMET
Scientific Research Journal for Metal Engineering and Technologies
Volume No.02 Issue No. 01,pp:91-99
ISSN:399-2017
01. Aug .2021

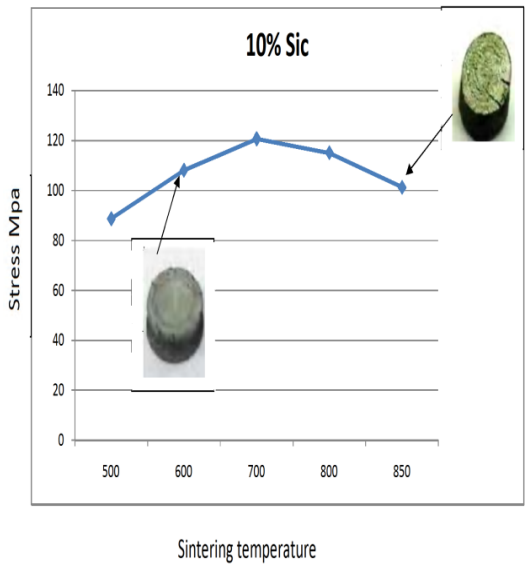

Figure 7: Effect of sintering temperature on the Compression strength for the specimens contain (90 %Al, 10%Sic).

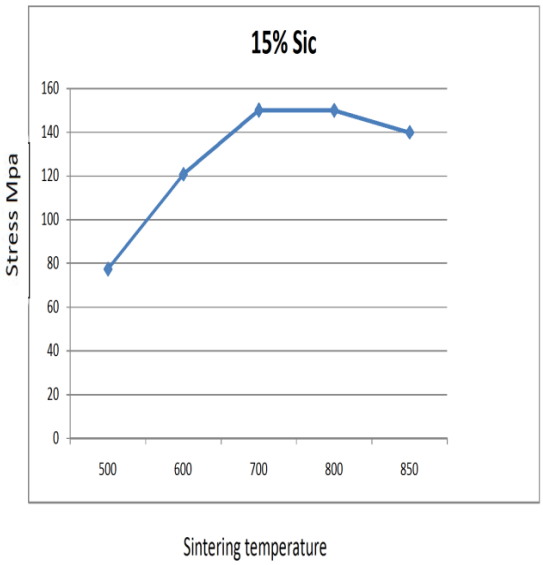

Figure 8: Effect of sintering temperature on the Compression strength for the specimens contain (85 %Al, 15 %Sic).

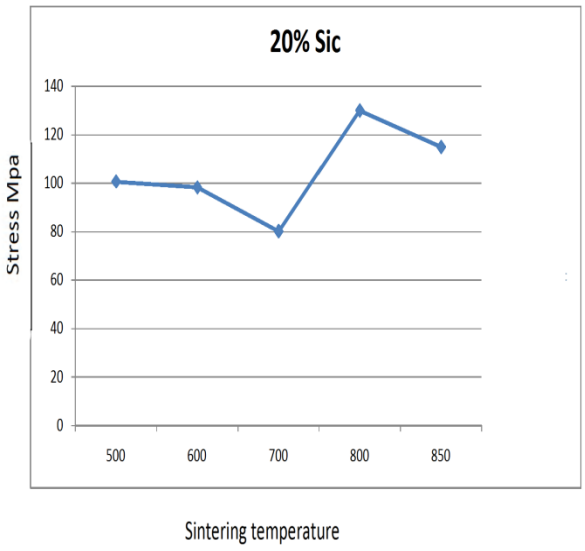

Figure 9: Effect of sintering temperature on the Compression strength for the specimens contain (80 %Al, 20%Sic).

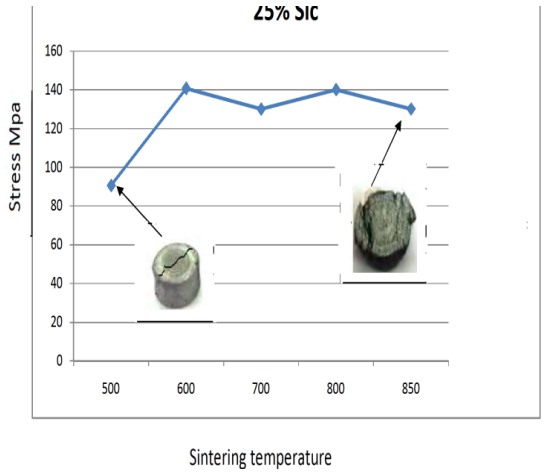

Figure 10: Effect of sintering temperature on the Compression strength for the specimens contain (75 %Al, 25%Sic).

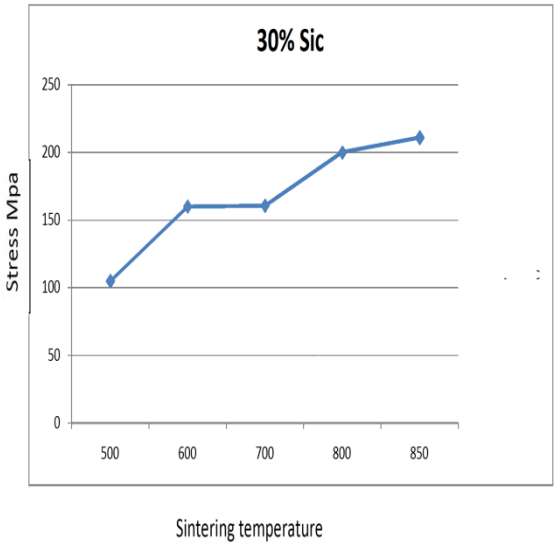

Figure 11: Effect of sintering temperature on the Compression strength for the specimens contain (70 %Al, 30%Sic).

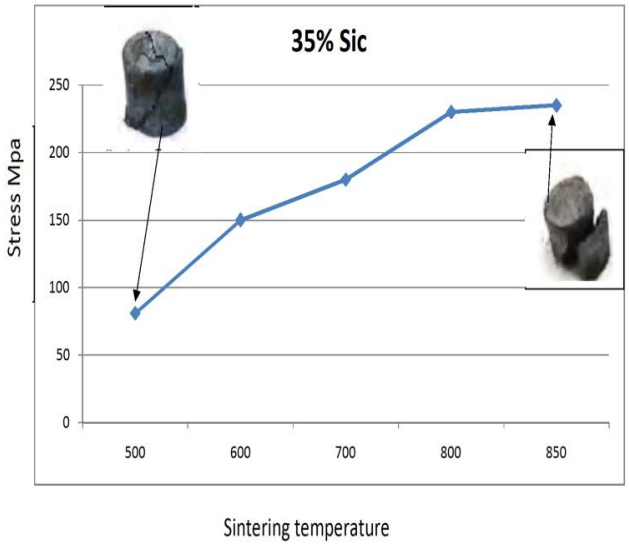

Figure 12: Effect of sintering temperature on the Compression strength for the specimens contain (65 %Al, 35%Sic).

4-Conclusions

1. The mechanical properties of the samples increases with increasing the silicon carbide percent.
2. Sintering temperature of 600°C is enough to produce a successful sintering for the aluminum with no silicon carbide content, while the composite containing 5% SiC requires a slightly increase in the sintering temperature.
3. The samples content 0% and 5% of silicon carbide are ductile. Moreover, the samples become brittle when the percent of silicon carbide increased.
4. The optimum mechanical properties of the composite under investigation can be obtained with 30% weight silicon carbide and 850°C sintering temperature.

References:

1 .G.Jiaug, Y.Fu,W,Wu,G.S.Daehn and R.H,Wagoner,"EnhancedDensificationof Metal Matrix Composites Under Cyclic Pressure", Material Science and Engineering Department, the Ohio State University ,2000.

2. F.V. Lenel, Powder Metallurgy--Principles and Applications, Metal Powder Industries Federation, 1980.

3. Powder Metallurgy, Vol 7, Metals Handbook, 9th ed., American Society for Metals, 1984.

4. Shen, Y.L., Williams, J.J., Piotrowski, G., Chawla, N. and Guo, Y.L. (2001), "Correlation between tensile and indentation behavior of particle reinforced metal matrix composites, Vol. 49 (16), pp.3219-3229,2001.

5. G. Staniek, E lehnert, M. Peters, W. Bunk and W.A. Kaysser,"Powder metallurgical processing of a Sic particle reinforcedAl-6wt.%Fe alloy", Institute of Materials Research, 51147Koln, Germany, pp1787,(1993).

6. W. M. Khairaldien, a.a. Khalil, and M. R. Bayoumi, Production of Aluminum-Silicon Carbide Composites Using Powder Metallurgy at Sintering Temperatures above the Aluminum Melting Point, J of ASTM international, Vol. 35,issue 6, 2007.

7. Yala S. Ahmed and Mohamed H. Alaalam, The influence of Sintering Temperature and Silicon Carbide Percent on the compression properties, AIP conference Proceedings, 2015.

SRJMET
Scientific Research Journal for Metal Engineering and Technologies
Volume No.02 Issue No. 01,pp:100-119
ISSN:399-2017
01. Aug .2021

Comparative Study Between Perception of 3D Printing Over Conventional Construction in Libya

Hamza Jarnaz,[1] **1 and Banu Numan Uyal**,[2]
Department of Engineering Management, Faculty of Engineering, Cyprus International University, Nicosia North Cyprus, via Mersin 10, Turkey.
jarnazhamza@yahoo.com

Abstract:

In recent years, 3D printing has received a growing interest in the construction industry. 3D printing in construction has proven to be very promising in terms of automating construction processes and has the potential to save hard work, material waste, construction time, and potentially dangerous human operations, among other things. This study evaluates the perception of both general public and professionals concerning 3D printing and compares the relative advantage of 3D printing over conventional construction. The study also investigates the difference in the average opinions of the professionals or publics about their perception of 3D printing over conventional construction in Libya. Convenient sampling approach was employed to generate primary data based on structured questionnaire administered to 400 respondents; 200 professionals working in construction and 200 general publics. Kolmogorov-Smirnov and Shapiro-Wilk Tests, Sign Test, Mann–Whitney U Test, Kruskal-Wallis Test, Correlation Coefficient Test and Microsoft Excel for the RII were used for data analysis. The empirical results showed that the professionals have a positive perception towards the feasibility of 3D printing building in Libya. The general public also has positive expectations towards 3D printing building in Libya. The results also show that there are differences between the professionals' responses about their perception of 3D printing over conventional construction due to years of experience in construction industry in favor of experience 11-20 years compared to other experiences, while there are no differences between the professionals and general public responses about their perception of 3D printing over conventional construction due to education level.

Keywords:3D Printing; Feasibility; Conventional Building; Civil Engineering; Construction**.**

1. Introduction

Construction industry is one of the industries that is highly concerned on safety which contribute to its slow adoption of new technologies. The risk associated with the industry is critical to implementation of newly developed or inventing method and products which are untested or required continuous evaluation and regulation for approval (Allouzi et al., 2020). However, many scholars perceived that conventional construction which revolves around the use of manually operated equipment or tools and traditional construction approach has reach it technological peak (Ikeda and Harada, 2006; Mydin et al., 2014; Hager et al., 2016).

As a result of technological advancement in the field of construction, conventional or traditional construction approach lagged behind in terms of customers' core standards of quality, cost, and timeliness (Bock, 2015; Wu et al., 2016). In comparison to other industries, the construction industry saw a decrease in productivity, reduced in profits margins (De Schutter et al., 2018). Moreover, even though with the increase in population and demand for houses, building standard houses from scratch is expensive for average working class and also the fear of mortgage by the general public which contributing to the stagnating productivity of the industry (Aghimien et al., 2020).

The advancement in science and technology has led to several scientific innovations. In the field of civil engineering, 3D printing of building has been trending throughout the 21st century. Consequently, while still in its infancy, three-dimensional (3D) printed construction is perceived as the promising technological advancement with the potential to revolutionize the construction industry. 3D-printed construction is regarded as an advanced construction approach which use machines and additives for construction of wide range of complex geometries and building structures without the need of framework

based on layer-by-layer material deposition approach (Biernacki et al., 2017; Sakin and Kiroglu, 2017).

Currently, some of the developed countries such as Germany adopted and regulated the use 3D printing for building apartment, residential homes, workplaces or offices, bridges, hotels etc. (Xu et al., 2017; Camacho et al., 2018). The use of this system has

shown a great potential for the construction industry in terms of timeliness (i.e., construction duration), cost (less expensive compare to conventional approach), as well as reducing the requirements for massive labour, decrease over usage of materials, improve quality of structures and efficiency, promotes sustainability, increase customization, improve flexibility, enable construction in extreme weather and harsh environment and eliminate the need for construction framework (Krieger et al., 2015; Camacho et al., 2018; Aghimien et al., 2020; Allouzi et al., 2020).

Thus, the main objective of this study is to investigate the perception of both general public and professional regarding the use of 3D printing for construction of buildings in Libya and also evaluate whether 3D printed construction can become a viable substitute for conventional or traditional construction methods. In addition, it examines the difference in the average opinions of the professionals or publics about their perception of 3D printing over conventional construction in Libya due to the general information of professionals (years of experience in construction industry, education level, primary area of professional practice).

The reminder of the paper is organized as: in section 2 the hypothesis of the study is presented. The methodology of the study is given in section 3. Section 4 contains the results and discussions of the data analysis. Finally, the conclusions are presented in section 5.

2. The study hypotheses

During the analysis, and in order to achieve the study objectives, the following hypothesis will be investigated which are related to both professionals and publics;

H1. professional workers on average have positive perceptions about relative advantage for 3D printing building in Libya.

H2. There is no statistically significant difference in the average opinions of the professional workers toward their perception of 3D printing over conventional construction due to years of experience in construction industry.

H3. There is no statistically significant difference in the average opinions of the professional workers toward their perception of 3D printing over conventional construction due to education level.

H4. There is no statistically significant difference in the average opinions of the professional workers toward their perception of 3D printing over conventional construction due to primary professional practice.

H5. General public on average have positive expectation toward 3D printing building in Libya.

H6. General public on average have positive knowledge toward 3D printing building in Libya.

H7. There is no statistically significant difference in the average opinions of the General Public toward feasibility of 3D printing building in Libya due to their age.

H8. There is no statistically significant difference in the average opinions of the General Public toward feasibility of 3D printing building in Libya due to their education level.

H9. There is no statistically significant difference in the average opinions of the General Public toward feasibility of 3D printing building in Libya due to their work sector.

H10. There is no statistically significant difference in the average opinions of the General Public toward feasibility of 3D printing building in Libya due to their marital status.

H11. There is no statistically significant difference in the average opinions of the General Public toward feasibility of 3D printing building in Libya due to their gender.

3. Research methodology

The used methodology for this research is quantitative research. The quantitative research methodology was chosen because efficient amounts of information can be gathered in a short period of time with low cost, analyzed more scientifically and objectively than the other forms, and it's practical. In this regard, questionnaire survey technique was selected for collecting data and further analysis. Two questionnaires (one for the professionals and the other for general public) were prepared based on well-established literature in the field, then the questionnaires were presented to experts and specialists for pilot study in order to enhance the quality of the questionnaires. The questionnaires were administered online using google forms which was the best way at the time considering the distances to travel, the time involved and

the political climate, this is in addition to the Corona Virus So, the researcher took advantage of technology and the willingness of companies to facilitate the participation of their workers in the study.

The study population includes two groups; the first is the professional specialized engineers in the Libyan construction companies, while the second is the non-professional public (general public) in Libya. The sample size was calculated according to (Suresh and Chandrashekara, 2012) and was set as 400 respondents; 200 professionals working in construction and 200 general publics. Convenient sampling approach was employed to generate primary.

data; 200 questionnaires related to professionals were collected, and 200 questionnaires were collected related to the general public.

4. Results and discussions.

1 Validity analysis

Before starting the analysis, the questionnaire was tested for validity and it was found that the questionnaire fields are valid to be measured what it was set for to achieve the main aims of study (Golafshani, 2003).

2 Reliability analysis

Cronbach's alpha test was used to know the level of reliability. A sample consisting of 15 questionnaires were used for conducting the test. and the questionnaires sections were found to be higher than 0.7, and these values are acceptable in SPSS reliability statistics (Garver and Mentzer, 1999

3 Demographic analysis of respondents

Demographıc analysıs of respondents (Professionals)

the general characteristics of the respondents (professionals) covered the years of experience in construction industry, education level and Respondent's primary area of professional practice

The experience in terms of years in the construction work is dominated by by (6 – 10) years with 40.5% followed by (1-5) years with 35.5% and just 7.0% have experiences more than 20 years

3.5% of the respondents, have attained at least a high school, 13.5% were diploma, 50.5% bachelor degree, 26.0% Masters, 6.5% Doctorate. 28% of the respondents their primary area of professional practice are engineering.

consulting Construction project management, 28% are Manufacturers and suppliers, followed by 12.5% are Developers and clients

4.3.2 Demographic analysis of respondents (general public)

the general characteristics of the respondents covered the gender, age, education level, marital status and sector of work is presented beginning from gender range down to their work sector and these comprised of five items.

the respondents were 66.5% males. Majority of the respondents were aged 26 - 40 years with a percentage of 55.0%, followed by the age range 18 - 25 with 26.5%. and 5.0% of the respondents, have attained at least a high school, 21.5% were diploma, 50.5% bachelor degree, 18.0% Masters, 5.0% Doctorate. Also, 45.0% of the respondents were married, 44.0% were single, 11.0% were divorced/separated. In addition 20.5% work in business sector, 14.5% in education sector, 15.5% work in finance and accounting sector, while only 3.5% work in army/pPolice/other force sector.

4.4 Hypothesis testing and the results

First hypothesis H1:

professional workers on average have positive perceptions about relative advantage for 3D printing building in Libya

For analyzing (First Hypothesis), Sign test was used and the test results are illustrated in Table 1.

Table 1:

Mean, SD, RII and P-Value Results for dimensions related to perceptions of professional workers toward feasibility of 3D printing building in Libya.

Dimensions	Mean	SD	RII (%)	Rank	p-value
Relative advantage	4.09	0.443	81.7%	1	0.000
Complexity	3.60	0.709	72.0%	9	0.000
Trialability	4.03	0.492	80.6%	2	0.000
Compatibility	3.97	0.386	79.4%	6	0.000
Absorptive capacity	3.98	0.444	79.6%	5	0.000
External Pressure	3.96	0.424	79.2%	7	0.000
Uncertainty	3.94	0.473	78.8%	8	0.000
Supply-side benefit	3.99	0.420	79.9%	4	0.000
Demand-side benefits	4.02	0.530	80.4%	3	0.000
Average	3.97	0.316	79.4%		0.000

As it can be seen from Table 1 that the dimension "Relative advantage", has the highest weight mean with 81.7%. Followed by the dimension "Trialability" with RII 80.6%. While the lowest RII was found for the dimension "Complexity" with RII 72.0%. Also, it can be noticed from the table that all the p-values are 0.000, which indicate that a significant difference does exist. In general, it was found that the overall mean of all the dimensions equal 3.97, with RII equal 79.4%, and the probability value is less than 0.05, which means that there is general agreement on all the dimensions. Therefore, the null hypothesis is rejected. It is stated that professional workers have a positive perception toward feasibility of 3D printing building in Libya.

Second hypothesis H2:

there is no statistically significant difference in the average opinions of the professional workers toward their perception of 3D printing over conventional construction due to years of experience in construction industry.

To test this hypothesis, Kruskal-Wallis test was used, the results are shown in Table 2 and Table 3.

Table 2

Kruskal-Wallis test- perception of 3D printing over conventional construction due to years of experience in construction industry..

	Years of experience in construction industry	N	Mean Rank	Chi-Square	P-value (Sig).
perception of 3D printing over conventional construction	1-5	71	75.16	36.184	0.000*
	6-10	81	99.28		
	11-20	34	141.74		
	Above 20	14	135.93		

Table 3

Multiple comparisons (Post Hoc Tests) due to years of experience in construction industry

Multiple Comparisons (Post Hoc Tests)				
(I) Experience	(J) Experience	Mean Difference (I-J)	Std. Error	Sig.
1-5	6-10	-0.09272	0.048	0.301
	11-20	-.32648*	0.062	0.000
	above 20	-.19387	0.087	0.177
6-10	1-5	0.09272	0.048	0.301
	11-20	-.23376*	0.061	0.002
	above 20	-.10115	0.086	0.710
11-20	1-5	.32648*	0.062	0.000
	6-10	.23376*	0.061	0.002
	above 20	0.13261	0.094	0.578
above 20	1-5	0.19387	0.087	0.177
	6-10	0.10115	0.086	0.710
	11-20	-.13261	0.094	0.578

The results in Table 2 showed that the probability value is less than 0.05, and this is evidence of differences between the respondents' responses about their perception of 3D printing over conventional construction due to years of

experience in construction industry, and to identify the direction of these differences and in favour of whom these differences were, it was found that the highest value of the average ranks was 141.74 corresponds to the 11-20 years (See Table 3). On the other hand, according to the results of Multiple Comparisons (Post Hoc Tests) table, it was found that there are significant differences between the categories, the probability value is less than 0.05, that meaning the level perception of 3D printing over conventional construction was higher for experience 11-20 years compared to other experiences. Therefore, the H2 was rejected.

Third hypothesis H3: there is no statistically significant difference in the average opinions of the professional workers toward their perception of 3D printing over conventional construction due to education level.

To test this hypothesis, Kruskal-Wallis test was used, as shown in Table 4.

Table 4

Kruskal-Wallis test- perception of 3D printing over conventional construction due to education level

	Education level	N	Mean Rank	Chi-Square	P-value (Sig).
perception of 3D printing over conventional construction	High school	7	83.79	4.948	0.293
	Diploma	27	104.78		
	Bachelor degree	101	96.54		
	Master's degree	52	100.46		
	Doctorate degree	13	131.54		

The results in Table 4 showed that the probability value is greater than 0.05, and this is evidence of no differences between the respondents' responses about their perception of 3D printing over conventional construction due to education level. As a result, the third hypothesis was not rejected.

Fourth hypothesis H4: there is no statistically significant difference in the average opinions of the professional workers toward their perception of 3D printing over conventional construction due to primary professional practice.

To test this hypothesis, Kruskal-Wallis test was used, as shown in Table 5 and Table 6.

Table 5

Kruskal-Wallis test- perception of 3D printing over conventional construction due to primary professional practice.

	Primary professional practice	N	Mean Rank	Chi-Square	P-value (Sig).
Perception of 3D printing over conventional construction	3D printing organizations and manufacturing	6	170.08	23.240	0.003*
	Academic and professional institutions	10	75.15		
	Developers and clients	25	90.9		
	Engineering consulting Construction project management	56	107.29		
	Quantity surveying	12	94.75		
	Manufacturers and suppliers	56	90.68		
	Estate and facilities management	22	109.39		
	Government organizations	7	153.21		

Other	6	58.83	

Table 6

Multiple comparisons (Post Hoc Tests) due to primary professional practice.

Multiple Comparisons (Post Hoc Tests)				
(I) Primary professional Practice	(J) Primary professional Practice	Mean Difference (I-J)	Std. Error	Sig.
3D printing organizations and manufacturing	Academic and professional institutions	0.52764	0.154	0.170
	Developers and clients	0.45642	0.135	0.190
	Engineering consulting Construction project management	0.33914	0.128	0.536
	Quantity surveying	0.46545	0.149	0.289
	Manufacturers and suppliers	0.43844	0.128	0.171
	Estate and facilities management	0.33186	0.137	0.664
	Government organizations	0.10743	0.166	1.000
	Other	.73984*	0.172	0.022
Academic and professional institutions	3D printing organizations and manufacturing	-.52764-	0.154	0.170
	Developers and clients	-.07122-	0.111	1.000
	Engineering consulting Construction project management	-.18850-	0.102	0.905
	Quantity surveying	-.06220-	0.128	1.000
	Manufacturers and suppliers	-.08920-	0.102	0.999
	Estate and facilities management	-.19579-	0.114	0.935
	Government organizations	-.42021-	0.147	0.419
	Other	0.21220	0.154	0.983
Developers and clients	3D printing organizations and manufacturing	-.45642-	0.135	0.190
	Academic and professional institutions	0.07122	0.111	1.000
	Engineering consulting Construction project management	-.11728-	0.072	0.952
	Quantity surveying	0.00902	0.105	1.000
	Manufacturers and suppliers	-.01798-	0.072	1.000
	Estate and facilities management	-.12457-	0.087	0.979
	Government organizations	-.34899-	0.127	0.486
	Other	0.28341	0.135	0.820
Engineering consulting Construction project management	3D printing organizations and manufacturing	-.33914-	0.128	0.536
	Academic and professional	0.18850	0.102	0.905

	institutions			
	Developers and clients	0.11728	0.072	0.952
	Quantity surveying	0.12631	0.095	0.987
	Manufacturers and suppliers	0.09930	0.056	0.926
	Estate and facilities management	-.00729-	0.075	1.000
	Government organizations	-.23171-	0.119	0.876
	Other	0.40070	0.128	0.286
	3D printing organizations and manufacturing	-.46545-	0.149	0.289
	Academic and professional institutions	0.06220	0.128	1.000
	Developers and clients	-.00902-	0.105	1.000
Quantity surveying	Engineering Construction project management	-.12631-	0.095	0.987
	Manufacturers and suppliers	-.02700-	0.095	1.000
	Estate and facilities management	-.13359-	0.107	0.991
	Government organizations	-.35801-	0.142	0.605
	Other	0.27439	0.149	0.906
	3D printing organizations and manufacturing	-.43844-	0.128	0.171
	Academic and professional institutions	0.08920	0.102	0.999
	Developers and clients	0.01798	0.072	1.000
Manufacturers and suppliers	Engineering Construction project management	-.09930-	0.056	0.926
	Quantity surveying	0.02700	0.095	1.000
	Estate and facilities management	-.10659-	0.075	0.980
	Government organizations	-.33101-	0.119	0.468
	Other	0.30139	0.128	0.697
	3D printing organizations and manufacturing	-.33186-	0.137	0.664
	Academic and professional institutions	0.19579	0.114	0.935
	Developers and clients	0.12457	0.087	0.979
Estate and facilities management	Engineering Construction project management	0.00729	0.075	1.000
	Quantity surveying	0.13359	0.107	0.991
	Manufacturers and suppliers	0.10659	0.075	0.980
	Government organizations	-.22442-	0.129	0.932
	Other	0.40798	0.137	0.361
Government	3D printing organizations	-.10743-	0.166	1.000

organizations	and manufacturing			
	Academic and professional institutions	0.42021	0.147	0.419
	Developers and clients	0.34899	0.127	0.486
	Engineering consulting			
	Construction project management	0.23171	0.119	0.876
	Quantity surveying	0.35801	0.142	0.605
	Manufacturers and suppliers	0.33101	0.119	0.468
	Estate and facilities management	0.22442	0.129	0.932
	Other	0.63240	0.166	0.075
Other	3D printing organizations and manufacturing	-.73984-*	0.172	0.022
	Academic and professional institutions	-.21220-	0.154	0.983
	Developers and clients	-.28341-	0.135	0.820
	Engineering consulting			
	Construction project management	-.40070-	0.128	0.286
	Quantity surveying	-.27439-	0.149	0.906
	Manufacturers and suppliers	-.30139-	0.128	0.697
	Estate and facilities management	-.40798-	0.137	0.361
	Government organizations	-.63240-	0.166	0.075

The results in Table 5 showed that the probability value is less than 0.05, and this is evidence of differences between the respondents' responses about their perception of 3D printing over conventional construction due to primary professional practice, and to identify the direction of these differences and in favor of whom these differences were, it was found that the highest value of the average ranks was 170.08 corresponds to the 3D printing organizations and manufacturing (See Table 16). On the other hand, according to the results of Multiple Comparisons (Post Hoc Tests) Table, it was found that there are significant differences between the categories, the probability value is less than 0.05, that meaning the level perception of 3D printing over conventional construction was higher for 3D printing organizations and manufacturing compared to other primary area of professional practice. Therefore, the H4 was rejected.

Fifth hypothesis H5: general public on average have positive expectation toward 3D printing building in Libya.

For analyzing (H6), Sign test was used and the test results are illustrated in Table 8.

Table 8

Mean, SD, RII and P-Value Results for knowledge of general public toward 3D printing building.

Items	Mean	SD	RII (%)	Rank	p-value
3D printing is a great modern technology that allows for the development of new building	4.27	0.825	85.4%	2	0.000
I will prefer to live in a house build using 3D building	3.96	0.912	79.2%	13	0.000
I believe building house using 3D printing will be cheaper	3.81	1.016	76.1%	16	0.000
I will be scared to live in a house built using 3D printing	3.61	1.050	72.2%	18	0.000
I will strongly recommend people to build house using 3D printing	3.81	0.986	76.1%	16	0.000
Building houses using 3DP printing can enhance sustainability	4.11	0.804	82.1%	8	0.000
3D printing building will benefit us in the future	4.17	0.801	83.3%	6	0.000
In comparison to conventional building, 3D printed building would reduce construction waste	4.25	0.719	84.9%	3	0.000
3D printing of building will be easier and save time	4.23	0.773	84.5%	4	0.000
Building houses and constructions using 3D printed building will be safer and reliable compare to conventional building	4.09	0.809	81.8%	10	0.000
3D building will replace human labor and can lead to increase of unemployment	4.07	0.780	81.4%	12	0.000
I believe the use of 3DP will replace conventional traditional building in Libya by 2030	3.88	1.002	77.5%	15	0.000
I will prefer to hire constructors that build houses using 3D Printing	3.92	0.926	78.4%	14	0.000
The use of 3DP will help constructors' engineers to build houses faster with less human errors	4.22	0.708	84.3%	5	0.000
The government should permit the use of this technology	4.10	0.830	81.9%	9	0.000
I believe innovation in construction is crucial for development of Libya	4.14	0.761	82.7%	7	0.000
I believe building houses using 3DP will solve housing crisis in Libya	4.08	0.952	81.6%	11	0.000
Technological advancement is key to development of every country and 3D building will transform Libyan construction sector	4.32	0.734	86.3%	1	0.000
Average	4.06	0.434	81.1%		0.000

Results in Table 8 showed that the item "Technological advancement is key to development of every country and 3D building will transform Libyan construction sector", has the highest weight mean with 86.3%. Followed by the item "3D printing is a great modern technology that allows for the development of new building" with a RII 85.4%, then the item "In comparison to conventional building, 3D printed building would reduce construction waste" with a RII 84.9%. While the lowest RII was found for the item "I will be scared to live in a house built using 3D printing" with 72.2%. Also, it can be noticed from the table that all the p-values are 0.000, which indicate that a significant difference does exist. Overall, it was found that the overall mean of all the paragraphs related to knowledge of general public toward 3D printing building dimension equals 4.06, with RII equal 81.1%, and the probability value is less than 0.05, which means that there is general agreement on all the paragraphs related to knowledge of general public toward 3D printing building dimension. Therefore, the null hypothesis is rejected. It is stated that general public on average have positive knowledge toward 3D printing building in Libya.

Seventh hypothesis H7: there is no statistically significant difference in the average opinions of the General Public toward feasibility of 3D printing building in Libya due to their age.

To test this hypothesis, Kruskal-Wallis test was used, and the results are shown in Table 9 and Table 10.

Table 9

Kruskal-Wallis test- feasibility of 3D printing building in Libya due to their age.

	Age	N	Mean Rank	Chi-Square	P-value (Sig).
feasibility of 3D printing building in Libya	18-25	53	69.98	25.745	0.000*
	26-40	110	104.95		
	41-60	33	131.71		
	Above 60	4	124.88		

Table 10

Multiple comparisons (Post Hoc Tests) due to age

Multiple Comparisons (Post Hoc Tests)				
(I) Experience	(J) Experience	Mean Difference (I-J)	Std. Error	Sig.
18-25	26-40	.25181-*	0.065	0.002
	41-60	.42302-*	0.086	0.000
	Above 60	-0.37929	0.202	0.319
26-40	18-25	.25181*	0.065	0.002
	41-60	-0.17121	0.077	0.181
	Above 60	-0.12748	0.198	0.937
41-60	18-25	.42302*	0.086	0.000
	26-40	0.17121	0.077	0.181
	Above 60	0.04373	0.206	0.997
Above 60	18-25	0.37929	0.202	0.319
	26-40	0.12748	0.198	0.937
	41-60	-0.04373	0.206	0.997

The results in Table 9 showed that the probability value is less than 0.05, and this is evidence of differences between the respondents' responses about their opinion toward feasibility of 3D printing over conventional construction due to their age, and to identify the direction of these differences and in favor of whom these differences were, it was found that the highest value of the average ranks was 131.71 corresponds to the 41 - 60 years. On the other hand, according to the results of Multiple Comparisons (Post Hoc Tests) Table 10, it was found that there are significant differences between the categories, the probability value is less than 0.05, that meaning the level feasibility of 3D printing over conventional construction was higher for age 41 - 60 years compared to other ages. Therefore, the H7 was rejected.

Eightieth hypothesis H8: there is no statistically significant difference in the average opinions of the General Public toward feasibility of 3D printing building in Libya due to their education level.

To test this hypothesis, Kruskal-Wallis test was used, as shown in Table 11.

Table 11

Kruskal-Wallis test- feasibility of 3D printing building in Libya due to education level.

	Education level	N	Mean Rank	Chi-Square	P-value (Sig).
Feasibility of 3D printing building in Libya	High school	10	69.05	8.190	0.085
	Diploma	43	110.19		
	Bachelor degree	101	93.87		
	Master's degree	36	109.38		
	Doctorate degree	10	125.35		

* The differences are significant

The results in Table 11 showed that the probability value is greater than 0.05, and this is evidence of no differences between the respondents' responses about their opinion toward

feasibility of 3D printing over conventional construction due to their education level. As a result, the Eightieth hypothesis is not rejected.

Ninth hypothesis H9: there is no statistically significant difference in the average opinions of the General Public toward feasibility of 3D printing building in Libya due to their work sector.

To test this hypothesis, Kruskal-Wallis test was used, as shown in Table 12.

Table 12

Kruskal-Wallis test- feasibility of 3D printing building in Libya due to work sector.

	Work sector	N	Mean Rank	Chi-Square	P-value (Sig).
Feasibility of 3D printing building in Libya	Education	29	107.43	9.958	0.191
	Business	41	88		
	Finance and Accounting	31	108.53		
	Agriculture	16	95.06		
	Army/Police/other force	7	154.43		
	Healthcare	23	102.2		
	Industries	23	89.91		
	Others	30	99.72		

The results in Table 12 showed that the probability value is greater than 0.05, and this is evidence of no differences between the respondents' responses about their opinion toward feasibility of 3D printing over conventional construction due to their work sector. As a result, the Ninth hypothesis was not rejected.

Tenth hypothesis H10: there is no statistically significant difference in the average opinions of the General Public toward feasibility of 3D printing building in Libya due to their marital status.

To test this hypothesis, Kruskal-Wallis test was used, the results are shown in Table 13 and Table 14.

Table 13

Kruskal-Wallis test- feasibility of 3D printing building in Libya due to their marital status.

	Marital status	N	Mean Rank	Chi-Square	P-value (Sig).
Feasibility of 3D printing building in Libya	Single	88	79.38	21.316	0.000*
	Married	90	115.52		
	Divorced/separated	22	123.55		

Table 14

Multiple Comparisons (Post Hoc Tests) due to marital status.

Multiple Comparisons (Post Hoc Tests)				
(I) Marital status	(J) Marital status	Mean Difference (I-J)	Std. Error	Sig.
Single	Married	.24704-*	0.059	0.000
	Divorced/separated	.32128-*	0.093	0.003
Married	Single	.24704*	0.059	0.000
	Divorced/separated	-.07424	0.093	0.729
Divorced/separated	Single	.32128*	0.093	0.003
	Married	0.07424	0.093	0.729

It is evident from the results of Table 13 related to the differences between the averages of the respondents' responses about the feasibility of construction due to the marital status variable. The probability value is less than the significance level of 0.05, and this is evidence of the existence of differences between the respondents' opinions according to their marital status, and to identify the direction of these differences and in favor of whom these differences were, it was found that the highest value of the average ranks was 123.55 corresponds to the Divorced/separated. On the other hand, according to the results of Multiple Comparisons (Post Hoc Tests) Table 14, it was found that there are significant differences between the categories, the probability value is less than 0.05, that meaning the level feasibility of 3D printing over

conventional construction was higher for Marital status (Divorced/separated) compared to other marital status. Therefore, the H10 was rejected.

Eleventh hypothesis H11: there is no statistically significant difference in the average opinions of the General Public toward feasibility of 3D printing building in Libya due to their gender.

To test this hypothesis, Mann-Whitney U test was used, as shown in Table 15.

Table 15

Man-Whitney U test- feasibility of 3D printing building in Libya due to gender.

	Gender	N	Mean Rank	Test value	P-value (Sig).
Feasibility of 3D printing building in Libya	Male	133	100.62	0.04	0.96
	Female	67	100.26	1	7

The results in Table 15 showed that the probability value is greater than 0.05, and this is evidence of no differences between the respondents' responses about their opinion toward feasibility of 3D printing over conventional construction due to their gender. As a result, the tenth hypothesis was not rejected.

5. Conclusions

In this study, perceptions of 3D printing over conventional construction in Libya have been studied. Two groups in Libya were selected for collecting the data, professional specialized engineers and general public. SPSS version 19 was used for analyzing the data, and the results of the analyzing led to draw the following conclusions:

- It was found that the professional workers have positive perceptions toward feasibility of 3D printing building in Libya. Moreover, general public on average have positive expectation toward 3D printing building in Libya.
- For years of experience, it was found that the level of perception of 3D printing over conventional construction is higher for experience 11-20 years of experience than for other experiences.
- For primary professional practice, the level perception of 3D printing over conventional construction was higher for 3D printing organizations and manufacturing compared to other primary area of professional practice.

- The level perception of 3D printing over conventional construction was higher for age 41 - 60 years compared to other ages.
- The level perception of 3D printing over conventional construction was higher for marital status (Divorced/separated) compared to other marital status.

References

[1] Aghimien, D., Aigbavboa, C., Aghimien, L., Thwala, W. D., & Ndlovu, L. (2020). Making a case for 3D printing for housing delivery in South Africa. *International Journal of Housing Markets and Analysis, 13*(4), 565-581. https://doi.org/10.1108/IJHMA-11-2019-0111

[2] Allouzi, R., Al-Azhari, W., & Allouzi, R. (2020). Conventional Construction and 3D Printing: A Comparison Study on Material Cost in Jordan. *Journal of Engineering, 2020,* 1-14. https://doi.org/10.1155/2020/1424682

[3] Biernacki, J. J., Bullard, J. W., Sant, G., Brown, K., Glasser, F. P., Jones, S., ... & Prater, T. (2017). Cements in the 21st century: challenges, perspectives, and opportunities. *Journal of the American Ceramic Society*, *100*(7), 2746-2773. https://doi.org/10.1111/jace.14948

[4] Bock, T. (2015). The future of construction automation: Technological disruption and the upcoming ubiquity of robotics. *Automation in Construction, 59*, 113-121. https://doi.org/10.1016/j.autcon.2015.07.022

[5] Camacho, D. D., Clayton, P., O'Brien, W. J., Seepersad, C., Juenger, M., Ferron, R., & Salamone, S. (2018). Applications of additive manufacturing in the construction industry–A forward-looking review. *Automation in construction*, *89*, 110-119. https://doi.org/10.1016/j.autcon.2017.12.031

[6] Garver, M. S., & Mentzer, J. T. (1999). Logistics research methods: employing structural equation modeling to test for construct validity. *Journal of business logistics, 20*(1), 33-57.

[7] Golafshani, N. (2003). Understanding reliability and validity in qualitative research. *The qualitative report*, *8*(4), 597-607.

[8] De Schutter, G., Lesage, K., Mechtcherine, V., Nerella, V. N., Habert, G., & Agusti-Juan, I. (2018). Vision of 3D printing with concrete—Technical, economic and environmental potentials. *Cement and Concrete Research*, *112*, 25-36. https://doi.org/10.1016/j.cemconres.2018.06.001

[9] Hager, I., Golonka, A., & Putanowicz, R. (2016). 3D printing of buildings and building components as the future of sustainable construction?. Procedia Engineering, 151, 292-299. https://doi.org/10.1016/j.proeng.2016.07.357

[10] Kreiger, M. A., MacAllister, B. A., Wilhoit, J. M., & Case, M. P. (2015). The current state of 3D printing for use in construction. In *The Proceedings of the 2015 Conference*

[11] Ikeda, Y., & Harada, T. (2006). Application of the automated building construction system using the conventional construction method together. In *Proceedings of 23rd International Symposium on Automation and Robotics in Construction. 3*(1), 722-727.

[12] Mydin, M. O., Sani, N. M., & Phius, A. F. (2014). Investigation of industrialised building system performance in comparison to conventional construction method. In *MATEC Web of Conferences, 10*, 04001. https://doi.org/10.1051/matecconf/20141004001

[13] Sakin, M., & Kiroglu, Y. C. (2017). 3D Printing of Buildings: Construction of the Sustainable Houses of the Future by BIM. *Energy Procedia*, *134*, 702-711. https://doi.org/10.1016/j.egypro.2017.09.562

[14] Suresh, K. P., & Chandrashekara, S. (2012). Sample size estimation and power analysis for clinical research studies. *Journal of human reproductive sciences*, *5*(1), 7. https://dx.doi.org/10.4103/0974-1208.97779

[15] Wu, P., Wang, J., & Wang, X. (2016). A critical review of the use of 3-D printing in the construction industry. *Automation in Construction*, *68*, 21-31. https://doi.org/10.1016/j.autcon.2016.04.005

[16] Xu, J., Ding, L., & Love, P. E. (2017). Digital reproduction of historical building ornamental components: From 3D scanning to 3D printing. *Automation in Construction*, *76*, 85-96. https://doi.org/10.1016/j.autcon.2017.01.010